



# VCU

Virginia Commonwealth University  
VCU Scholars Compass

---

Theses and Dissertations

Graduate School


---

2019

## Differential Mobility Classifiers in the Non-Ideal Assembly

Thamir Alsharifi  
*Virginia Commonwealth University*

Follow this and additional works at: <https://scholarscompass.vcu.edu/etd>

 Part of the [Manufacturing Commons](#), [Nanoscience and Nanotechnology Commons](#), [Other Engineering Commons](#), and the [Other Mechanical Engineering Commons](#)

© Thamir Alsharifi

---

Downloaded from

<https://scholarscompass.vcu.edu/etd/6054>

This Dissertation is brought to you for free and open access by the Graduate School at VCU Scholars Compass. It has been accepted for inclusion in Theses and Dissertations by an authorized administrator of VCU Scholars Compass. For more information, please contact [libcompass@vcu.edu](mailto:libcompass@vcu.edu).

# Differential Mobility Classifiers in the Non-Ideal Assembly

A dissertation submitted in partial fulfillment of the requirements for the degree of  
Doctor of Philosophy at Virginia Commonwealth University.

by

THAMIR HARETH ALI ALSHARIFI

M.Sc., Mechanical Engineering, University of Technology, Iraq, 2008

B.Sc., Mechanical Engineering, University of Technology, Iraq, 2005

Director: DR. DA-REN CHEN

PROFESSOR AND FLOYD D. GOTTWALD, SR. CHAIR IN MECHANICAL AND  
NUCLEAR ENGINEERING

Virginia Commonwealth University

Richmond, Virginia

December 2019

**COPYRIGHT PAGE**

© Thamir Hareth Ali Alsharifi, 2019

All Rights Reserved

## **Acknowledgment**

I would like to express my sincere appreciation and gratitude to my supervisor and committee chair, Professor Da-Ren Chen, for introducing me to the aerosols science, and for his guidance and never-ending support. Without his valuable guidance and broad experience, this dissertation would not be possible. I wish to acknowledge the members of my Ph.D. committee, Dr. Hong Zhao, Dr. Shawn Chen, Dr. Jing Wang, and Dr. Weijun Xiao for taking interest in my research work, examining my dissertation, and supporting this research work with their fruitful comments and feedbacks.

I am extremely grateful to the Higher Committee for Education Development in Iraq for its scholarship program and its professional staff. Without their gracious scholarship, I would not have been able to complete this research at Virginia Commonwealth University (VCU). I am blessed to travel abroad to glean great knowledge and experience.

I like to thank my parents for raising me to reach my PhD in mechanical and nuclear engineering, and for their love and patience as I left them for long years to study abroad.

I am grateful for my colleagues, alumni, and visiting scholars at the Particle Lab at VCU for their nice attitude and encouragement. I especially attribute Charlie (Hsi-Wei Yeh), Di Liu, Zhenzhong Zhang, Qiaoling Liu, Peng Wang, Zhen Li, Hao Tu, and Nan Zhou. Also, I would like to thank a very good friend in the Electrical and Computer Engineering department at VCU, Ammar Hoori.

I am very thankful to the faculty and the staff of the Mechanical and Nuclear Engineering Department for supporting me by all means. I especially appreciate the Department Chair, Dr. Gary C. Tepper, and the graduate student director, Dr. Karla Mossi.

I would also like to thank my friends that have become like family: the Browns (Gilpin & Pam) and the Seiberts (Dave & Amanda).

Many nice people in the VCU community deserve to be thanked for their, educational, linguistic, technical, and emotional supports. They are a lot and space is not enough to mention them all. Thank you all!

Thamir Alsharifi

Virginia Commonwealth University

December 2019

# Table of Contents

	Page
COPYRIGHT PAGE.....	ii
Acknowledgment.....	iii
Table of Contents .....	v
List of Tables.....	viii
List of Figures .....	ix
Abstract .....	xi
CHAPTER 1 Introduction and Overview.....	1
<b>1.1 Background</b> .....	1
<b>1.2 The Dissertation Motivation</b> .....	6
<b>1.3 Overall Objective</b> .....	8
<b>1.4 Dissertation Structure</b> .....	11
CHAPTER 2 Review of the Differential Mobility Classifier.....	12
<b>2.1 Review of the Differential Mobility Classifier (DMC)</b> .....	12
<b>2.2 An Overview of the DMC Configurations</b> .....	16
<b>2.2.1 Cylindrical DMC</b> .....	16
<b>2.2.2 Parallel plate DMC</b> .....	24
<b>2.3 DMC Transfer Function Calculation Methods</b> .....	26
CHAPTER 3 Eccentric Cylindrical Differential Mobility Classifier .....	29
<b>3.1 Introduction</b> .....	29
<b>3.2 The Numerical Model</b> .....	33
<b>For the flow and electrical fields</b> .....	34
<b>For particle trajectory</b> .....	34
<b>For the DMC transfer function</b> .....	35
<b>3.3 Model Verification</b> .....	38
<b>3.3.1 Cylindrical Model Verification</b> .....	38
<b>3.3.2 Eccentric Model Verification</b> .....	39

<b>3.4 Results and Discussion</b> .....	41
<b>3.4.1 Flow and electrical fields inside the eccentric DMC</b> .....	41
<b>3.4.2 Transfer function of an eccentric DMC</b> .....	43
<b>3.4.4 Effect of sheath-to-aerosol flow ratio and total flow rate on the eccentric transfer function</b> .....	48
<b>3.4.5 Effect of DMC geometry on the eccentric transfer function.</b> .....	51
<b>3.4.6 Effect of particle diffusivity on the eccentric DMC transfer function</b> .....	54
CHAPTER 4 Inner Rod Tilting / Cylindrical Differential Mobility Classifier .....	57
<b>4.1 Introduction</b> .....	57
<b>4.2 The Numerical Model</b> .....	59
<b>4.3 Result and Discussion</b> .....	62
<b>4.3.1 Distorted flow and electrical fields in a tilted DMC classifying channel</b> .....	62
<b>4.3.2 Transfer function of a DMC having a tilted inner rod</b> .....	64
<b>4.3.3 Tilted DMC transfer function at different sheath-to-aerosol flow rate ratios and total flow rates</b> .....	69
<b>4.3.4 Effect of the geometrical parameters of classification channel on tilted DMC transfer function</b> .....	71
<b>4.3.5 Effect of particle diffusivity on the tilted DMC transfer function</b> .....	72
<b>4.3.6 Classification of the tilted DMC transfer function</b> .....	73
CHAPTER 5 Parallel Plates Differential Mobility Classifier .....	75
<b>5.1 Introduction</b> .....	75
<b>5.2 The Numerical Model</b> .....	78
<b>5.3. Modeling Results</b> .....	83
<b>5.3.1 Validation of numerical modeling</b> .....	83
<b>5.3.2 Effect of the classification-channel aspect ratio (CAR)</b> .....	84
<b>5.3.3 Effect of the aerosol slit opening</b> .....	88
<b>5.3.4 Effects of cross-sectional area and aerosol injection angle of the particle classification channel</b> .....	92
CHAPTER 6 Plates Tilting/ Parallel Plates Differential Mobility Classifier .....	94

<b>6.1 Introduction</b> .....	94
<b>6.2 Numerical Modeling of the Tilted-plate DMCs</b> .....	97
<b>6.3 Model verification</b> .....	101
<b>6.4 Modeling Result</b> .....	101
<b>6.4.1 Typical flow and electrical fields inside the tilted DMC classifying channel</b> .....	101
<b>6.4.2 Side Tiled Transfer Function</b> .....	104
<b>6.4.3 Channel Aspect Ratio (AR)</b> .....	106
<b>6.4.4 Channel Length</b> .....	107
<b>6.4.5 Flow Ratio <math>\beta</math> and Total Flow</b> .....	108
<b>6.4.6 Slits opening <math>\eta</math></b> .....	109
<b>6.4.7 Particle Size/Diffusivity</b> .....	110
<b>6.4.8 Tilting Type</b> .....	110
CHAPTER 7 Dissertation Summary and Future Work.....	114
<b>7.1 Dissertation Summary</b> .....	114
<b>7.1.1 Eccentric Cylindrical Classifier</b> .....	114
<b>7.1.2 Tilted Cylindrical Classifier</b> .....	116
<b>7.1.3 Parallel Plates Classifier</b> .....	118
<b>7.1.4 Parallelism of the Parallel Plates Classifier</b> .....	120
<b>7.2 Recommendations for Future Research</b> .....	121
Literature Cited.....	123
Appendices .....	135
APPENDIX A: Bipolar Coordinate System.....	136
APPENDIX B: The Developing Length for the Eccentric DMC.....	140
APPENDIX C: The Transfer Function Slope.....	142
APPENDIX D: Maximum Inner Rod Tilting Angle $\theta_m$ for The Cylindrical DMC .....	144
VITA .....	145



## List of Tables

	Page
Table 3. 1 Properties of gas and particles, and flow rates for cylindrical DMC.....	38
Table 4. 1 Properties of gas and particles utilized in the tilted cylindrical DMC.....	62
Table 4. 2 Geometrical dimensions and parameters for tilted cylindrical DMC.....	62
Table 5. 1 Properties of the flow and particles used for parallel-plates DMC.....	82
Table 5. 2 List of geometrical variables of miniature parallel-plate DMCs .....	85
Table 6. 1 Constants and physical properties inside the plates-tilted DMC.....	100
Table 6. 2 The key dimensions for plates-tilted DMC. ....	100

## List of Figures

	Page
Figure 1. 1 Particle size range.....	2
Figure 1. 2 The schematic diagram of the SMPS system .....	5
Figure 2. 1 Whitby electrical counter system .....	18
Figure 2. 2 Differential mobility analyzer designed by Knutson.....	19
Figure 2. 3 A cross-section of Vienna classifier .....	22
Figure 2. 4 The perfect concentric DMC .....	23
Figure 2. 5 Perfect parallel plate DMC.....	24
Figure 3. 1 The schematic diagram of a cylindrical differential mobility classifier.....	31
Figure 3. 2 The comparison of numerical transfer functions.....	40
Figure 3. 3 The comparison of numerical non-diffusive transfer functions with the theoretical.....	41
Figure 3. 4 The illustration of flow and electrical fields in the classification channel .....	42
Figure 3. 5 The comparison of the numerical transfer function with the theoretical data	44
Figure 3. 6 The position of particles in the neighborhood of the classified particle exit slit .....	46
Figure 3. 7 The numerical transfer function of a DMC with 5% eccentricity .....	49
Figure 3. 8 The numerical transfer function with different flow ratios .....	50
Figure 3. 9 Comparison of the calculated transfer functions of a DMC.....	51
Figure 3. 10 The effect of DMC geometrical parameters on the transfer function .....	53
Figure 3. 11 Calculated transfer function of DMCs having the 0%, 1%, 2% and 5% eccentricity.....	55
Figure 3. 12 Eccentric DMC transfer function peaks zones .....	56
Figure 4. 1 The schematic diagram of a cylindrical differential mobility classifier.....	61
Figure 4. 2 The illustration of the flow field in the classification channel .....	65
Figure 4. 3 The illustration of the electrical potential contours.....	66
Figure 4. 4 The variation of the non-diffusive transfer function of tilted cylindrical DMCs .....	66
Figure 4. 5 The position of particles in the neighborhood of classified particle exit slit..	68
Figure 4. 6 The effect of the electrical field vs. the combined effects of flow and electrical field .....	69
Figure 4. 7 Tilted DMC transfer function at different flow rate ratios and total flow rates .....	70

Figure 4. 8 The effect of DMC geometrical parameters on the transfer function of DMCs .....	72
Figure 4. 9 Comparison of non-diffusive and diffusive transfer functions for the 10% rod-tilted DMC. ....	73
Figure 4. 10 The rods tilted DMCs transfer functions peaks regions .....	74
Figure 5. 1 The schematic diagram of the computational domain for the plates DMC modeling .....	79
Figure 5. 2 Comparison of numerical results with the measured data given in the work of Liu .....	84
Figure 5. 3 DMC transfer functions at various channel aspect ratios, CARs .....	87
Figure 5. 4 The central voltage correction factor as a function of channel aspect ratio ...	88
Figure 5. 5 The transfer functions of studied DMCs with different slit opening percentages.....	89
Figure 5. 6 The comparison of numerical FWHMs with FWHMs calculated via the 2-D model.....	90
Figure 5. 7 The effect of varying the exit slit size .....	92
Figure 5. 8 The effect of channel cross-section areas (a) and aerosol injection angles (b) .....	93
Figure 6. 1 The schematic diagram of the plates tiled DMC .....	99
Figure 6. 2 The flow in the cross-section of the plate tilted DMC classification channel .....	102
Figure 6. 3 The electrical field inside the cross-section of the plate tilted DMC classification channel .....	103
Figure 6. 4 The transfer function at relative tilting percentages .....	104
Figure 6. 5 Comparison between the combined effect and separate effect of flow and electrical field.....	105
Figure 6. 6 The transfer function with channel aspect ratio for the plates tilted DMC ..	107
Figure 6. 7 The DMC transfer function for various particle residence time.....	108
Figure 6. 8 The flow effect on the plate tilted DMC transfer function.....	109
Figure 6. 9 The DMC transfer function with different slits openings .....	110
Figure 6. 10 Compare between the diffusive and non-diffusive DMC transfer function	111
Figure 6. 11 Tilting type effect on the DMC transfer function.....	113

# Abstract

## DIFFERENTIAL MOBILITY CLASSIFIERS IN THE NON-IDEAL ASSEMBLY

By Thamir Alsharifi, M.Sc.

A dissertation submitted in partial fulfillment of the requirements for the degree of Doctor of Philosophy at Virginia Commonwealth University.

Virginia Commonwealth University, 2019

Major Director: Dr. Da-Ren Chen  
Professor and Floyd D. Gottwald, Sr. Chair in Mechanical and Nuclear Engineering

The differential mobility classifier (DMC) is one of the core components in electrical mobility particle sizers for sizing sub-micrometer particles, which have wide medical, industrial, technological and environmental applications. Designing the DMC requires knowledge of the geometrical and constructional imperfection (or tolerance). For example, disassembling and assembling DMC parts for maintenance and routine cleaning can result in misalignment and tolerance issues, which requires continuous recalibration. Studying the effects of geometrical imperfection on the performance of the DMC is necessary to provide

manufacturing tolerance, and helps to predict the performance of geometrically imperfect classifiers, as well as providing a calibration curve for the DMC.

The overall objectives of this dissertation are: to investigate the geometrical imperfections of the DMC performance; to perform a parametric study on imperfect DMC performance; and to provide general guidance about DMC tolerance. Consequently, the objectives of the thesis have been accomplished via two major parts: 1) studying the cylindrical classifier, and 2) studying the parallel plate classifier. The numerical model was built using the most recent versions of COMSOL Multiphysics® and MATLAB®.

For the cylindrical DMC, (i.e., constructed by axial aligning of the inner and outer cylinders), two major geometrical imperfections (tolerances) were studied: the eccentric annular classifying channel, and the tilted inner cylinder/rod. A parametric study was conducted for several tolerances under various geometrical factors (i.e., cylinders radii and length magnitudes, cylinders radii ratio, ratio of length to spacing between cylinders, etc...). For the parallel-plates DMC, the first study examined for the perfectly designed plates to optimize its dimensions and working conditions, while the second study conducted the plates' parallelism as a major geometrical imperfection. Three possible misalignments were studied: plate side tilting in stream spanwise, plates point tilting in both forward and backward directions around the diagonal of the classifying channel. A parametric study examined several tolerance limits under various geometrical factors (i.e., channel cross-section size and aspect ratio, channel length, aerosols slits opening, spacing between plates, etc). For both DMCs, the flow conditions (i.e., sheath-to-aerosol flow ratio, total flow rate), and several particles sizes were studied.

The results of the cylindrical DMC show that transfer function deteriorated as the axial eccentricity or inner rod tilt was increased (i.e., the peak is reduced and the width at the half peak height is broadened). The high axial eccentricity caused the transfer function peak to split into two. On the other hand, the parallel plate DMC results show that the aspect ratio of the classifying channel cross-section (width-to-height) was recommended to be above 8. For the plates tilted DMCs, the transfer function was disrupted. For both types of DMCs, particle diffusivity reduce the effect of geometrical imperfection on DMC transfer function, especially for particles with sizes less than 10 nm.

# CHAPTER 1 Introduction and Overview

## 1.1 Background

The aerosol's submicrometer (nanometer nm) particles are defined as any solid shape objects or liquid droplets (spray) immersed in gas, often air, with effective diameter sizes between 1-1000 nm. They are diverse in size, surface area, mass, number concentrations, physical properties, chemical composition, and particle's source (Liu, 2015).

The airborne ultra-fine (<100 nm) and nano-particles are present in nature and mostly generated by human activity. Naturally, existing nanoparticles are some viruses, atmospheric particles, sea salt nuclei, organic matter, etc. The human-generated nanoparticles are varied from welding fumes, combustion nuclei products, tobacco smoke, metallurgical dust and fumes, photochemical smog, oil smoke, etc. These human- synthetic nanoparticles get a great deal of attention as they have wide applications in medicine and most of the new fields in science and technology (Zhang et al., 2007; Sergeev & Klabunde, 2013). [Figure 1.1](#) illustrates examples of existing particles and their size range in micrometer  $\mu\text{m}$  ( $1\mu\text{m} = 10^3$  nm).

Car traffic is the most serious source of ultra-fine particles in urban air. Its potential hazards on human health and environmental aspects are the main importance of the nanoparticles' study (Geiser et al., 2005; Hattori et al., 2017; Oberdörster et al., 2005; Oberdörster et al., 2004; Oliveira et al., 2017; Zhu et al., 2002).

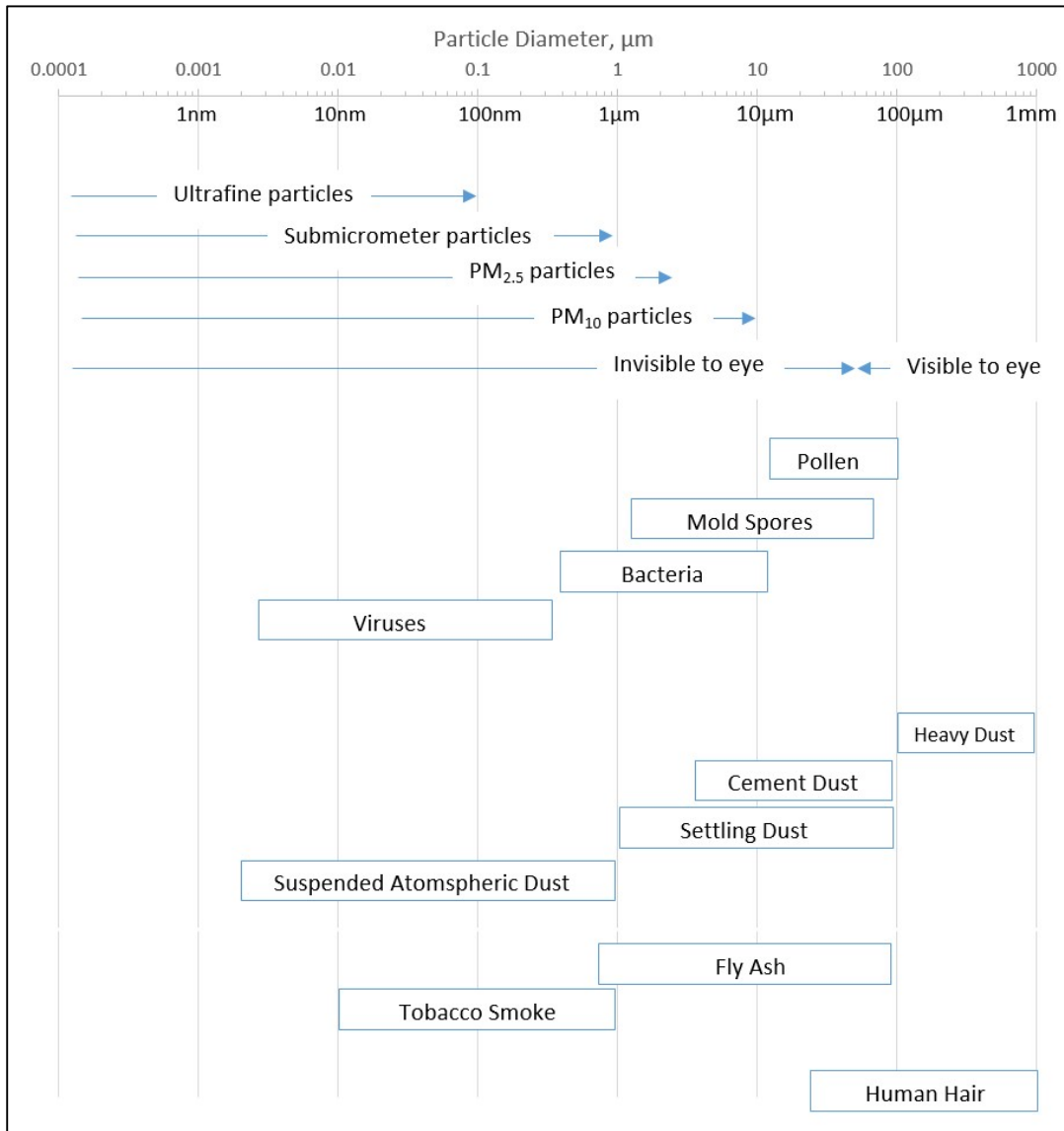


Figure 1. 1 Particle size range. The chart's data collected mainly from Hinds (2011), and from Wikipedia.com ( <https://en.wikipedia.org/wiki/Particulates>).



The particulate air pollution (i.e. the environmental airborne solid particles and liquid droplets) are measured via the two particulate matter PM standards<sup>1</sup>: 1) the PM<sub>10</sub> is used for inhalable particles, with aerodynamic diameters of 10 µm and smaller, and 2) the PM<sub>2.5</sub> is used for fine inhalable particles with aerodynamic diameters of 2.5 µm and smaller. This includes all small particle sizes (less than 10 or 2.5 µm up to 1 nm) that make up a large proportion of the inhaled particles. These small size particles tend to be deposited deep into the lungs as larger particles are trapped at the beginning of the respiratory tract in the nose, mouth or throat (Dahl & Mygind, 1998; Grassin-Delyle et al., 2012). Those small particles can penetrate through human cells, are carried through the blood vessels, and accumulate inside vital organs and cause health consequences. However, this mechanism can also be used for targeted drug delivery and for tumor cell imaging by fluorescence or magnetic resonance (Azarmi, Roa, & Löbenberg, 2008; Choi et al., 2010; Montet, Montet-Abou, Reynolds, Weissleder, & Josephson, 2006).

Particle toxicity depends on the chemical properties, which can vary depending on the size of the particles. Toxicological studies conducted on some metal oxides concluded a rise in particle toxicity for ultrafine particles compared to microscale particles for the same chemical composition (Karlsson et al., 2009).

On the other hand, nanoparticle size matters in determining material physical properties. For example, the melting temperature of gold particles rapidly declines as the size decreases. Large gold particles appear yellow, while the 10 nm particles are red because

---

<sup>1</sup> Information about PM<sub>2.5</sub> and PM<sub>10</sub> standards is listed on USEPA website <https://www.epa.gov/pm-pollution>

they absorb the green light. The gold nanoparticles at 2–3 nm are considerably magnetic and metallic while smaller sized particles tend to be good insulators (Roduner, 2006).

The wide existence of nanoparticles brings the need for classifying and controlling these nanoparticles. The most decisive parameter to characterize the nanoparticles is their size (represented by their effective diameter). There are various techniques and devices for detecting and classifying aerosols nanoparticles by size. These techniques are either offline or online. The offline, which is also referred as a “manual” measurement, is performed on samples, and the results may differ from sample to the other and based on the experience of the operator. Examples include microscopic techniques like: Transmission Electron Microscopy (TEM), Scanning Electron Microscopy (SEM), and Atomic Force Microscopy (AFM). Conversely, the online measuring technique is constantly monitoring and referred to as “automatic,” which is not highly dependent on the experience of the operator, making it a very productive method. Examples of the devices that work with the online technique are: Photon Correlation Spectroscopy (PCS), Dynamic light scattering (DLS), Nanoparticle Surface Area Monitor (NSAM), Scanning Mobility Particle Sizer (SMPS), etc.

There are three methods for submicrometer particle size classification: inertial, optical, and electrical. The inertial method depends on particle shape, density, and size, and it is efficient for the particle size range of 0.1 to 100  $\mu\text{m}$ . Devices that follow the inertial method are the cyclone and the impactor. The optical method measures the particle diameter by light scattering detectors. It depends on the particle refractive index (chemical composition), shape, and size. The measured size range via the optical method is 0.01 to 10  $\mu\text{m}$  on the devices like photometers, laser system, etc. The electrical method measures the

particle electrical mobility by charging the particles and differentiating them with an electrical field. This technique depends on particle size and less on the shape. This method is determined by the rate of migration of charged particles in an electrostatic field. The efficiently measured size range of the electrical method is 0.001 to 1  $\mu\text{m}$  on the system like the Scanning Mobility Particle Sizer (SMPS), which is utilized by the differential mobility classifier DMC on its stages.

No one technique is rated as the best. Each method depends on many factors like the size range, chemical composition, reactivity or stability, etc. However, the electrical technique with the SMPS, which utilizes electrical methods in categorizing nanoparticles, is the most straightforward, cost-effective, and chemical composition independent method for classifying aerosols' nanoparticles. Through the SMPS system, particles are charged in the aerosols charger, which changes their electrohydrodynamic properties. Then these charged particles are passed through to the differential mobility classifier (DMC) at which point the electrical field is characterizing the charged particle based on their electrical mobility. Then the selected particle size is grown by the use of liquids and be counted in the condensation particle counter (CPC). Note that the CPC is also labeled as a condensation nucleation counter (CNC) in the early literature (Knutson, 1972). [Figure 1.2](#) shows these three stages of particle characterization via the electrical technique.

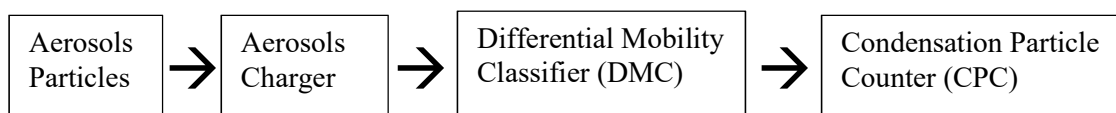


Figure 1. 2 The schematic diagram of the SMPS system

The working accuracy of the SMPS system is highly depending on the DMC performance, which is the basis of particle size selection. DMC provides online data for size distribution, while particle concentration can be retrieved simultaneously from the CPC. Combining the data for DMC and CPC gives the particle size distribution. The CPC can be substituted for an electrometer, which measures the electrical current and converts the signal to particle size. If the DMC works in voltage scanning mode, it detects particle size distribution. It is also used for particle characterization/classification if it works in the fixed voltage mode.

## **1.2 The Dissertation Motivation**

Particles in the nanoscale level are extremely important in various industrial, technological, therapeutic, and environmental applications (Liu, 2015). The ultrafine particles (particle below 100 nm in diameter) are mainly generated from motor vehicle emissions. These ultrafine airborne particles are very small and lightweight; therefore, they tend to stay longer in the air than larger (heavier) particles. This increases the chances of inhaling these tiny particles into the human body. Owing to their tiny size, these particles are able to bypass the nose and throat and be deposited deeper into the lung. These particles may penetrate the lungs tissues and reach to other vital organs via the circulatory system. Several studies found a close connection between exposure to pollutant particles via inhaling and early death rate, caused by cancer, heart and respiratory problems; as well as other chronic diseases like asthma, bronchitis, and cardiovascular disease as well as cognitive problems (Donaldson et al., 2002; Herbarth et al., 2001; Lee, Kim, & Lee, 2014; Liao et al., 2011; Ranft et al, 2009; von Klot et al., 2002). Therefore, monitoring the ultrafine particle

pollutant is essential for human health. On the other hand, the nanoparticle's high surface-to-volume ratio plays an important role in medicine (i.e. drug delivery, imaging agents, and penetrating some body parts) (Lin & Scott, 2012). These therapeutic applications for nanoparticles require a monodisperse particle size to improve the efficacy of the medical process. This physical property for the nanoparticles enables them to be quick and efficiently reactive with their containing solvent, which makes them advantageous to use in many chemical and industrial applications.

The Scanning Mobility Particle Sizer (SMPS) system is the most capable and efficient instrument to detect and characterize the ultrafine particle size range (B. T. Chen et al., 2016). Since the particle size is the most essential property in determining the toxicity of the nanoparticles, the performance of the SMPS is highly dependent on the particle classification stage at the DMC. Therefore, DMC design perfection is crucial in boosting the SMPS performance. Building the DMC requires providing tolerance on all key dimensions of the DMC when the blueprint technical drawing is produced for manufacturers. The tolerance requirement in the DMC design also affects how the DMC is constructed. Therefore, it is very important to understand the design/construction imperfection effects on the performance of a DMC.

Differential mobility classifiers in various configurations have been designed and evaluated in the literature. All previous research assumed the classifier dimensions were perfect. However, machining precision limits the tolerance when constructing the classifiers. The DMC needs periodic cleaning and maintenance, which is usually done by disassembling

the components. Reassembling the classifier parts can also cause minute variation in the dimensions. Thus, geometrical imperfection is always possible. However, it has not been studied before. Consequently, this research is focused on the geometrical imperfection of the DMCs.

The application of this research provides a comprehensive understanding of the geometrical imperfection effects and tolerance limitations when designing the DMCs. Also, the knowledge gained from this work can be utilized to design the new DMC, set tolerance limits, and can be an alternate method to calibrate the classifier prior to performing the experiment.

### **1.3 Overall Objective**

The main objectives of this work are: to investigate the effect of geometrical imperfections on the performance of DMC; to perform a parametric study on the imperfect DMC performance; and to provide general guidance to the DMC tolerance.

DMCs are the typical instruments that are used to classify the size distribution for the submicron particles based on their electrical mobility ( $Z_p$ ). The electrical mobility of a particle is defined as the velocity  $\vec{U}$  of the charged particle in response to the applied electrical field strength  $\vec{E}$  (Kulkarni et al, 2011; AMS, 2012). A typical DMC contains two electrodes between which the charged submicrometer particles are sheathed by clean air and flow through the device. A narrow range of mobilities can be classified to pass through aerosol's slit at the oppositely charged electrode.

This work is focused on evaluating the performance of the DMCs under all possible geometrical imperfections. This requires examining these DMCs with all sorts of geometrical tolerance limits, which will be a significant challenge experimentally due to the difficulty of building an accurate DMC with zero tolerance for all examined cases. Therefore, numerical modeling was the best tool for solving and analyzing this problem, and it is also more convenient to use than the experimental approach. The numerical capabilities to precisely solve the flow field, electrical field, and particle path inside the DMC are powerful and useful for imperfect geometry DMCs, which can be challenging to investigate experimentally. Also, establishing the design guidelines calls for error-independent results cases to perform the comparison between those cases; the numerical approach was the best fit for those needs. Our modeling was set via the combination of COMSOL Multiphysics® and MATLAB®.

For this work, our primary goal was to model both the cylindrical and parallel-plate DMCs with the perfect configuration to validate the performance of the perfect-geometry DMCs with the available experimental and theoretical DMC data from the literature. This established the foundation to model the imperfect-geometry DMCs to achieve our three main objectives: 1) to examine all the possible DMCs with geometrical imperfection, 2) to parametrically study the imperfect DMC performance, and 3) to establish design criteria for the DMCs.

We planned to model both the cylindrical and parallel-plate DMCs with all possible geometrical imperfections under different flow rates, particle sizes, geometrical parameters, and dimensional conditions. In this part, it was assumed the dimension and the geometry is

imperfect with different tolerance values. We isolated geometrical flaws and studied them separately for all possible cases. Wide ranges of flow and particle size were considered in order to investigate the limitation for each tolerance or flaw and examine how critical these flaws could be in affecting the performance of the DMC. Investigating the tolerance limitation helped to set the tolerance limit when the DMC was manufactured indicated whether or not the DMC had certain manufacturing flaws or alignment issues associated with regular maintenance and cleaning procedures throughout the calibration process. Pursuing this goal will enable manufacturers to design a DMC with the best possible performance.

Our goals started with analyzing and optimizing the available DMC designs, then developing a set of simple design guidelines for the most favorable DMC dimensional size and working conditions, as well as the best configurational aerosol's flow intake directions. Several independently repeated cases were performed to establish a stable design foundation. A wide range of flow and particle size were included in this part of the study to investigate the optimum design working conditions.

Despite the fact that the essential design concept of the DMC remains constant, the DMC geometrical design is varied from the cylindrical to the plate and disks configuration (Alsharifi & Chen, 2018; Flagan, 1998; Steer et al., 2014). Since the cylindrical design is available and widely commercialized in real-world applications, it was more beneficial to start studying its design details in all types of DMCs. The plate-design was the second to be investigated because it has received much attention recently and was proposed several times for portable measurement applications.



## 1.4 Dissertation Structure

To address the major objectives, the dissertation is constructed in **seven chapters** via the following structure: Part 1 focuses on the cylindrical differential mobility classifier, which is covered in chapters 3 and 4. Part 2 focuses on the parallel plate differential mobility classifier, which is covered in chapters 5 and 6.

Chapter 1 gives a general introduction, including an overview and background about aerosol's measuring techniques, and outlines the motivation and overall objectives for this study.

Chapter 2 reviews in depth all configurations of the differential mobility classifiers.

Chapter 3 deals with the eccentricity of the inner rod of the cylindrical DMC; establishes the numerical model; verifies the model with existing theoretical and experimental work from the literature for perfect and eccentric classifiers; and performs a parametric study for different geometries and flow conditions.

Chapter 4 handles the inner cylinder tilting of the cylindrical DMC to establish the numerical model and performs a study for different geometries and flow conditions.

Chapter 5 introduces the parallel plate DMC, establishes the numerical model for perfect parallel plates DMCs, and performs a parametric study for several conditions.

Chapter 6 studies in detail the plate's alignment for the parallel plate DMC.

Chapter 7 summarizes the conclusions and the outcomes of this dissertation study, as well as explores the challenges and recommendations for future research.

## **CHAPTER 2 Review of the Differential Mobility Classifier**

### **2.1 Review of the Differential Mobility Classifier (DMC)**

The differential mobility classifier (DMC) is a vital part of the electrical mobility particle sizer (SMPS) systems, which can work in variable (scanning) voltage or fixed voltage modes. The DMC measures particle size distribution and concentration. The DMC measures a selective size range of charged nanoparticles between 2 nm and 1  $\mu\text{m}$  in diameter and gives an online actual aerosol particle size distribution; then its data is integrated with those from the CPC to give the particle number concentration (Reischl, 1991; TSI INCORPORATED, 2018). The DMC is the current standard to measure submicrometer particles' size distributions because it is the most practical device to characterize submicron particles below 100nm (Kinney, et al., 1991; Kozlowski & Ferna, 2013; Liu & Pui, 1974).

The typical DMC consists of a classifying channel through which an electrical potential is applied through two electrodes on opposite sides, utilized to produce a steady direct current (DC) of an electrical field. The DMC's classifying zone has two inlets for polydisperse aerosol stream and clean sheath air stream, and two outlets for classified aerosol stream and excess flow. The electrical field will lead particles of a specific charge to shift to other sides of the DMC channel and exit through the monodisperse/classified aerosol exit slits (Intra & Tippayawong, 2008; Liu, 2015). Charged polydisperse aerosols are introduced

to the clean air flows from one electrode inside the channel. Both aerosol and sheath flow to the other side. The aerosol-free (or clean) airflow is used to carry and sheath the charged aerosol particles away from the other electrode. Due to the electrical field, charged aerosol particles gradually drift toward the other electrode as they propagate inside the channel. At the end of the classifying zone, particles of a certain charge number (electrical mobility) will reach the opposite electrode and exit from the aerosols' assembly as monodisperse size, while the remaining excess flow will continue to flow in the channel. Simultaneously, those particles with higher electrical mobility (with low charge numbers) will be deposited at the electrode on different locations prior the aerosols' exit, and particles of low mobility will exit from the excess main flow.

The particle electrical mobility is the response velocity as the charged particle is pulled by the electric field. The velocity of the particle will be directly proportional to both the number of ions (charges) that it carries and the electrical field strength, i.e. a particle with higher mobility can move faster in response to the electrical field, whereas the stronger the electrical field, the faster the particle response will be.

To understand particle electrical mobility, we should analyze the charged particle motion inside the electrical field, which is governed by the dragging and pulling forces. The drag force is directly caused by the particle flowing and colliding with the carrying medium molecules, which in this case are the air molecules. From Stoke's law, the drag force  $F_d$  is given for a spherical particle as

$$F_d = \frac{3\pi\mu d_p(u-v)}{C_c} \dots (2.1)$$

Where  $\mu$ : is the carrying fluid viscosity;  $d_p$ : particle diameter;  $u$ : particle velocity;  $v$ : flow velocity;  $C_c$ : is the Cunningham slip correction coefficient and is given through the empirical equation (Allen & Raabe, 1982; Allen & Raabe, 1985).

$$C_c = 1 + Kn \left( 1.155 + 0.471 e^{-\frac{0.596}{Kn}} \right) \dots (2.2)$$

Where  $Kn$ : is the Knudsen number and is given by the ratio of  $\frac{2\lambda}{d_p}$ ;  $\lambda$ : is air mean free bath and given by 0.066[um].

On the other hand, the pulling force is the electrical attraction between the charged particles (ions) and the electrode. It is axiomatic that the pulling or electrical force will be proportional to the electrical field strength and the amount of charge carried by the particles. As this pulling increases, the velocity of the particle will be increased, which leads to an increase in the particle collision with air molecules, which elevates the drag force. The electrical force  $F_e$  is given by the equation

$$F_e = neE \dots (2.3)$$

Where  $n$ : is the number of charge/ions that particle carries;  $e$ : the elementary charge and given as  $1.602 \times 10^{-19}$  C (Hinds, 1999).

Since particle mobility  $Z_p$  is defined as the ratio of particle relative velocity to the electrical field as  $Z_p = (u - v)/E$  and from both eq. (1) and eq. (3), particle mobility can drive as

$$Z_p = \frac{neC_c}{3\pi\mu d_p} \dots (2.4)$$

The DMC works on the physical principle of flowing charged particles on an electrical field. This allows us to differentiate particles based on their electrical mobility which is

highly related to particle size based on the electrohydrodynamic properties of these charged/ionized particles. The working principle of the DMC is balancing the forces that act on the particles that pass through its classifying zone. There are three main kinds of forces that act on the particles that flow inside the DMC. The first one is the drag force that acts on the particle due to friction between the particle and air molecules. This force highly depends on the temperature and the relative velocity between the particles and air. The second force is the electrical force which is acting on the charged particle only due to the electrical field. This force depends on the number of charges carried on the particle and the electrical field strength. Thus, the larger the particle size, the larger the number of charges particle can carry. The third force is the Brownian diffusion force, which is highly dependent on particle size, i.e. small particles tend to have a higher diffusive force. The diffusion force increases by raising the temperature. In this study, it is assumed that there is no variation in the temperature.

The performance of DMCs is characterized by their transfer function, which is defined as the probability of particles, with certain electrical mobility, to pass through the classification zone of a DMC (Knutson & Whitby, 1975). The theoretical non-diffusive transfer function of all three DMC designs, the cylindrical, the parallel-plate, and the disk, is triangular-shaped (Knutson & Whitby, 1975; Liu & Chen, 2016a; S. Zhang et al., 1995).

## 2.2 An Overview of the DMC Configurations

Several DMC design configurations that serve the same purpose of sorting and classifying sub-micrometer particles within a narrow size range window. The common DMC types are the cylindrical and the parallel-plates. Less common types of DMCs are the disks (or radial)<sup>2</sup>, and the circular design<sup>3</sup>.

### 2.2.1 Cylindrical DMC<sup>4, 5</sup>

The cylindrical DMC is the most popular type among all the DMC design configurations. It had an accumulated research experience which made it the predominant type to commercialize (Müschorn, 2007). Typically, it consists of two concentric cylinders, between them a hollow spacing which forms the classifying channel. The outer cylinder is electrically grounded and the inner is the electrode. The sheath air is flowing between these cylinders while applying the electrical field. Charged polydisperse aerosols enter through a circular slit that grooved on the outer cylinder and classified-size aerosols exit to a circular slit at the inner cylinder.

Early cylindrical DMC design starts at the end of the 19<sup>th</sup> century through scientists' efforts to investigate the atmospheric electricity and the conductivity produced by lightning. McClelland was the first researcher to utilize the coaxial cylinder to measure the ion electrical conductivity for hot gases emitted from the flame (McClelland, 1898). Later at the

---

<sup>2</sup> The radial DMC design was not commercialized yet and mostly researched by a few research groups (Brunelli, Flagan, & Giapis, 2009; S. Zhang et al., 1995).

<sup>3</sup> The circular DMC design is patent recently by Chen and Liu (2019).

<sup>4</sup> Some material in this section is taken from a publication-Alsharifi, T., & Chen, D.-R (2019), "Effect of axial eccentricity on the performance of a cylindrical differential mobility classifier," *Aerosol Science and Technology*, 53:7, 735-748: <https://doi.org/10.1080/02786826.2019.1599097>.

<sup>5</sup> Extended details about the DMCs, or DMAs, history of developments are illustrated in Flagan (1998).

University of Minnesota, John Zeleny utilized a hollow cylinder configuration to analyze the ion migration (Zeleny, 1900).

As the science of ion measurement was progressing, it was appropriate to employ this field to analyze aerosol particles. Submicrometer aerosol particles have a very wide range of sizes and can be characterized through several techniques. Large particles can be sieved, and if the particle is dense, it can be gravitationally classified. Small and ultrafine (those below 100 nm in size) particles are characterized efficiently via the electrical method. Particles need to be charged first then analyzed via the same technique as atmospheric ions.

A breakthrough in the ultrafine particles characterization happened at the University of Minnesota through the invention of a complete system consisting of a particle charger, cylindrical classifier, and condensation measurement. The classifier had a coaxial design and was successfully capable of sorting particles with a small mobility window (Hewitt, 1957). This design is the basis for all modern cylindrical differential mobility classifiers.

Whitby & Clark followed the same steps to design a complete system consisting of a particle charger, coaxial aerosols channel, and particle counter shown in [Figure 2.1](#). This instrument collects particles in a filter at the very end of the classifier channel. They detect particle concentration and size distribution for the size range from 0.015 to 1.2  $\mu\text{m}$  (Whitby & Clark, 1966).

Liu and Pui at the University of Minnesota were able to expand Hewitt's work further and sort a wide size range of particles at which they extract the classified mono-disperse aerosols out of the classifier instead of collecting it (Liu & Pui, 1974). They were the first to term the classifier as a "differential mobility analyzer" (Flagan, 1998).

Later, Knutson and Whitby were the first to outline the cylindrical classifier theory (Knutson & Whitby, 1975). The analyzer was a spacing between two concentric cylinders, and this channel had two inlets and two outlets as shown in Figure 2.2. The sheath flow is flowing from the top of the channel while aerosol is smoothly entering from the aerosols inlet slit on the outer cylinder. The inner cylinder is an electrode and the outer cylinder is grounded, and that leads charged aerosol particles to flow toward the inner cylinder and deposit there due to the electrical field. Particles with a specific mobility (size) range lay on the carved exit slit on the inner cylinder and are withdrawn out of the classifier through classified aerosol exit flow at the center of the inner cylinder. The remaining sheath and aerosol stream will flow to the end of the channel and exit from the main air outlet.

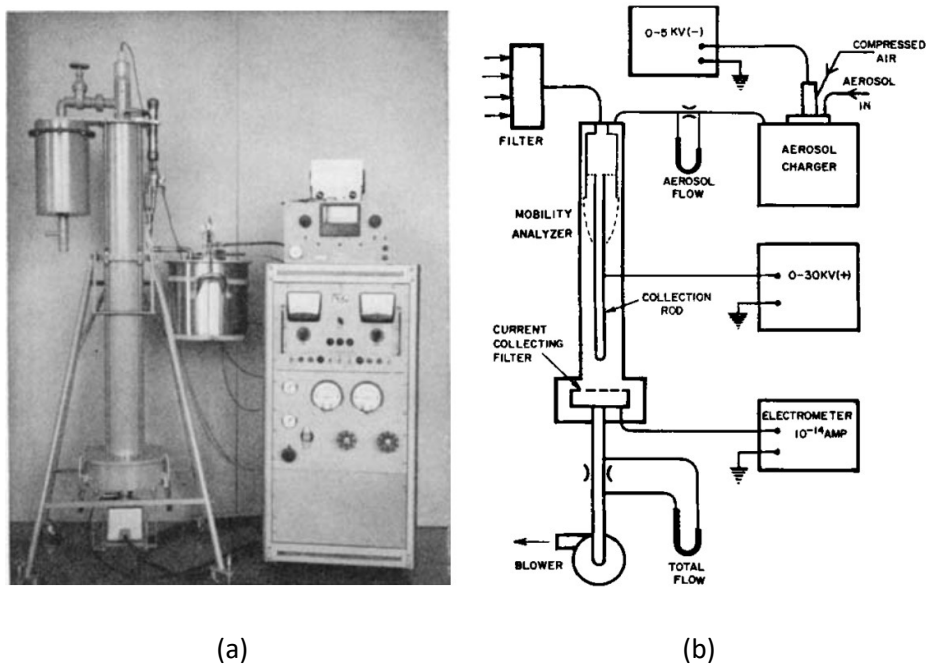


Figure 2. 1 Whitby electrical counter system : (a) the mobility analyzer, aerosols charger and both flow and electric equipment (b) schematic diagram of the system (Whitby & Clark, 1966).



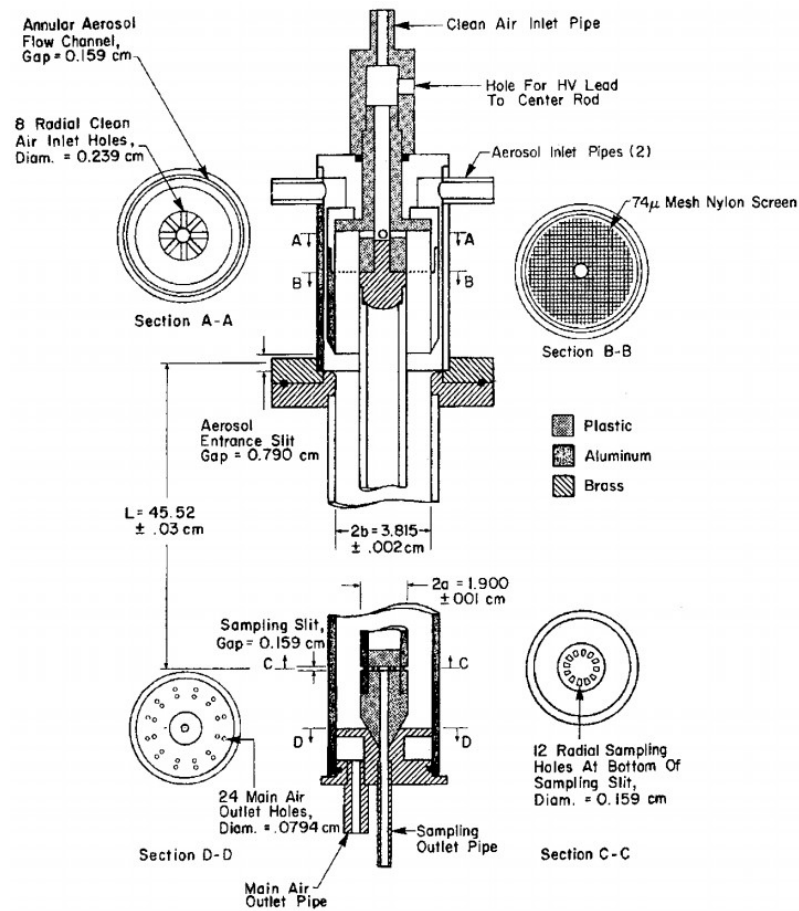


Figure 2. 2 Differential mobility analyzer designed by Knutson and Whitby (1975).

Knutson describes the performance of the classifier in terms of particle transfer function  $\Omega$ ; which he defines as the probability that a particle entering the classifier through the aerosol's inlet will leave with the aerosol classified flow. This effort led to commercialize the classifiers and the first generation was TSI Model 3071, which became the standard classifier. Aganval was the first to standardize the tandem technique to calibrate the classifier, and that was done by repassing a classified particle to a second classifier (Aganval et al., 1978). Based on Knutson's transfer function, a model for the tandem system was developed by Kousaka (Kousaka et al., 1985). This model does not match with the

experiment due to diffusion bordering effects, which shift researcher attention to investigate the particle's diffusion inside classifiers (Kousaka et al., 1986; Stolzenburg, 1988). The last researcher, Stolzenburg, had provided a complete theoretical model for the diffusive transfer function. Later, Llompart used the convective-diffusive flow equation to provide an approximate solution and explain the particle diffusivity in the classifier channel (Rosell-Llompart et al., 1996). The limitation of the DMC to deal with particle diffusion losses inside the classifier channel as it travels inside leads to a preference for the shorter classifying channel DMCs to measure ultrafine particles.

Considering the length of the DMC classifying channel, we can go back and observe the early development of the cylindrical DMCs that were designed by Particle Technology Laboratory at the University of Minnesota by Hewitt and later developed by Knutson (Intra & Tippayawong, 2008; Knutson & Whitby, 1975; Whitby & Clark, 1966). Knutson's design was a long hollow spacing in a 45.52 cm length channel and targeted a wide particle size range of 5 to 1000 nm. However, due to diffusion effects, such a longer channel DMC would not be efficient in detecting small particle size without high flow conditions to overcome particle diffusion toward the walls. That led to the development of a shorter cylindrical classifier (11 cm) at the University of Vienna to address the narrower particle size range of 1 to 40nm (Winklmayr et al., 1991). This design utilized a higher flow rate of 28 lpm and 5 lpm for the aerosols and sheath flow respectively. Later, a shorter (5 cm) cylindrical DMC was developed by Chen which is known as a "nano-classifier" (D. R. Chen et al., 1998a). This short DMC specialized in detecting a smaller size range 3-50 nm with a reasonable sheath flow of 16.5 lpm and aerosols flow of 1.5 lpm. The shortest classifier was 1.8cm and

achieved by Seto at which the classifier works under a low-pressure range of 60-760 Torr (Seto et al., 1997). The DMC was able to measure particle size 4-10nm. Another approach to reduce the losses of small particle sizes on the DMC channel is by adjusting the length for different particle size measurements. Seol's design was an adjustable column length classifier with a size range of 1 to a few hundred nanometers (Seol, Yabumoto, & Takeuchi, 2002). Although working with low pressure is not as easy as atmospheric pressure, in which most of the designs are based in that era, the complexity of the moving part was another drawback of the low-pressure design which required an extra cost and contained parts that were more susceptible to breaking down or misaligning. Also, the device needs to be calibrated after each adjustment.

In general, the design of the cylindrical DMC had utilized sliding rings on the inner cylinder to minimize the shifting or the tilting of the inner cylinder which affects the performance of the device (Knutson & Whitby, 1975; Seol et al., 2002). Even though these rings will reduce the eccentricity by constraining the inner electrode, it is also susceptible for further eccentricity or relocation after reassembling the DMC when doing the regular cleaning.

In all DMC designs, the sheath flow prior to entering the classifying channel has a Dacron screen (filter) in order to make the flow uniform. That means the flow and the velocity profile will continue to develop all over the DMC channel. All the research and analysis assumes the DMC is following the typical design of concentric cylinders, however, the alignment of these two cylinders could be a challenge due to the limitation of manufacturing tolerance which leads to two eccentric cylinder cases. Having an eccentric

DMC channel will impact the flow (velocity development) and electrical field required, which will affect the particle path and the performance of the DMC. Any small relative eccentricity between the DMC cylinder's center will double the transfer function widening (Rosser & de la Mora, 2005).

Until this point in the cylindrical DMC's development, all the designs had an axial aerosols flow from the top part, on the head of the classifier. Winklmayr at the University of Vienna changed the common stereotype of entering the flows axially and introduced both (aerosol and sheath) flows tangentially as shown in [Figure 2.3](#) below (Winklmayr et al, 1991). No research efforts had focused on comparing the two designs and their capability on the particle classification system.

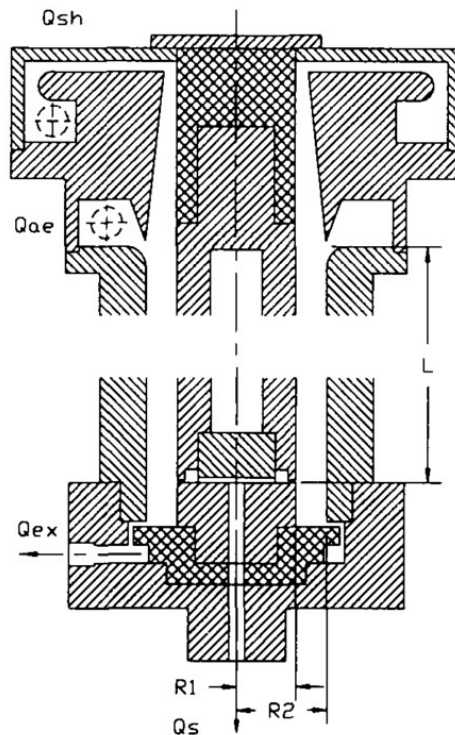


Figure 2. 3 A cross-section of Vienna classifier(Winklmayr et al, 1991).

From all the reviewed literature, it is obvious that the geometrical imperfection like the eccentricity or tilting of the inner cylinder has not been investigated thoroughly in a detailed study to understand and improve the performance of the classifier. Due to the difficulty of examining imperfect classifiers experimentally, the numerical approach will be utilized in the study. From using the cylindrical DMC in our lab, we recognized that the cylindrical classifier tends to have problems with the central rod clearance (i.e eccentricity of the centers ), and the tilting of the central rod. All these flaws can create a malfunction and deter the achievement of the best performance of the cylindrical DMC. Figure 2.4 illustrates the computational domain of the perfect cylindrical DMC, which will be the reference to all modeling studies that we are going to perform.

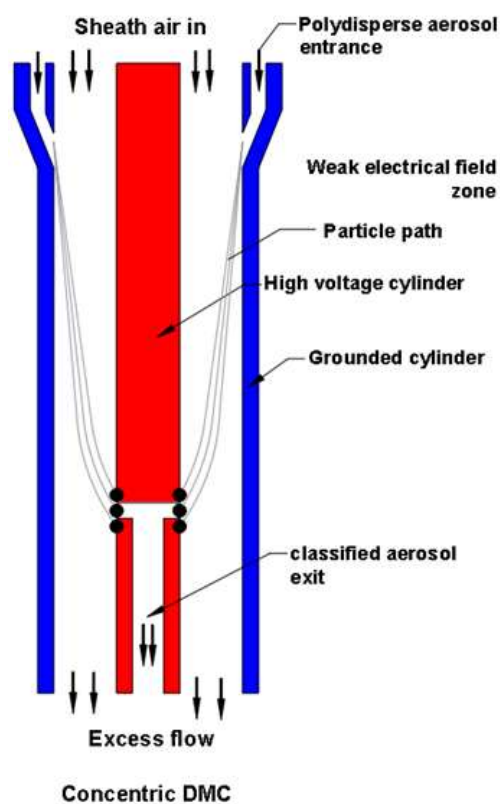


Figure 2. 4 The perfect concentric DMC

### 2.2.2 Parallel plate DMC

The simplest DMC configuration is the **parallel plates design** DMC. It has two parallel-plates (electrodes) at which the polydisperse aerosols enter from the top plate and exit from the exit slit at the bottom, as shown in [Figure 2.5](#).

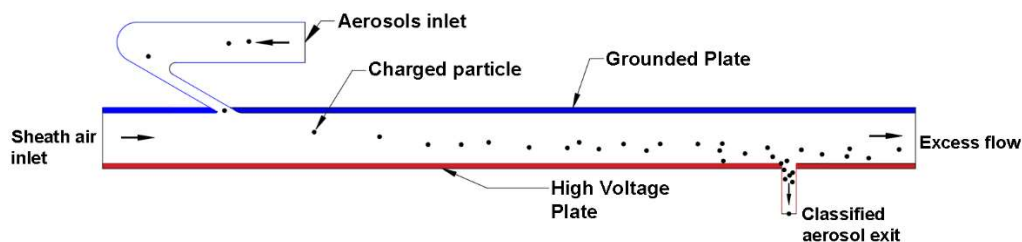


Figure 2. 5 Perfect parallel plate DMC

The simplicity of the plates design made it the earliest to be utilized as a parallel screen in the duct configuration to measure the atmospheric charged particles (Zeleny, 1898). Later on, the first developed DMC was the parallel-plate configuration (Erikson, 1921). The focus of DMC design later changed to the cylindrical configuration because of the undesired side-wall effect encountered in parallel-plate DMCs (Hewitt, 1957; Knutson & Whitby, 1975). The development of parallel-plate DMCs has not made significant progress since the commercialization of the cylindrical DMC, originally designed by Particle Technology Laboratory, at the University of Minnesota (Intra & Tippayawong, 2008; Whitby & Clark, 1966). The cylindrical DMC thus has become the standard instrument for sizing or classifying particles in the submicrometer and nanometer size range. Parallel-plate DMCs have recently gained the attention of aerosol scientists in the characterization of ions, macromolecules, or single-digit nanoparticles by coupling them with atmospheric pressure

ionization(API)-mass spectrometers (MS), or molecular analyzers (de la Mora, Ude, & Thomson, 2006). This is because of the uniform electric field in the particle-classification channel of a parallel-plate DMC and its low manufacturing cost compared with cylindrical DMCs. The uniform electric field in the classification zone is believed to result in less broadening on the DMC transfer function due to the particle diffusion (Alonso & Endo, 2001). The performance of a high-resolution parallel-plate DMC has been investigated both experimentally and theoretically (Santos et al., 2009). A different parallel-plate DMC has also been applied to measure air ions produced by corona discharge and  $^{241}\text{Am}$  radiation sources (Alonso et al., 2009). When coupled with commercial atmospheric pressure ionization mass spectrometers (API-MS), parallel-plate DMCs have been proposed for sizing nanoparticles, measuring atmospheric ion spectra or detecting volatile organic compound (VOC) molecules (Pomareda et al., 2013; Rus et al., 2010). A parallel-plate DMC with multiple electrometers (instead of having one classified particle exit), named as cross-flow ion mobility spectrometer, has further been designed and evaluated for characterizing atmospheric ions (Zhang & Wexler, 2006). Notice that relatively high sheath flow rates (typically greater than 1000 lpm) were used in the operation of these developed parallel-plate DMCs. For example, sheath flow rates of 1000 lpm or more were used in the DMCs (with the flow channel cross-section of 1–2 cm<sup>2</sup> only) described in the work of Rus (Rus et al., 2010). Another DMC with the flow channel cross-sectional area of 0.25 cm<sup>2</sup> was operated at a sheath flow rate of 100–800 lpm (Pomareda, et al., 2013).

Due to the potential of low production costs, the mini-plate DMCs have been designed and their performance has been experimentally evaluated for cost-effective

electrical-mobility-based ultrafine particle sizers (Liu & Chen, 2016a, 2016b; Steer et al., 2014). Different from the parallel-plate DMCs operating at high sheath flow rates, these compact/miniature parallel-plate DMCs are typically operated at low sheath flow rates (usually less than 5.0 lpm). A compact multi-electrode parallel-plate DMC with the feature of ESP (electrostatic precipitation) has also been proposed for submicrometer particle characterization (Ranjan & Dhaniyala, 2008). In addition to the hardware development, 2-D theoretical models have predicted the performance of parallel-plate DMCs/EAAs, i.e., the transfer function, for non-diffusive or diffusive particles (Liu & Chen, 2016a; Rus et al., 2010). Although both experimental and theoretical work has been carried out for parallel-plate DMCs, the general design guideline for compact/miniature parallel-plate DMCs has not yet been established. Understanding the effect of design parameters of particle classification channels on the transfer function of compact parallel-plate DMCs, operated at a low sheath flow rate, will set up the foundation for the future design guidelines.

### **2.3 DMC Transfer Function Calculation Methods**

The performance of the DMC is characterized by its transfer function, which simply quantifies the capability of the DMC to classify particles within a narrow size range window. However, throughout stages of DMC's development, there are several approaches are utilized for quantifying the value of the DMC transfer function: numerical, theoretical, and experimental.

The numerical approach is based on the flux of the aerosol particles that flow through the aerosols entrance. This assumes a homogenous distribution of particle concentration,



while the flow of the aerosol stream is varies based on the location of the flow element (i.e. it is slow near the wall and in its max value near the farthest point from the walls of the channel). As a result, the flux is mainly dependent on the flow. However, aerosol flux is calculated based on the integrated number of flux segments (mesh elements) over the entrance of the aerosols. These elements are always non-uniformly distributed to consider the boundary layer of the flow because it is efficient to be utilized in the numerical solution technique. All DMC numerical modeling calculations are performed via three steps: 1) calculating the flow and the electrical field, 2) solving particle equation of motion, 3) and finding the particle that exits from the DMC channel and considering its flux value (D. Chen, 1996; D. R. Chen et al., 1998a; Mai & Flagan, 2018; Steer et al., 2014).

On the other hand, the theoretical approach is based on deriving the transfer function directly based on the stream and electrical flux function and based on the probability theory for both aerosols and sheath inside the DMC channel (Knutson & Whitby, 1975; Knutson, 1972; Stolzenburg & McMurry, 2008; Stolzenburg, 1988). However, despite that this approach does not require expensive computational power; it is neither capable of predicting the performance in the complicated designs nor assessing particle loss outside the classification channel especially at the aerosol entrance zone.

The experimental approach is based on counting the exact number of particles of a specific size range that successfully pass through the DMC classification channel. It has been reported in the work of several nanoparticle experimentalists (D. Chen, 1996; Fissan et al., 1996; E. O. Knutson & Whitby, 1975; Earl Owen Knutson, 1972; Q. Liu, 2015; Stolzenburg,

1988). The system of instruments is sorted as illustrated in [figure 1.2](#) with three consecutive stages: charging, sorting, and counting. Charging is done through the charger prior to sorting the particles inside the DMC channel. Counting the selected particle size is the last stage that is done through the Condensation Particles Counter (CPC). The CPC counts particles based on the optical technique, which requires the particle to be larger than the wavelength of the light source. Therefore, the particle has to grow in size from several nanometers to several micrometers.

The experimental setup of the DMC can operate in a parallel series of two consecutive DMCs, such a setup called Tandem Differential Mobility Classifier TDMC (or Analyzer TDMA). It is usually used in a humid aerosol's measurement and studies related to the size change of submicron particles (Rader & McMurry, 1986). The sorted particle size range of the first DMC can be further sorted to a narrower window on the second DMC. The data of both DMCs is processed in a single computer with a de-convoluted scheme to find the actual transfer function for the single DMC (Gysel et. al, 2009; Li et. al, 2006; Stratmann et. al, 1995; Vlasenko et. al, 2016).

## CHAPTER 3 Eccentric Cylindrical Differential Mobility Classifier<sup>6</sup>

### 3.1 Introduction

The differential mobility classifier (or analyzer), DMC (or DMA), has been applied in aerosol particle studies for sizing and classifying particles in sub-micrometer and nanometer size ranges (by the electrical mobility of particles). It is one of the core components in electrical particle mobility sizers for measuring the size distribution of particles. The DMC has also been applied by the National Institute of Standards and Technology (NIST) to certify the sizes of standard PSL particles in the diameters less than 100 nm (Kinney et al., 1991; Liu & Pui, 1974).

DMCs in different configurations have been designed and their performance has been reported in the literature. The basic design of a DMC is either in the cylindrical, parallel-plate or disk configuration (Ramechecandane et al., 2011; Steer et al., 2014; Zhang et al., 1995). Among them, cylindrical DMCs are the most popular because there is no sidewall presence in the particle classification channel. [Figure 3.1](#) shows the schematic diagram of a cylindrical DMC. It is generally constructed by coaxially aligning one inner and one outer cylinder. Two inlets for polydisperse particle and clean sheath flows and two

---

<sup>6</sup> The material of this is chapter is taken from a publication-Alsharifi, T., & Chen, D.-R (201X), "Effect of axial eccentricity on the performance of a cylindrical differential mobility classifier," *Aerosol Science and Technology*, 53:7, 735-748: <https://doi.org/10.1080/02786826.2019.1599097>.

outlets for classified particle and excess flows, respectively, are designed in a DMC. Prior to entering a DMC, particles are required to be electrically charged to a well-known charge distribution. Once they enter, particles flow into the classification channel via the particle entrance slit. The clean sheath flow in the DMC serves as the barrier to prevent charged particles from reaching the classified particle exit slit as they follow the flow downstream. For the particle sizing or classification, an electrical field is established in the annular spacing between the inner and outer cylinders to drive charged particles crossing the sheath flow. Once crossed, charged particles in a certain range of electric mobility will exit from the classified particle exit slit. Particles with electrical mobility greater or less than a certain range will be either deposited in the inner cylinder or carried out by excess flow. In principle, the flow direction in a DMC shall be different from that of an electrical field in order to achieve the particle separation. For design simplicity, the flow direction is typically perpendicular to the electrical field direction.

The development of modern cylindrical DMCs stems from the success of sorting particles in a narrow electrical mobility window and collecting the sorted ones by a filter created by Hewitt (1957). Liu and Pui (1974) improved Hewitt's design, enabling the extraction of classified particles from the DMC classification channel and counting the concentration of classified particles via an aerosol electrometer. They were the first to term the classifier as the "differential mobility analyzer" (Flagan, 1998). Knutson and Whitby (1975) further developed the fundamental theory to describe the performance of a cylindrical DMC, i.e., transfer function (defined as the probability of a particle entering the classifier through the aerosol's inlet and leaving with the classified aerosol flow), for non-diffusive

particles. Their effort eventually led to the commercialization of the DMC originally designed by Liu and Pui (1974).

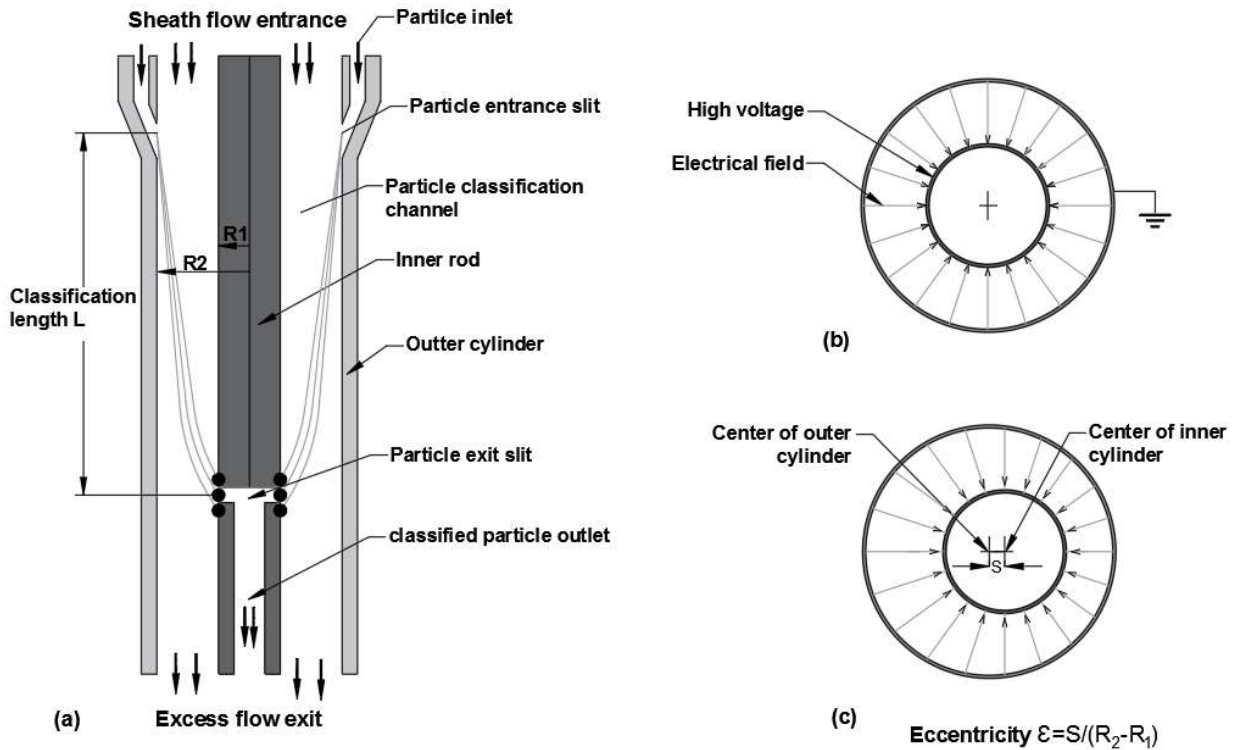


Figure 3. 1 The schematic diagram of a cylindrical differential mobility classifier (DMC) and computational domain in this modeling: (a) side view (with the illustration of the particle movement in the classification channel); (b) for the axial view of a concentric DMC; (c) for the axial view of an eccentric DMC.

The effect of particle diffusivity on the DMC transfer function was first investigated by Kousaka et al. (1985, 1986) through the comparison of theoretical calculation and experimental data obtained from the tandem DMC (TDMC), or tandem DMA (TDMA), setup. The theoretical transfer function of a cylindrical DMC for diffusive particles was later derived by Stolzenburg (1988). Note that the summary of the derivation could be found in the paper of Stolzenburg and McMurry, (2008). Due to the requirement to study the particle

nucleation events in the atmosphere, the late development of a scientific DMC is primarily on the sizing of particles in single-digit nanometers (Fissan et al., 1996; Kozlowski & Ferna, 2013; Tanaka & Takeuchi, 2002;. Zhang & Flagan, 1996; S. Zhang et al., 1995).

The axial alignment of outer and inner cylinders in a cylindrical DMC is assumed perfect in all the DMC studies. In the real DMC construction, the axial eccentricity indeed exists when aligning the outer cylinder with the inner one (due to the presence of machining and construction tolerance). Unfortunately, our knowledge of the effect of axial eccentricity on the performance of a cylindrical DMC is very limited. The above knowledge, on the other hand, becomes essential in the design phase of a cylindrical DMC. To the authors' knowledge, the effect of axial eccentricity on the performance of a cylindrical DMC was only investigated in the dissertation work of Knutson (1972) with the assumptions of 2-D flow and electrical fields in the particle classification channel and for non-diffusive particles. Note that the above work is in fact presented in the appendix, not in the main content of the dissertation. Uin et al., (2011) applied Knutson's theory to investigate the transfer function of a very long DMC with the construction imperfection. The assumption of a 2-D flow field, i.e., either uniform or fully developed velocity profiles, in the particle classification channel of a cylindrical DMC is questionable. It is because the velocity profile of sheath flow is developing into a fully-developed profile as the flow initially enters the DMC classification channel in the uniform profile. The developing flow in the classification channel should be considered in 3-D, not 2-D, in an eccentric DMC. The numerical modeling will lift the assumption made in the Knutson's derivation.

The objective of this chapter work is thus to investigate the effect of axial eccentricity on the performance of cylindrical DMCs. A numerical approach was applied because of its cost-effectiveness compared with the experimental approach and its ability to lift the fully-developed velocity profile assumption made in the Knutson's derivation. The COMSOL Multiphysics 5.3a<sup>®</sup> and MATLAB R2017a<sup>®</sup> were used to model the DMC performance. Prior to our investigation, the model was verified by the comparison of numerical results obtained for both concentric and eccentric DMCs with those calculated by the theory given in the work of Knutson (1972) and in the experimental work of Chen et al., (1998). The studied parameters include the geometrical variables, i.e., the axial eccentricity, the ratio of outer to inner cylinder radii, the aspect ratio of the particle classification channel (i.e., the ratio of hydraulic diameter of the annular spacing and the length of the particle classification channel), and the cross-sectional area of the particle classification channel in addition to the flow parameters, i.e., the sheath-to-aerosol flow rate ratio and total flow rate (i.e., the sum of sheath and aerosol flow rates). Furthermore, the effect of particle diffusivity on the eccentric DMC transfer function was also studied.

### **3.2 The Numerical Model**

Both COMSOL Multiphysics 5.3a<sup>®</sup> and MATLAB R2017a<sup>®</sup> Multiphysics were used to set up the DMC modeling. A typical computational domain for modeling the performance of a cylindrical DMC is shown in [Figure 3.1](#). [Figure. 3.1a](#) and [3.1b](#) are the cross-sectional views of the computational domain in the longitudinal and radial directions, respectively, for a concentric DMC. [Figure. 3.1c](#) shows a typical cross-sectional view of an eccentric DMC. Note that the eccentricity,  $\epsilon$ , of the axial alignment of inner and outer cylinders is

defined as the ratio of the axial displacement of the inner rod and outer cylinder,  $S$ , to the annular spacing,  $(R_2 - R_1)$ , between them.

$$\epsilon = \frac{S}{(R_2 - R_1)} \quad (3.1)$$

### **For the flow and electrical fields**

The steady and incompressible Navier-Stokes and continuity equations were applied to model the flow field in a DMC. The electrical field in the classification channel of a DMC was calculated by the Laplace equation for the electrical potential,  $\phi$ , and the electrical field intensity,  $\vec{E}$ , was calculated as  $\vec{E} = -\nabla\phi$ .

For the flow field calculation, the velocity at the sheath flow entrance was assumed either in the uniform or fully developed profile, while a uniform velocity profile was assumed at the particle inlet. A uniform velocity profile was assumed at the classified particle outlet. The pressure boundary condition was set at the exit of excess flow. The no-slip boundary condition was applied to all the solid walls in contact with fluid flow. For the electrical field, the inner cylinder was set at an elevated voltage, and the outer one was on the electrical ground.

### **For particle trajectory**

Because of the small sizes of studied particles (i.e., negligible particle inertia effect), the motion of non-diffusive particles in a DMC was assumed to follow the flow and electrical fields (i.e., negligible particle inertial effect), the trajectory of a singly-charged particle in a DMC was thus computed via

$$x_{(t+1)} = x_{(t)} + \int_t^{t+dt} u dt + Z_p E_x \quad (3.2a)$$



$$y_{(t+1)} = y_{(t)} + \int_t^{t+dt} v dt + Z_p E_y \quad (3.2b)$$

$$z_{(t+1)} = z_{(t)} + \int_t^{t+dt} w dt + Z_p E_z \quad (3.2c)$$

where  $x_{(t)}, y_{(t)}, z_{(t)}$  are the initial particle location;  $x_{(t+1)}, y_{(t+1)}, z_{(t+1)}$  are the location of the particle after  $\Delta t$  time;  $u, v, w$ : are the three velocity component in the  $x, y, z$  coordinates respectively where  $y$  is the axial direction of particle traveling distance;  $Z_p$  is particle mobility and  $E_x, E_y$  and  $E_z$  are the electrical field in  $x, y$ , and  $z$  coordinates. Note that for eccentric classification channel, there was no electrical field in axial direction. The initial velocity of particle released at the particle inlet was assumed the same as the flow velocity at the same location.

The modeling of diffusive particle motion was done by the Monte Carlo method (Hagwood et al., 1999). The additional random displacement terms,  $g(\sqrt{\sigma_i^2})$ , where  $i = x, y$ , and  $z$ , are included in Eq. (3.2). The random displacement was generated from the normal data distribution and its standard deviation of  $\sigma$  is given as:

$$\sigma_i^2 = 2D\Delta t \quad (3.3)$$

where  $i$  is the Cartesian coordinates ( $x, y, z$ );  $D$  is the particle diffusivity and  $\Delta t$  is the time step; and  $g$  is the random generator function.

### **For the DMC transfer function**

The performance of a DMC is characterized by its transfer function, defined as the probability of a particle with given electrical mobility ( $Z_p$ ) entering the DMC classification region and reaching the classified aerosol exit. The calculation of the transfer function of a DMC for singly charged particles of a given size was based on the particle flux. In the

computation, the annular spacing for the particle entrance was partitioned into fine meshes distributed based on the meshing scheme suggested in the works of Masset et al. (2011) and Becker and Becker (2012). For non-diffusive particles, a representative particle was released from the centroid of each mesh at the particle entrance. The trajectories of representative particles were calculated and their fates (i.e., either deposited in or transmitted through the classification channel) were recorded. With the assumption of uniform particle concentration at the particle entrance, the transfer function of a DMC was calculated as

$$\Omega = \frac{\sum_1^n p_i w_i A_i}{\sum_1^n w_i A_i} \quad (3.4)$$

where  $\Omega$  is the numerical transfer function of a DMC for singly charged particles of a given size;  $n$  is the total number of particles released from the aerosol entrance;  $w_i$  is the flow velocity at the released particle location;  $A_i$  is the area of the mesh associated with the released particle,  $i$ , and  $p_i$  is the probability of particles released from the mesh,  $i$ , and penetrating through the particle classification channel of a DMC. For non-diffusive particles, the value of  $p_i$  is 1.0 if a representative particle released from the centroid of the mesh,  $i$ , was penetrating through the classification channel and is 0 if the particle were either deposited or carried out by excess flow. For diffusive particles, at least 100 particles were released from the mesh,  $i$ , to access the probability of a particle exiting the classification channel through the classified particle slit.

Note that, for a concentric DMC, the theoretical transfer function for non-diffusive particles under the assumption of 2-D flow and electrical fields in the particle classification channel, is given by Knutson (1975) and can be re-expressed by Stolzenburg (1988) as

$$\Omega(\bar{Z}_p) = \frac{1}{2\beta(1-\delta)} [|\bar{Z}_p - (1 + \beta)| + |\bar{Z}_p - (1 - \beta)| - |\bar{Z}_p - (1 + \beta\delta)| - |\bar{Z}_p - (1 - \beta\delta)|] \quad (3.5)$$

where  $\bar{Z}_p = \frac{Z_p}{Z_p^*}$  in which  $Z_p$  is the particle electrical mobility and  $Z_p^*$  is the electrical mobility of particles at the maximum penetration at the same voltage;  $\beta = \frac{Q_s + Q_a}{Q_m + Q_c}$  and  $\delta = \frac{Q_s - Q_a}{Q_s + Q_a}$  are the flow ratios as  $Q_s$  is the classified aerosol flow rate,  $Q_a$  is the polydisperse aerosols flow,  $Q_m$  is the excess flow rate, and  $Q_c$  is the clean sheath flow rate. The required voltage for the maximal penetration through the classification channel for particles of given electrical mobility is given by Hewitt (1957),

$$V = \frac{Q_c \ln \frac{R_2}{R_1}}{2\pi L Z_p^*} \quad (3.6)$$

where  $R_2$  and  $R_1$  are the radii of the outer and inner cylinders, respectively;  $L$  is the length of particle classification channel; and  $Z_p$  is the electrical mobility of singly charged particles of a given size.

The theoretical transfer function of an eccentric DMC for non-diffusive particles was derived by Knutson (1972). For reference, the derivation is briefly summarized in Appendix A.

Table 3.1 gives the values of the physical properties of gas and particles used in our modeling. The effect of axial eccentricity on the performance of a cylindrical DMC was investigated for particles in the diameters of 3, 5, 10, 50, 160, 340 and 815 nm and under the various conditions of sheath-to-aerosol flow rate ratio,  $\beta$ , of 3.33, 4, 5, 6.67, 10, 20, 50 (at which both sheath and aerosols flow rates were varied from 5 to 20 lpm and from 0.5 to 2

lpm, respectively). The diffusivity of particles was considered for the particle sizes less than 50 nm.

Table 3. 1 Properties of gas and particles, and flow rates for cylindrical DMC

CONSTANT		VALUES AND FORMULAS
PARTICLE	diameter, $dp$	3, 5, 10, 50, 160, 340, 815 nm
	mass density, $\rho_p$	1000 kg/m <sup>3</sup>
	slip correction factor $C_c$	$C_c = 1 + Kn \left( 1.155 + 0.471 e^{-\frac{0.596}{Kn}} \right)$
	Elementary charge e	$1.602 \times 10^{-19}$ C
AIR	temperature, t	293.15 K
	dynamic viscosity, $\mu$	$18.5 \times 10^{-6}$ N.s/m <sup>2</sup>
	density, $\rho$	1.2047 kg/m <sup>3</sup>
	mean free path $\lambda$	0.066 [um]
	Boltzmann constant	$1.38064852 \times 10^{-23}$ [J/K]
FLOW	Aerosols inlet and exit flow	0.5-1.5 lpm
	Sheath flow rate range	0.1-20.0 lpm

### 3.3 Model Verification

#### 3.3.1 Cylindrical Model Verification

Figures 3.2a and 3.2b show the comparison of the height and the full width at half maximum (FWHM) of the numerical transfer function with the experimental data given in Chen et al., (1998) for Nano-DMC, or Nano-DMA, when operated at the aerosol and sheath flow rates of 1.5 and 15 lpm. The height and FWHM data shown in the mentioned above figures were obtained from the de-convolution of Tandem DMC (TDMC) curves, calculated first by the convolution of numerical transfer functions and then by the de-convolution of

TDMC, assuming the functional form of the DMC transfer function is in the triangular shape. A reasonable agreement between the numerical and experimental data was obtained. The height of the DMC transfer function decreases as the particle size reduces and the FWHM of the DMC transfer function remains constant at 0.1 and increases as the particle size is less than 10 nm. The above observed trends are because of the Brownian diffusion of particles.

The comparison of the numerical transfer function of Nano-DMC with the theoretical one, for Stolzenburg & McMurry (2008), for the particle size of 3 nm is also given in [figure 3.2c](#) when it was operated at the aerosol and sheath flow rates of 1.5 and 15 lpm, respectively. A good agreement was achieved in the above comparison. [Figure 3.2d](#) illustrates the comparison between the numerical and theoretical transfer function for a long classification channel of 45cm for the particle size of 160 nm and for the aerosol and sheath flow rates of 1.5 and 15 lpm, respectively. The inner and outer diameters are 1 and 2 cm respectively. Obvious compatibility appears between both the numerical and theoretical data.

### **3.3.2 Eccentric Model Verification**

[The figure 3.3](#) shows the comparison of the DMC transfer function for the numerical with the theoretical calculation obtained based on the work of Knutson, (1972) for eccentricities of 1,2, and 5% respectively, and for 160 nm particle size. The Nano-DMC was operated at the aerosol and sheath flow rates of 1.5 and 15 lpm. The inner and outer diameters are 1 and 2 cm respectively. A good agreement between the numerical and experimental data was obtained.

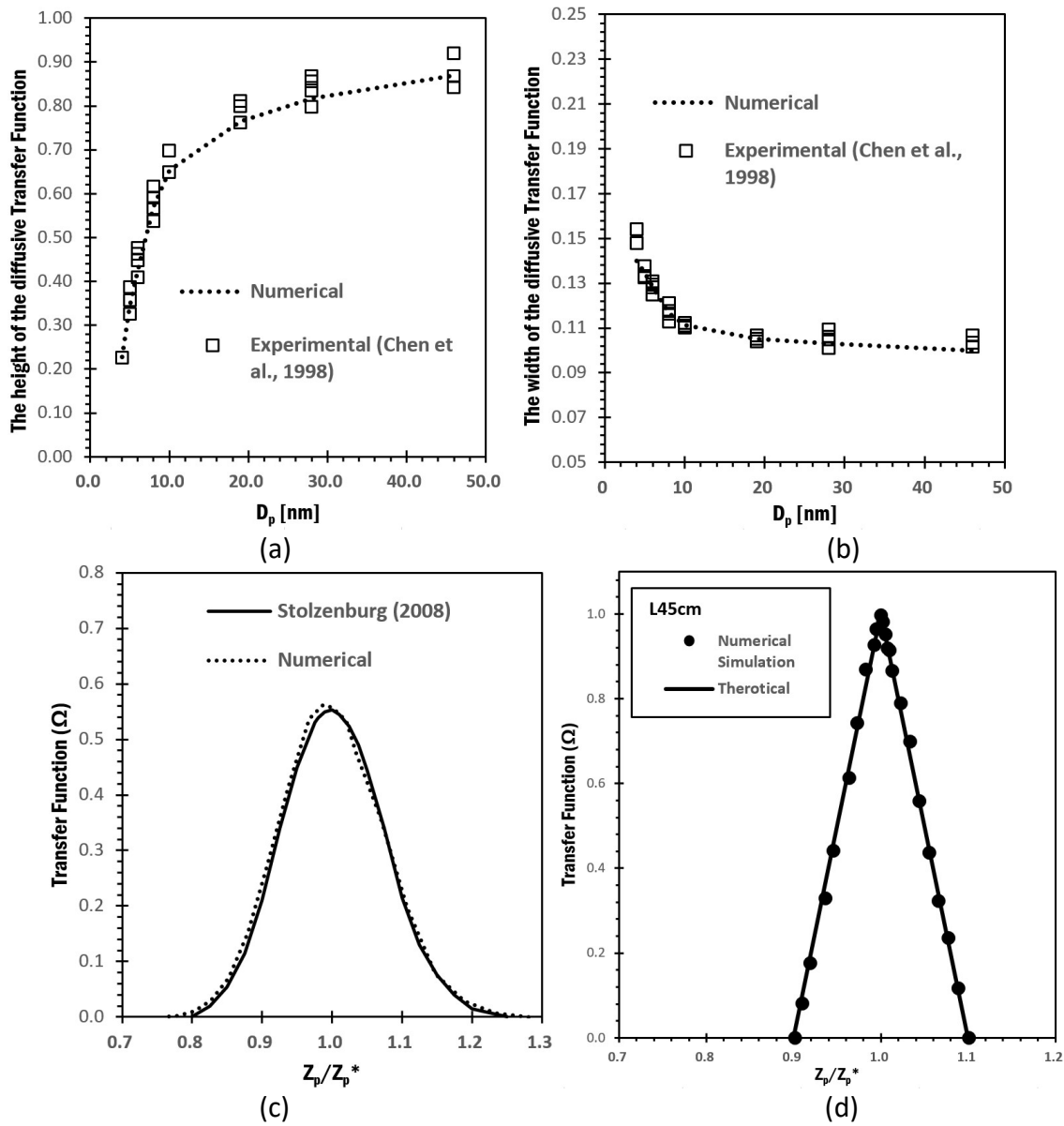


Figure 3. 2 The comparison of numerical transfer functions with the experimental data for (Chen et al., 1998) and diffusive transfer function (Stolzenburg, 1988) for Nano-DMC: (a) the height and (b) the full width at half maximum (FWHM) of transfer function (assumed in triangular shape) as the function of particle size; (c) the diffusive transfer function of Stolzenburg (1988) for 3 nm particle size; and (d) the non-diffusive transfer function theoretical transfer function. Both, the Nano-DMC and long DMC was operated at the aerosol and sheath flow rates of 1.5 and 15 lpm.

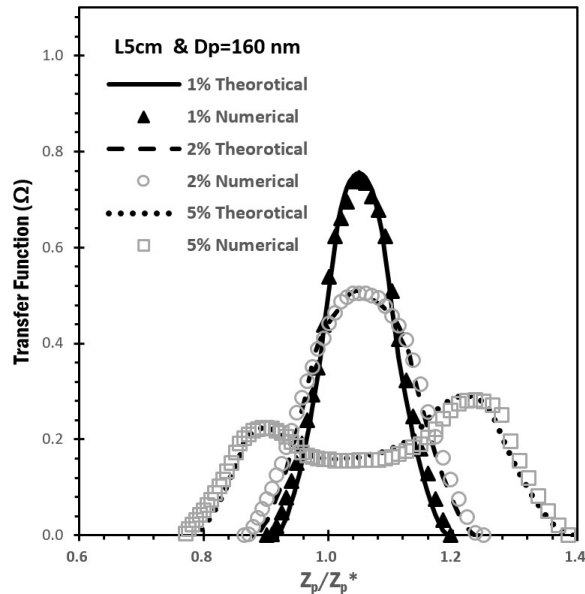


Figure 3.3 The comparison of numerical non-diffusive transfer functions with the theoretical calculation obtained based on the work of Knutson, (1972) for eccentricities of 1,2, and 5% respectively, and for 160 nm particle size. The Nano-DMC was operated at the aerosol and sheath flow rates of 1.5 and 15 lpm.

### 3.4 Results and Discussion

#### 3.4.1 Flow and electrical fields inside the eccentric DMC

For illustration, the flow field (at the cross-section of 20 cm from the sheath flow entrance) in the particle classification channel of an eccentric DMC having the inner and outer diameters of 20 and 40 mm, respectively, and with 40% eccentricity when operated at the sheath flow rate of 10 lpm is given in [figure 3.4a](#) and [3.4b](#). [Figure 3.4a](#) is the velocity in the circumferential direction (whose magnitude was scaled up by a factor of 1,500) and [figure 3.4b](#) is the contour of the velocity magnitude in the axial direction. The velocity profile of sheath flow at the entrance of the particle classification channel was assumed uniform. Because of the axial eccentricity, the annular spacing between the inner and outer cylinders of the DMC is not constant. As a result, the maximum axial velocity value is located at the

widest spacing and it reduces as the spacing became smaller, eventually reaching the minimum value at the location with the narrowest spacing. The circumferential velocity is minimal at the location with the narrowest spacing and maximal at the location with the widest spacing. For the same spacing reason, the electrical field intensity is the highest at the narrowest spacing and the lowest at the widest spacing (as shown in [figure 3.3c](#)). Note that the developing length for the flow in an eccentric DMC channel under different flow rates and DMC eccentricity was further obtained in this dissertation work. A brief summary of this part of the work is given in the in Appendix B, for reference.

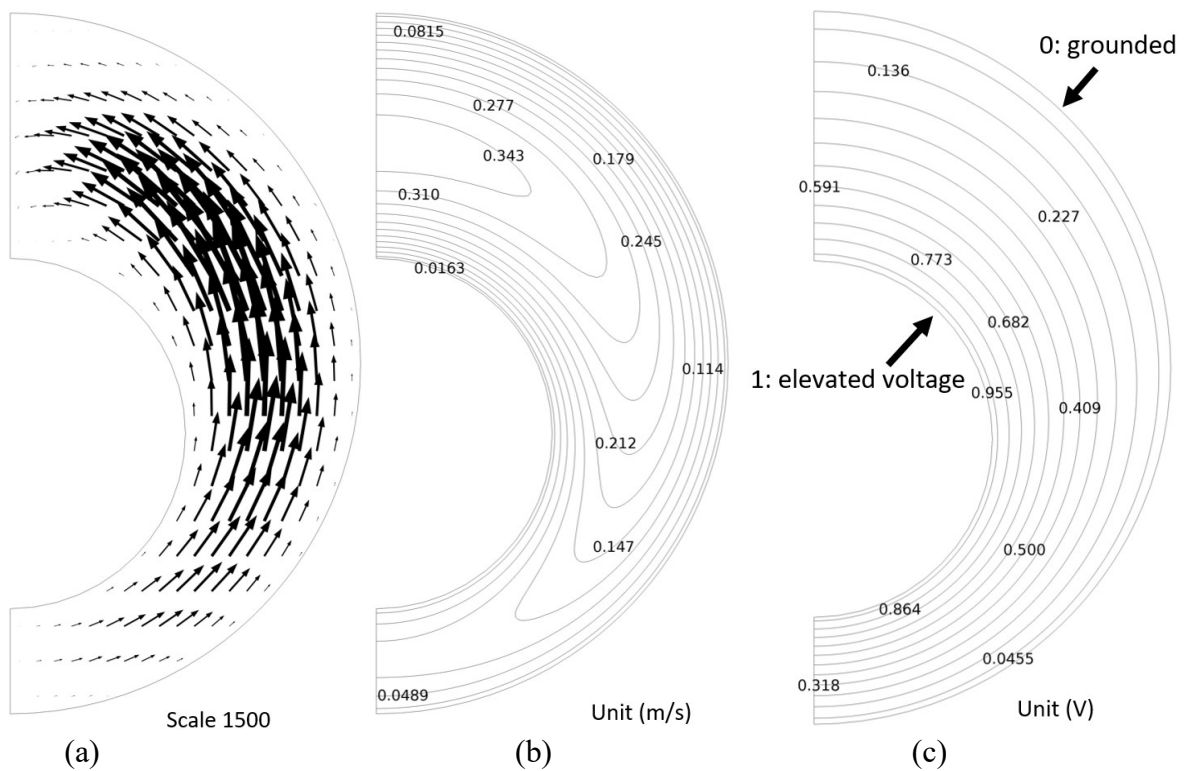


Figure 3. 4 The illustration of flow and electrical fields in the classification channel of a cylindrical DMC with outer and inner cylinder radii of 40 and 20 mm, respectively, and at 40% eccentricity. The shown data is at the cross-section located at 20 cm downstream the sheath flow entrance: (a) the circumferential component of sheath flow velocity (with the magnification of 1,500); (b) the contour of axial component of sheath flow velocity; (c) the contour of electrical potential (normalized by the applied voltage,  $V_0$ ).



### 3.4.2 Transfer function of an eccentric DMC

Figure 3.5 shows the numerical transfer function of cylindrical DMCs with the axial eccentricity of 1%, 2% and 5% for the particle size of 160 nm. These DMCs, operated at the aerosol and sheath flow rates of 1 and 10 lpm, respectively, had the particle classification length, inner and outer cylinder diameters of 5, 2 and 4 cm, respectively. Also included in the same figure is the theoretical transfer function calculated by the eccentric DMC theory given by Knutson (1972). Both uniform and fully developed velocity profiles at the sheath flow entrance of each studied DMC were assumed. In the cases with a uniform velocity profile assumption, the flow in the particle classification channel was 3-D (i.e., with the presence of the circumferential flow component) because of the sheath flow velocity profile developing to a fully developed one. In the cases of assuming the fully developed profile at the sheath flow entrance, no circumferential velocity component was present in the classification channel of a DMC.

It is observed that, in general, the peak of DMC transfer function was reduced while the FWHM was broadened as the axial eccentricity of the DMC was increased. In the case of 5% eccentricity, the peak of transfer function was split into two (i.e., double-peaked) with one peak in the low electrical mobility range, lower than the other one in high mobility range. Note that the theoretical transfer functions with the assumption of fully developed velocity profiles are comparable to numerical ones, assuming the fully-developed profile at the sheath flow entrance, but not with the ones assuming the uniform profile.

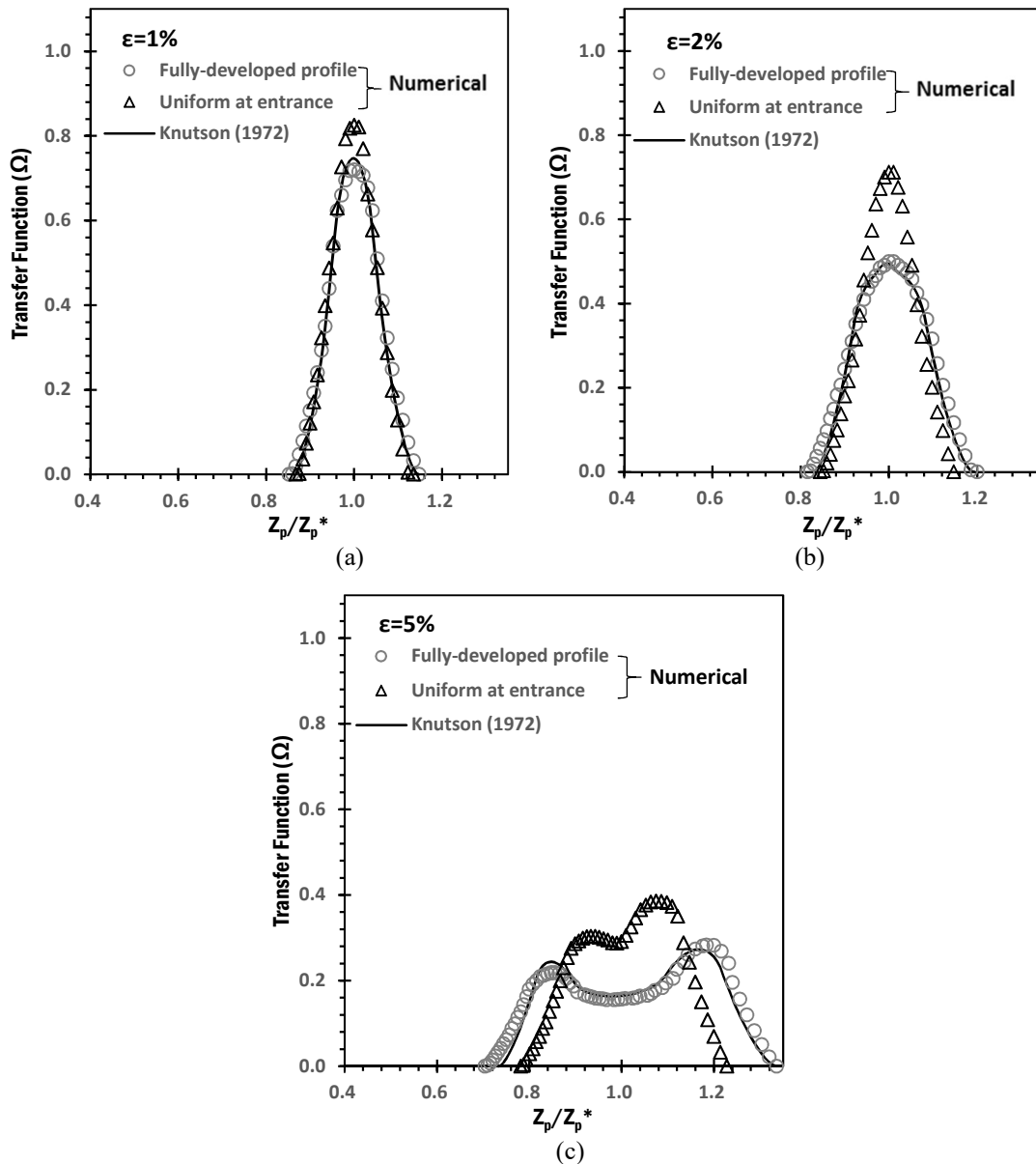


Figure 3. 5 The comparison of the numerical transfer function with the theoretical data of Knutson (1972) for the eccentric DMC with the assumption of uniform and fully-developed velocity profiles at the sheath flow entrance for the particle size of 160 nm. The studied DMC has the particle classification length of 5 cm, and an inner and outer cylinder radii of 10 and 20 mm, respectively. The sheath and aerosol flow rates of the studied DMCs are 10 and 1 lpm, respectively. (a) for 1% eccentricity, (b) 2% and (c) 5%.

To better understand the splitting of transfer function peak in the case of 5% eccentricity, the locations of 160nm particles in the neighborhood of the classified particle exit slit after

they were released from the particle inlet for the DMCs with eccentricities of 1% and 5%, and under the assumption of uniform and fully-developed flow profiles at the sheath flow entrance (plotted as the function of circumferential angle from 0 to  $2\pi$ ) is shown in [Figure 3.6](#) (a and b for the DMC with 1% and 5% eccentricity, respectively). Note that the circumferential angles related to the location at the narrowest and widest spacing of the DMC particle classification channel are 0 and  $\pi$ , respectively. Because of the variation of particle traveling distance and time, the particle position when moving close to the classified particle exit slit was varied at different angles. Only particles moved in the spacing nearby the classified particle exit slit (shown as the lines in the figure) are expected to exit the classification channel. From the figure, the location variation of particles in the neighborhood of the exit slit was increased with the increase in DMC eccentricity, resulting in more particle loss in the classification channel. The variation status of particle position nearby the classified particle exit slit is also dependent on the electrical mobility of particles. The nearby-the-exit-slit location of particles with higher electrical mobility is less varied than that of ones with low electrical mobility. It is why the peak in low mobility range is lower than that in high mobility range once the peak of the transfer function is split.

Moreover, the peak of the transfer function is calculated by assuming the fully developed profile at the DMC sheath flow entrance is lower and its FWHM is wider compared to those in the cases with the uniform profile assumption. The reason for the above observation is illustrated in [Figure 3.6](#) as the variation status of particle position at the exit slit in the case with the uniform flow assumption is less than that in the case with fully developed flow assumption.

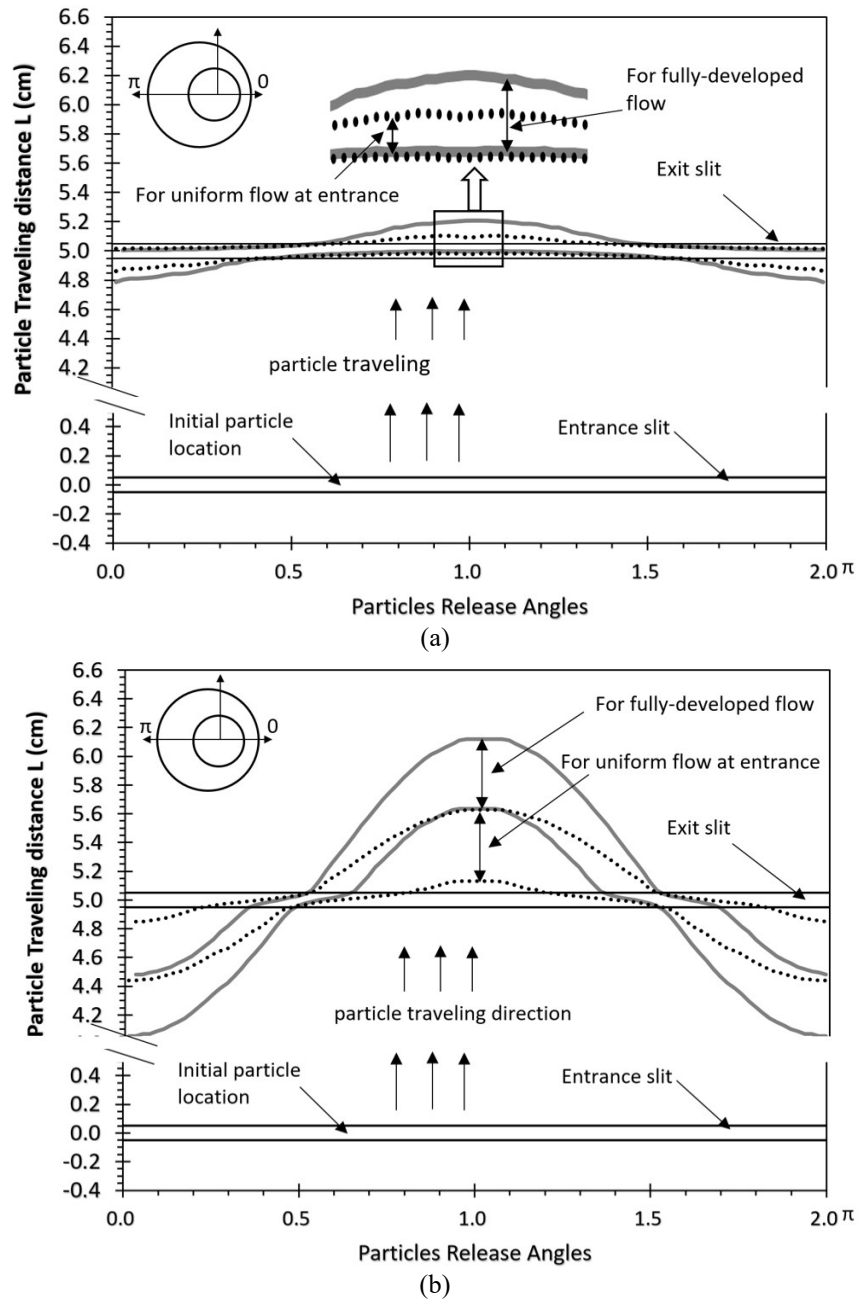


Figure 3. 6 The position of particles in the neighborhood of the classified particle exit slit after they were released from their initial location under the assumption of a uniform and fully developed velocity profile at the sheath flow entrance of studied DMC: the angle of  $0$  is associated with the narrowest spacing and  $\pi$  with the widest spacing of the annular classification channel. The annular classification channel of an eccentric DMC having the 5 cm classification length, and inner and outer radii of 10 and 20 mm (operated at the aerosol and sheath flow rates of 1 and 10 lpm, respectively): (a) 1% eccentricity and (b) 5%.

### 3.4.3 Dominant factor for the shape of the eccentric DMC transfer function

The distortion of flow and electrical field in the particle classification channel of an eccentric DMC is attributable to the shape change of the DMC transfer function. In this part of the work, we investigated which one is the dominant factor influencing the shape of the DMC transfer function. [Figure 3.7](#) shows the numerical transfer functions calculated with the assumption of uniform and fully developed velocity profiles at the sheath flow entrance for a cylindrical DMC with 5% eccentricity, operated at the aerosol and sheath flow rates of 1 and 10 lpm, respectively. Also included in the figure is the calculated transfer function with the assumption of uniform velocity profile in the entire particle classification channel. The particle classification length of studied DMCs was varied from 5 to 45 cm. The studied particle size was 160 nm.

[Figure 3.7a](#) shows the shape variation in the transfer function of a DMC with the inner and outer cylinder radii of 10 and 20 mm (operated at the aerosol and sheath flow rates of 1 and 10 lpm) as the classification length of the eccentric DMC was increased. Also included in the figure is the transfer function calculated with the fully developed flow profile assumption. It is found that the transfer function of an eccentric DMC approached the one calculated with the assumption of a fully developed velocity profile as the DMC classification length increased. It is because, under the same sheath flow rate, the percentage of the developing flow length relative to the entire classification channel length was reduced as the DMC particle classification length was increased. [Figure 3.7b](#) gives the transfer functions of an eccentric DMC under different flow fields in the particle classification channel (i.e., uniform profile at the sheath flow entrance, uniform and fully developed flow

profile in the entire classification channel). The particle classification length of the DMC was 45 cm. It is found that the effect of flow field variation on the transfer function of the eccentric DMC is in fact secondary.

Figure 3.7c shows the comparison of a calculated transfer function of a DMC with the classification length of 5 cm and 5% eccentricity under the assumptions of uniform velocity profile in the entire particle classification and only at the sheath flow entrance. The resulting transfer function calculated by assuming a uniform flow profile in the classification channel is attributed to the effect of electric field distortion. The difference between the two transfer functions is attributed to the effect of flow field distortion. It is thus found that the shape and peak split of an eccentric DMC transfer function is primarily due to the distortion of the electric field. The distortion of the flow field makes the transfer function broader.

#### **3.4.4 Effect of sheath-to-aerosol flow ratio and total flow rate on the eccentric transfer function**

The effect of sheath-to-aerosol flow rate ratio ( $\beta$ ) on the transfer function of an eccentric DMC was investigated in this part of the study. The studied DMC with the 2.5% eccentricity has the classification length of 45 cm, and the inner and outer cylinder diameters of 20 and 40 mm, respectively. Figure 3.8 shows the numerical transfer functions of the studied DMCs when operated at  $\beta = 4, 5, 10$  and 20. It is noticed that the effect of eccentricity on the transfer function of an eccentric DMC is much more severe when operated at a high sheath-to-aerosol flow rate ratio (i.e., at high sizing resolution power). Also, notice that it is confirmed by our modeling that the eccentric DMC transfer function for non-diffusive particles remained the same when the sheath-to-aerosol flow rate ratio was kept constant.

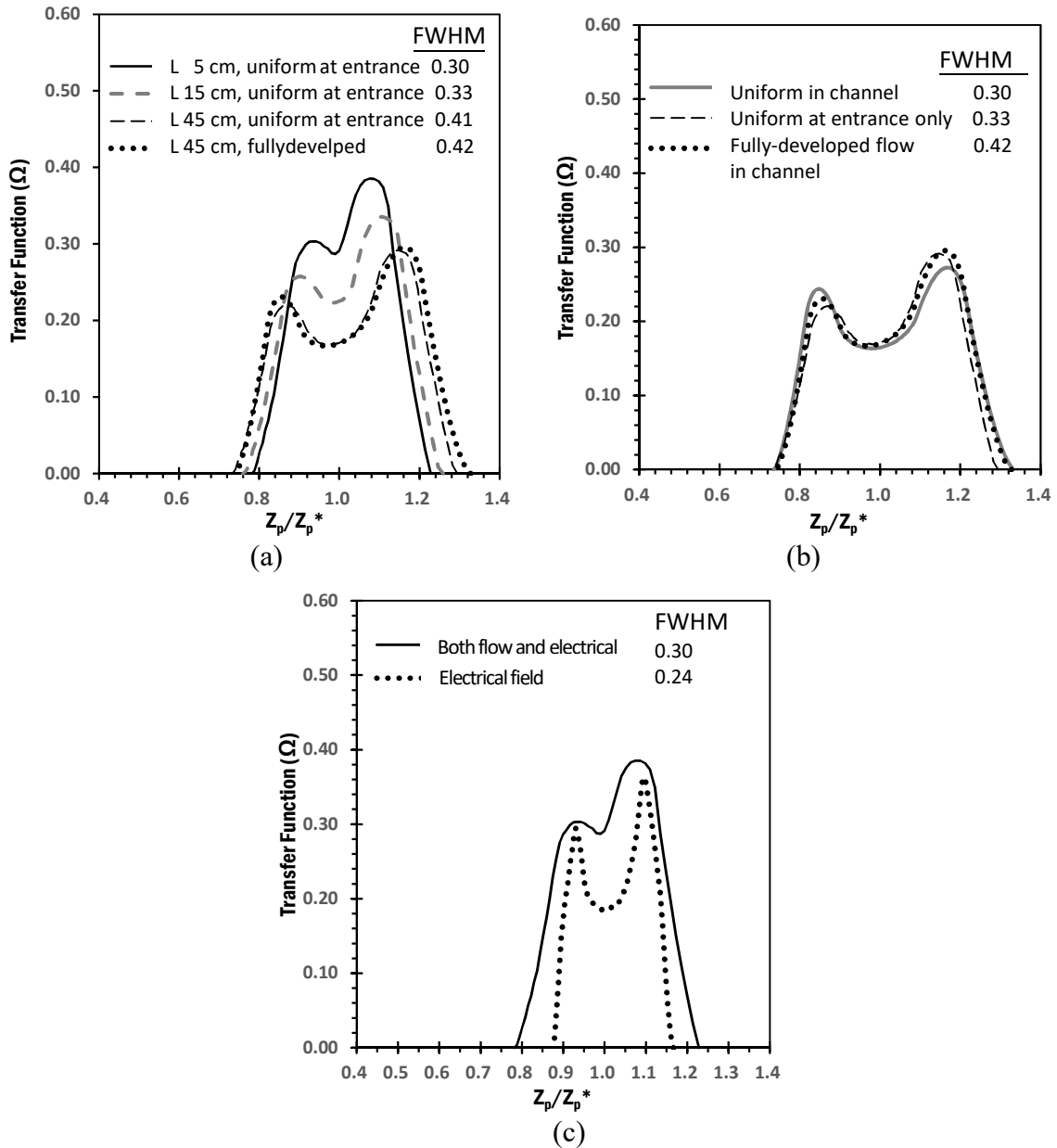


Figure 3. 7 The numerical transfer function of a DMC with 5% eccentricity and operated at the aerosol and sheath flow rates of 1 and 10 lpm, respectively. The inner and outer cylinder radii of studied DMCs were 10 and 20 mm, respectively. The studied particle size is 160 nm. (a) is for the cases with the classification channel lengths of 5, 15, and 45 cm under the uniform velocity profile at the sheath flow entrance, and under the fully developed profile; (b) is for the cases under the assumption of both fully-develop and uniform velocity profiles at the sheath flow entrance, and under the assumption of uniform sheath flow in the entire channel. The DMC channel length was fixed at 45 cm; (c) is for the cases with both flow and electrical field distortion, and with the distortion of the electrical field only. The DMC classification length was fixed at 5 cm. For the reference, the full width at half maximum (FWHM) of shown transfer functions is also given.

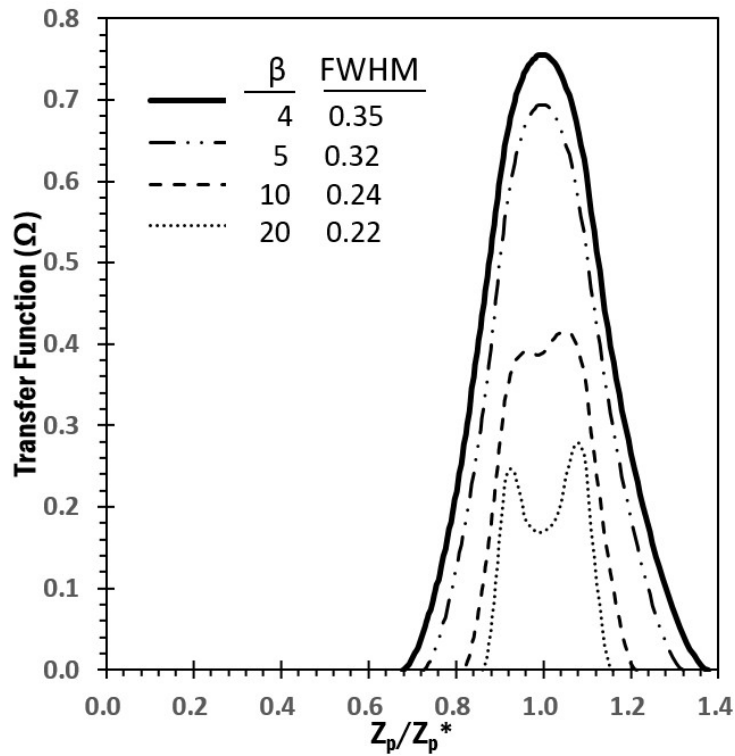


Figure 3. 8 The numerical transfer function with different flow ratios for a DMC with an inner and outer cylinder radii of 10 and 20 mm, respectively and with 2.5% eccentricity when operated at sheath-to-aerosol flow rate ratios  $\beta$  of 4, 5, 10, 20 (for sheath flow of 10 lpm and areoles flow of 2.5, 2, 1, and 0.5, respectively). The classification length of studied DMCs was 45 cm. For the reference, the full width at half maximum (FWHM) of shown transfer functions is also given.

Figure 3.9 shows the numerical transfer function of a cylindrical DMC with the 5% axial eccentricity and the particle classification length of 5 cm (operated at the sheath-to-aerosol flow rate ratio of 10 under different total flow rates). It is found that the reduction of total flow rate while keeping the sheath-to-aerosol flow rate ratio constant increased in the particle loss, resulting in the reduction of the transfer function. It is because of flow velocity reduction at the classified particle exit slit (to overcome the electric force for particle exiting).



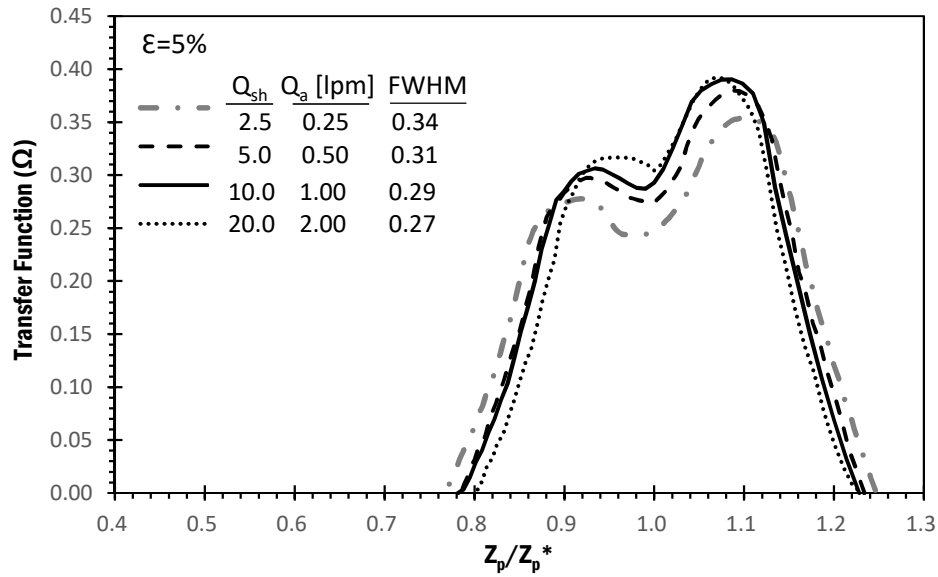


Figure 3. 9 Comparison of the calculated transfer functions of a DMC having  $R_1$ ,  $R_2$ , and  $L$  of 10, 20 and 50 mm, respectively when operated at the total flow rates of 2.75, 5.5, 11 and 22 while keeping the value of  $\beta$  at 10. The studied DMCs have an eccentricity of 5%. For the reference, the full width at half maximum (FWHM) of shown transfer functions is also given.

### 3.4.5 Effect of DMC geometry on the eccentric transfer function.

Three geometrical parameters of a cylindrical DMC (i.e.,  $L$ ,  $R_2/R_1$ ,  $L/(R_2 - R_1)$ ) where  $L$  is the particle classification length, and  $R_1$  and  $R_2$  are the radii of inner and outer cylinders) were considered in this part of the investigation.

Figure 10a illustrates the effect of the particle classification channel,  $L$ , on the transfer function of a DMC having 5% eccentricity and operated at the aerosol and sheath flow rates of 1 and 10 lpm, respectively, while keeping both the radial ratio  $R_2/R_1$  and the channel aspect ratio  $L/(R_2 - R_1)$  of 2 and 5, respectively. It is found that the value of the transfer function was decreased as the length of the particle classification channel was

increased. It is because of the increased effect of circumferential velocity component in a long DMC channel, causing more particle loss to the walls of the inner cylinder. [Figure 9b](#) gives the numerical transfer functions for the DMCs with 5% eccentricity and a particle classification length of 5 cm while having radial ratios of 1.2, 2, and 4 (for the radii ratios  $R_2:R_1$  of 6:5, 2:1 and 1.33:0.33 cm, respectively). The result shows the increase of the radii ratio (which is associated with the decrease of the cross-sectional area of the annular channel) decreased the height of the eccentric DMC transfer function. It is because, at the same flow rate and classification channel length, the small cross-sectional area resulted in high circumferential velocity during the flow developing, leading to more particle loss to the inner cylinder walls. [Figure 10c](#) presents the calculated transfer function of cylindrical DMCs with the 5% eccentricity, 5 cm particle classification length and radial ratio of 2 while varying the channel aspect ratios of 1, 5 and 10 (for the  $R_2:R_1$  ratio of 10:5, 2:1, 1:0.5, respectively). It is found that the effect of the channel aspect ratio on an eccentric transfer function is minor. The DMC with a high channel aspect ratio has a slightly lower transfer function compared to those of DMC with lower channel aspect ratios (due to the same reason described above).

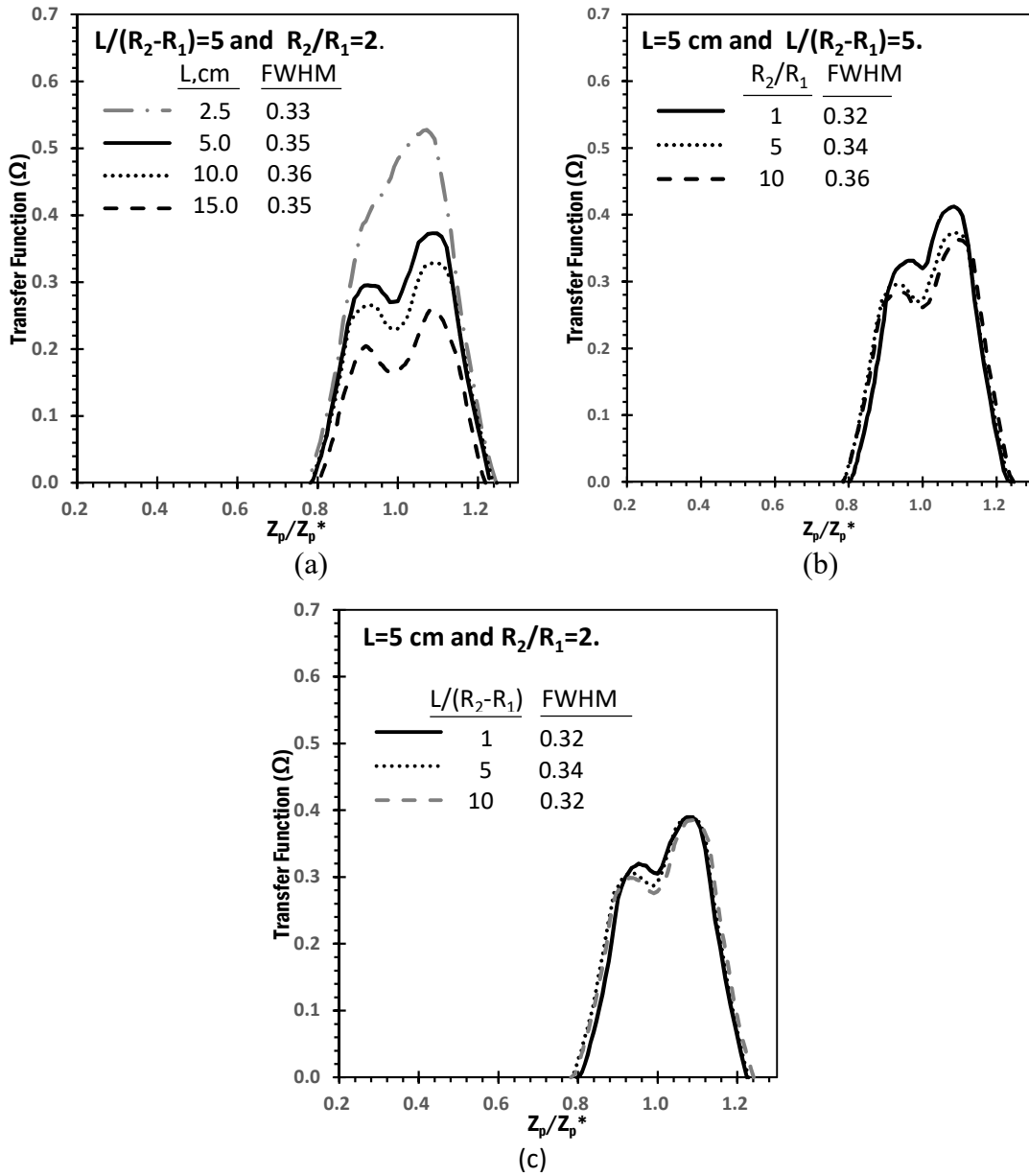


Figure 3. 10 The effect of DMC geometrical parameters on the transfer function of an eccentric DMC; (a) varying particle classification length ( $L=2.5, 5, 10$  and  $15$  cm) of a DMC while keeping the radii ratio and channel aspect ratio constant ( $2$  and  $5$ ); (b) varying the radii ratio ( $R_2/R_1 = 1.2, 2$  and  $4$ ) while keeping the channel length and aspect ratio constant ( $5$  cm and  $5$ ); (c) varying the channel aspect ratio,  $L/(R_2-R_1) = 1, 5$  and  $10$ ) while keeping the channel length and the radii ratio constant ( $5$  cm and  $2$ ). For the reference, the full width at half maximum (FWHM) of shown transfer functions is also given.

### 3.4.6 Effect of particle diffusivity on the eccentric DMC transfer function

Figure 3.11 shows the transfer functions for DMCs with the eccentricity of 0, 1%, 2%, and 5% for particles in the sizes of 5, 10, and 50 nm. The DMCs with the particle classification length of 5 cm were operated at the aerosol and sheath flow rates of 1 and 10 lpm. In all the studied cases, the increase of particle diffusivity reduced the peak and increased FWHM of the DMC transfer functions. It is found that the combinational effects of axial eccentricity and particle diffusivity make the peak and FWHM of the DMC transfer function lower and broader, compared with those observed due to individual effects. In addition, the particle diffusivity smeared the double-peaked transfer functions, making the peak splitting occur at the higher eccentricity. As shown in the figure, the double-peaked transfer function was not observed for the particle size less than 10 nm (which was observed for all the particle sizes without the consideration of particle diffusivity, given in Figure 3.5c) for the same DMC operated under the same flow rate conditions.

### 4.7 Classification of Eccentric DMC transfer function

For a given DMC operated at the fixed rates of aerosol and sheath flows, the shape of the transfer function is varied as the axial eccentricity is increased. An example of such variation of DMC transfer function is shown in Figure 3.12a for the DMC having the  $R_1$ ,  $R_2$ , and  $L$  of 1, 2 and 45 cm, and operated at the aerosol and sheath flow rates of 1 and 10 lpm, respectively. The shape of the transfer function for the concentric DMC is in the triangular (once the electrical mobility,  $Z_p$  was normalized by the central mobility,  $Z_p^*$ ). With the increase of axial eccentricity, the peak of DMC transfer function is decreased, flattened and

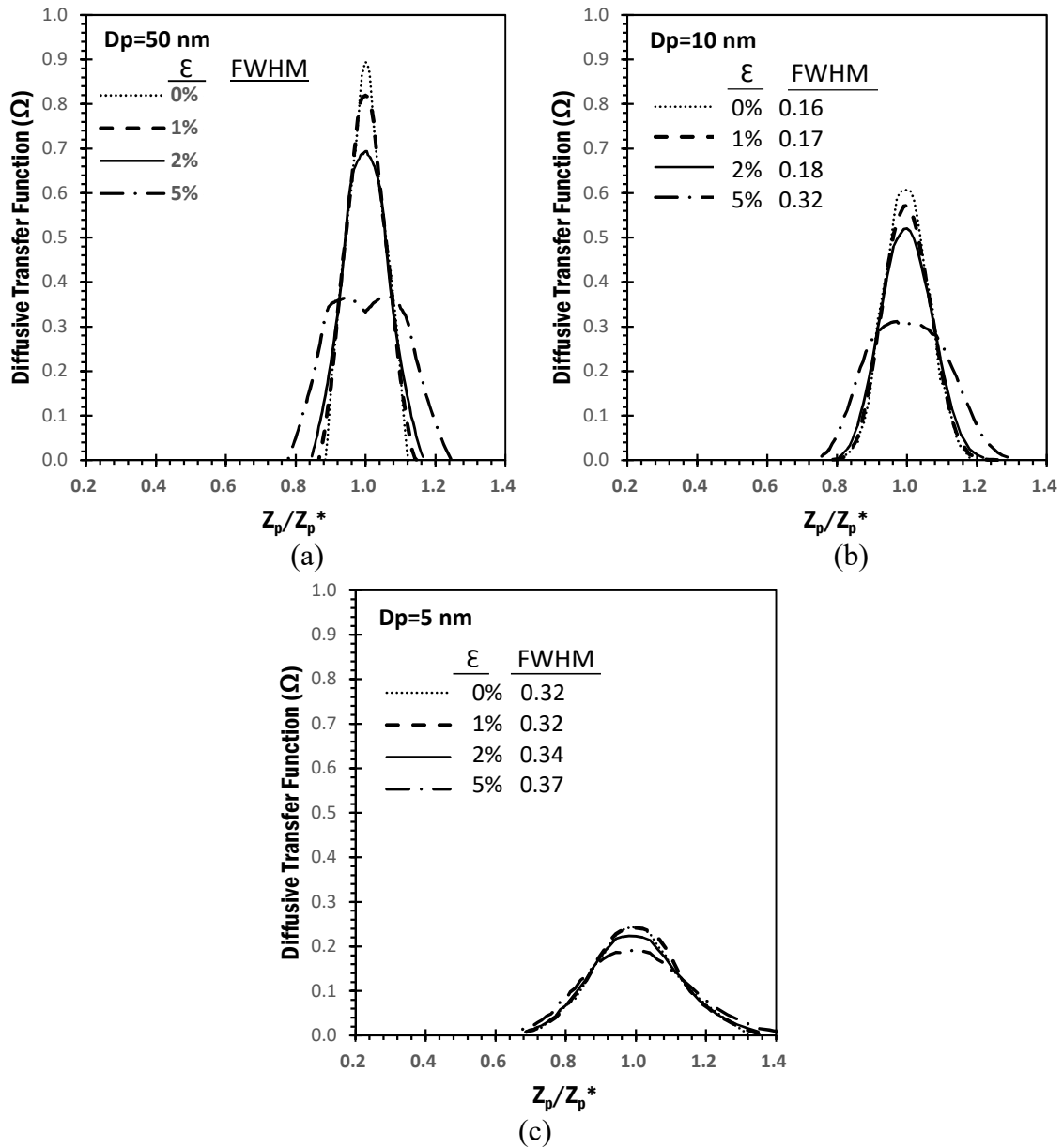


Figure 3. 11 Calculated transfer function of DMCs having the 0%, 1%, 2% and 5% eccentricity for diffusive particles: (a) 50 nm particles; (b) 10 nm particles; (c) 5 nm particles. The studied DMCs have inner and outer radii of 10 and 20 mm, and classification length of 5 cm were operated at the aerosol and sheath flow rates of 1 and 10 lpm, respectively. For the reference, the full width at half maximum (FWHM) of shown transfer functions is also given.

eventually double-peaked. Such shape variation is also dependent on the sheath-to-aerosol flow rate ratio,  $\beta$ . Accordingly, the evolution of transfer function shape for a cylindrical DMC due to the axial eccentricity could be classified into three regions: single-peaked, transient, and double-peaked regions (as shown in figure 3.12b). The determination of transfer function in three regions was based on the slopes at the peak of the transfer function, which are described in the Appendix C, for the reference. From the above figure, it is shown that a DMC is required to have very tight tolerance on the axial eccentricity to well perform the particle sizing measurement in high sizing resolution, especially for the one with long particle classification channel.

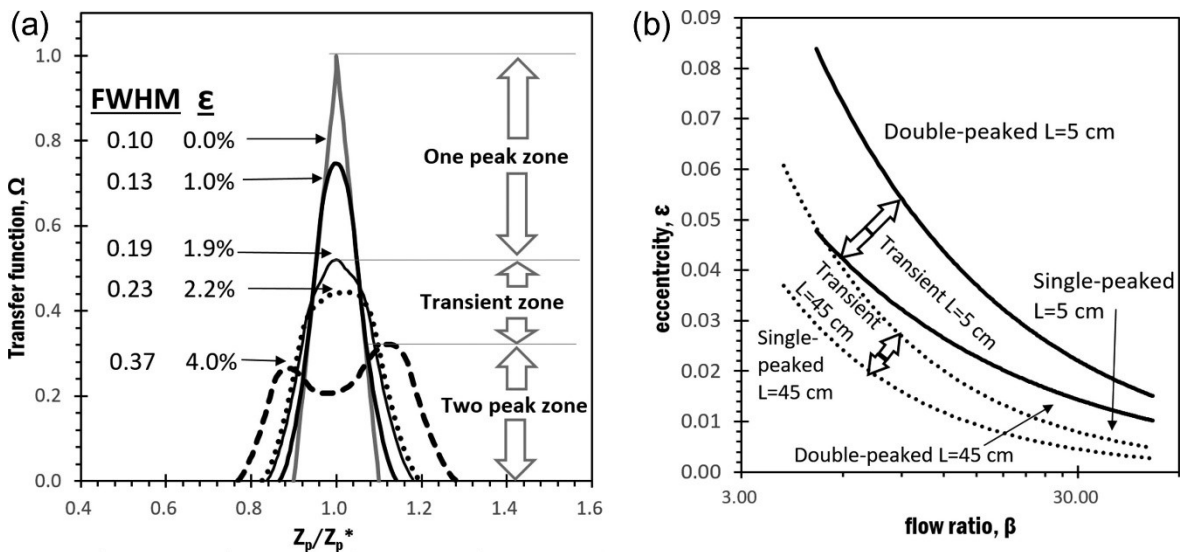


Figure 3. 12 Eccentric DMC transfer function peaks zones (a) The classification of non-diffusive transfer function of eccentric DMCs with inner and outer radii of 10 and 20 mm, and a classification length of 45 cm. The aerosol and sheath flow rates of the DMCs were 1 and 10 lpm, respectively; (b) Three classified zones for eccentric DMC transfer function as the functions of the eccentricity  $\epsilon$  and the flow ratio  $\beta$  for DMCs with the classification lengths of 5 and 45 cm. For the reference, the full width at half maximum (FWHM) of shown transfer functions is also given.

## CHAPTER 4 Inner Rod Tilting / Cylindrical Differential Mobility Classifier <sup>7</sup>

### 4.1 Introduction

The sizing/classification of sub-micrometer-sized particles is primarily accomplished in the aerosol research community by a differential mobility classifier (DMC). DMC differentiates particles based on their electrical mobility. The cylindrical type is predominant among various DMC designs because there is no sidewall presence in the particle classification channel (Müschelborn, 2007). A cylindrical DMC is composed of an inner rod and an outer cylinder coaxially aligned. The annular spacing between the inner rod and outer cylinder defines the particle classification channel, in which the clean sheath gas flows and serves as the barrier for charged particles introduced from the outer cylinder. Having an electrical field set up in the annular channel, charged particles cross the sheath flow barrier and move towards the inner rod. Downstream of the classification channel, a circular exit slit is designed in the inner rod to extract classified particles out from the classification channel. Relative to the exit slit, particles with high electrical mobility are deposited on the upper portion of the rod, and ones with low mobility are either deposited

---

<sup>7</sup> The material of this is chapter is taken from the publication- Alsharifi, T., & Chen (2019), "Effect of Inner Rod Tilting on the Performance of a Cylindrical Differential Electrical Mobility Analyzer (DEMC)," Published online 2019, Aerosol and Air Quality Research <https://doi.org/10.4209/aaqr.2019.01.0037>.

on to the lower part of the rod or carried out of the channel by excess flow. Only particles within a narrow mobility range are extracted from the exit slit.

All the DMCs were designed and constructed with the assumption that the DMC would be perfectly assembled. In reality, the presence of tolerance in the DMC construction often makes it imperfect in the DMC construction. Two types of basic geometrical imperfection have been observed in the DMCs (if not carefully designed/assembled): axial misalignment and tilting of the inner rod relative to the outer cylinder. To the authors' knowledge, limited attention has been paid to investigate the effect of axial misalignment and tilting on the performance of a cylindrical DMC (i.e., transfer function). However, the knowledge on how significantly the geometrical imperfection affects the DMC performance is essential to the DMC design. Intensive investigation on the effect of axial misalignment on the performance of a cylindrical DMC has been presented in chapter 3 of this dissertation. In the work of chapter three, the flow and electrical fields in the annular classification channel of a DMC were considered 2-D (i.e., fully developed for the flow).

However, no study on the effect of axial tilting on the performance of a cylindrical DMC has been reported. Under the axial tilting condition, the flow and electrical fields in the classification channel of a cylindrical DMC are completely in 3D. It is because the cross-section of the flow channel continuously varying along the axial direction of a DMC, resulting in the continuous flow developing in the tilted DMC classification channel. Notice that the flow in the channel of an eccentric DMC will eventually become fully developed so long as the channel length is sufficiently long. The effect of axial tilting on the DMC performance is thus expected to be different from that of axial misalignment (eccentricity).



The objective of this study is thus to investigate the effect of inner rod tilting on the performance of a cylindrical DMC. The numerical modeling approach was again applied in this study. Our modeling of the DMC performance was set up via the combination of COMSOL Multiphysics 5.4<sup>®</sup> and MATLAB R2018a<sup>®</sup>. Prior to the parametric study, the setup model was verified by the comparison of numerical results with theoretical ones (Knutson & Whitby, 1975; Stolzenburg, 2008), and the experimental work of (D. R. Chen et al., 1998b). The parametric study was performed to investigate the effect of geometrical variables on the transfer function of cylindrical DMCs. The studied geometrical and flow variables included the tilting angle, the classification channel length, the outer to inner radii ratio, cross-sectional area, and the aspect ratio (i.e., channel length: hydraulic diameter of the annular spacing). The effect of sheath-to-aerosol flow ratio ( $\beta$ ) on the performance of tilted DMCs was also investigated. Diffusive particles were also considered in this study.

## 4.2 The Numerical Model

Both COMSOL Multiphysics 5.4<sup>®</sup> and MATLAB R2018a<sup>®</sup> Multiphysics were applied to set up the DMC model. A typical computational domain to model the performance of a DMC having the tilted inner rod is shown in [Figure 4.1](#) (a is the side view; and both b and c are the selected cross-sectional views). In this study, we define the DMC inner rod tilting,  $\tau$ , as the ratio of the angle,  $\theta$ , between the axis of the inner rod and the outer cylinder to the maximal tilting angle,  $\theta_m$ , which depends on the inner rod radius,  $R_i$ , outer cylinder radius,  $R_o$ , and the classifying channel length,  $L$ . The formula for the  $\theta_m$  calculation is given in the in the Appendix D. Polydisperse particles flow into the particle classification channel from the particle entrance slit at the outer cylinder, and classified particles leave the channel

from the exit slit at the inner rod. A clean sheath flow enters the classification channel from the top and the excess flow exits the channel from the bottom exit. A high voltage was applied on the inner rod and the outer was electrically ground.

Steady and incompressible Navier-Stokes and continuity equations were applied to calculate the flow field in the classification channel of a DMC. The Laplace equation was used to calculate the electrical potential,  $\phi$ , in the DMC's classification channel. The intensity of the electrical field,  $\vec{E}$ , was derived by  $\vec{E} = -\nabla\phi$ .

For the flow field calculation, the velocity profile at the sheath flow entrance was assumed uniform because the channel flow would not be fully developed in the studied channel (due to the continuous variation of channel cross-section). A uniform velocity profile was assumed at the classified particle exit (because of the installation of the flow straightener) . The pressure boundary condition was set at the excess flow exit. No-slip boundary conditions were applied to all the solid walls in contact with fluid flow. For the electrical field, the inner rod was set at an elevated voltage, and the outer cylinder was on the electrical ground.

The performance of a DMC is characterized by its transfer function, defined as the probability of a particle with a given electrical mobility ( $Z_p$ ) entering the DMC classification region and reaching the classified aerosol exit. The calculation of the transfer function of a DMC for singly charged particles of a given size was based on the particle flux. The detail can be found in the previous chapter and also in the work of Alsharifi and Chen (2019).

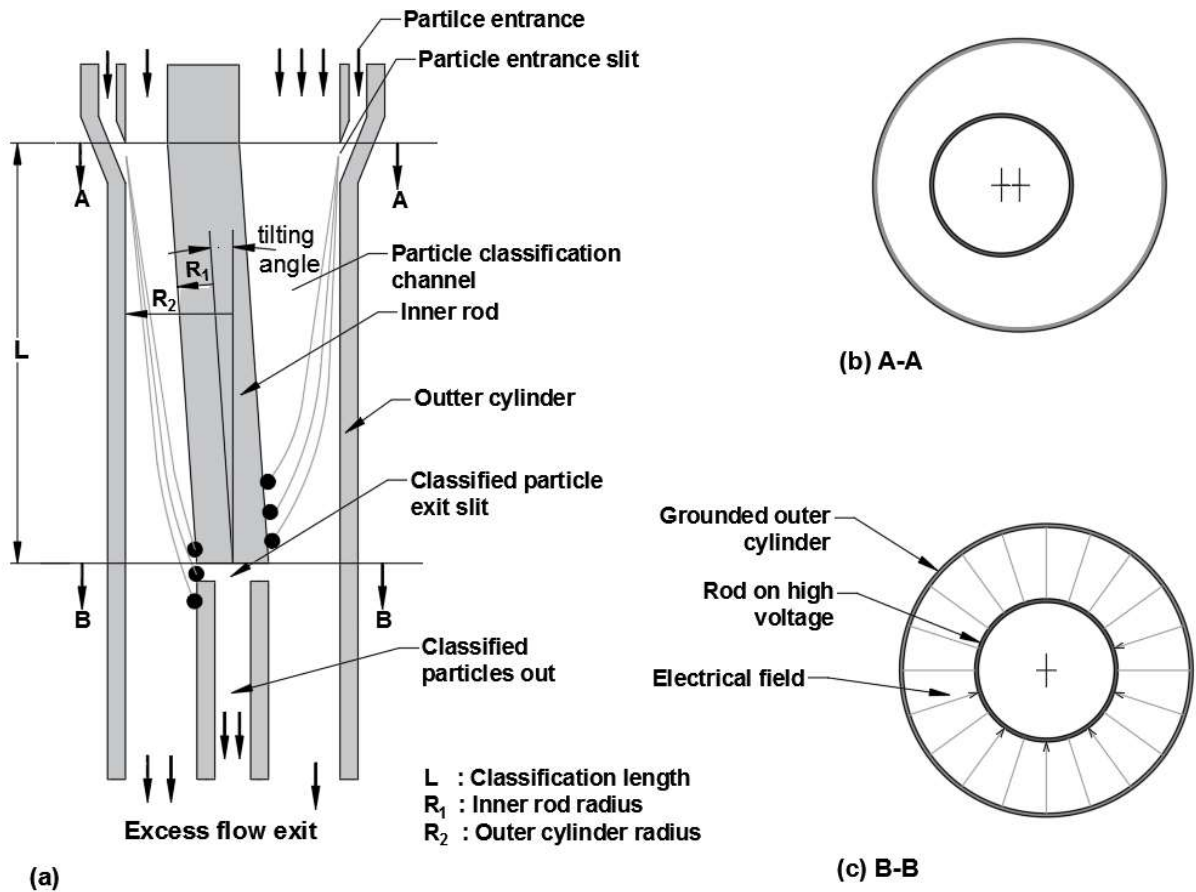


Figure 4. 1 The schematic diagram of a cylindrical differential mobility classifier (DMC) with a tilted inner rod and the computational domain used in the DMC modeling: (a) side view (with the illustration of the particle movement in the classification channel); (b) the cross-sectional view at the location near the particle entrance; (c) the cross-sectional view at the location near the particle exit slit.

Table 4.1 summarizes the values of the physical properties of gas and particles used in our modeling. The effect of axial tilting on the performance of a cylindrical DMC was investigated for particles with the sizes of 3, 4, 5, 10, 50 and 160 nm and under the condition of different sheath-to-aerosol flow rate ratios,  $\beta$ , of 3.33, 4, 5, 6.66, 10, 20 and 50 (i.e., both sheath and particle flow rates were varied in 5-20 lpm and in 0.5-2 lpm, respectively). The particle diffusivity was considered for particles with sizes less than 50 nm. Table 4.2 summarizes the ranges of DMC dimensions studied.

Table 4. 1 Properties of gas and particles utilized in the tilted cylindrical DMC

CONSTANT		VALUES AND FORMULAS
<b>PARTICLE</b>	Diameter, $dp$	5, 10, 50, 160, 340, 815 nm
	Mass density, $\rho_p$	1000 kg/m <sup>3</sup>
	Slip correction factor $C_c$	$C_c = 1 + Kn \left( 1.155 + 0.471 e^{-\frac{0.596}{Kn}} \right)$
	Elementary charge e	$1.602 \times 10^{-19}$ C
<b>AIR</b>	temperature, t	293.15 K
	dynamic viscosity, $\mu$	$18.5 \times 10^{-6}$ N.s/m <sup>2</sup>
	density, $\rho$	1.2047 kg/m <sup>3</sup>
	mean free path $\lambda$	0.066[um]
	Boltzmann constant	$1.38064852e-23$ [J/K]
<b>FLOW</b>	Aerosols inlet and exit flow	0.5-4.0 lpm
	Sheath flow rate range	5.0-20.0 lpm

Table 4. 2 Geometrical dimensions and parameters for tilted cylindrical DMC

GEOMETRICAL PARAMETER	RANGE
Inner cylinder radius $R_1$	0.5-2 [cm]
Outer cylinder radius $R_2$	1.2-4 [cm]
Channel length L	5-45 [cm]
Radial ratio ( $R_2/R_1$ )	2-4
Aspect ratio ( $L/R_1$ )	2.5-10

## 4.3 Result and Discussion

### 4.3.1 Distorted flow and electrical fields in a tilted DMC classifying channel

Figure 4.2 shows a distorted flow field in the particle classification channel of a cylindrical DMC having the inner rod tilted. For better visualization, the DMC with 50% inner rod tilting was selected. Because of the tilting of the inner rod, the channel cross-

section is varied along the primary flow direction. The selected DMC, operated at the particle and sheath flow rates of 1 and 10 lpm, has the inner rod and outer cylinder radii of 1 and 2 cm, respectively and the channel length of 12 cm. The side view of the DMC classification channel illustrates the convergent (left) and divergent (right) spacing on both sides of the inner rod. [Figure 4.2a](#) gives the axial flow velocity profiles along the convergent and divergent spacing. As expected, in each spacing, the axial flow was developing to a parabolic-like one (having the maximal axial velocity). [Figure 4.2b](#) plots the axial velocity contours at two selected cross-sections (i.e., section A-A near the flow entrance and section B-B near the flow exit). Because of uneven spacing on both sides of the inner rod, the location of maximal axial velocity shifted from the narrowest gap to the widest gap. It is because the pressure drop is higher for the flow moving in the narrow gap as compared to that in the wide gap.

[Figure 4.2c](#) shows the radial and circumferential velocity vector fields at two selected cross-sections, A-A and B-B (at the same levels as those in [figure 4.2b](#)). Note that, for the illustration, the magnitude of shown velocities was magnified 70 times. At the A-A section, the velocity is primarily in the radial direction because of flow developing from the uniform profile to the parabolic-like one. At the B-B section, the circumferential velocity component became more obvious compared to that at the A-A section. It is because of the flow moving toward the wider gap (due to lower pressure drop for axial flow). As the axial flow increased in the wide gap and decreased in the narrow gap, the secondary flow at each cross-section of the DMC classification channel was then developed.

Figure 4.3 illustrates the distorted electrical field at the cross-section located at the middle level of the DMC classification channel. Because of the uneven gap in the circumferential direction of the classification channel (due to the inner rod tilting), the electrical potential was intensified in the narrow gap compared to that in the wide spacing.

### 4.3.2 Transfer function of a DMC having a tilted inner rod

Figure 4.4 shows the transfer function of a cylindrical DMC having a tilted inner rod at various tilting values (0%, 2%, 5%, 6%, 7%, and 10%), defined as the ratio of actual tilting angle to the maximal angle. The DMC, operated at the particle and sheath flow rates of 1 and 10 lpm, has the inner rod and outer cylinder radii of 1 and 2 cm, respectively and the channel length of 25 cm. The shape of the transfer function for the 0% tilting (i.e., non-tilted DMC) is triangular (once the electrical mobility,  $Z_p$  was normalized by the central mobility,  $Z_p^*$ ). With the increase of inner rod tilting, the peak of the DMC transfer function was decreased, flattened, and eventually double-peaked. In conjunction with the peak change, the full width at half maximum (FWHM) was increased as the inner rod tilting was increased. The deterioration of the transfer function could be explained by understanding the particle fate near the exit slit of the classification channel of studied DMC.

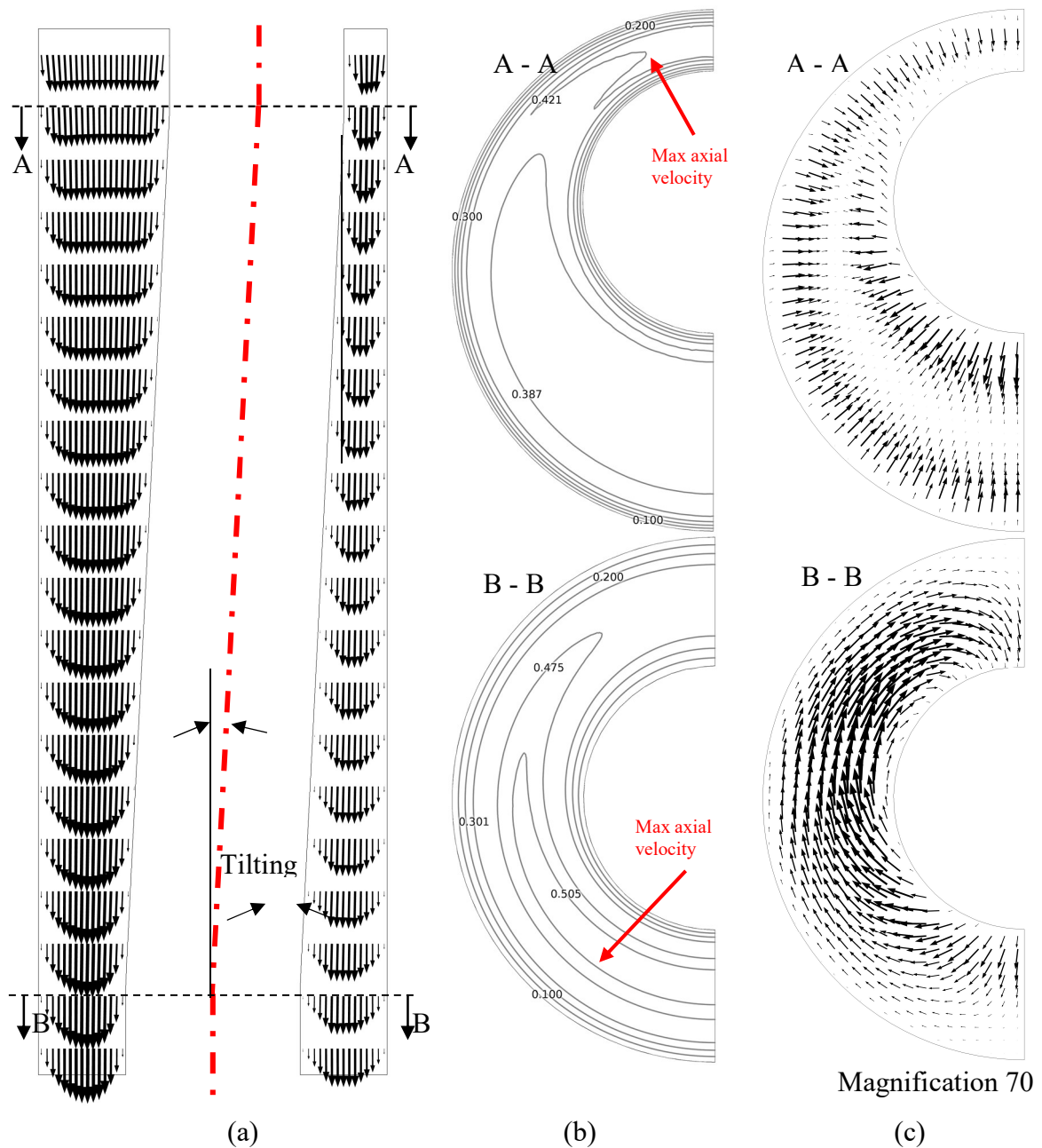


Figure 4. 2 The illustration of the flow field in the classification channel of a cylindrical DMC having the outer and inner cylinder radii of 1 and 2 cm, respectively, and a 12 cm in length. The tilting of inner rod is 50% tilting and the DMC is operated at the sheath flow rate of 10 lpm. The selected cross-sections A-A, and B-B are located at the 1, and 11 cm, respectively, measured from the sheath flow entrance: (a) the side view showing the axial velocity profiles along the classifying channel; (b) Cross-sectional view showing of velocity contours of the sheath flow axial velocity; (c) Cross-section view showing of the circumferential velocity of sheath flow (with the magnification of 70).

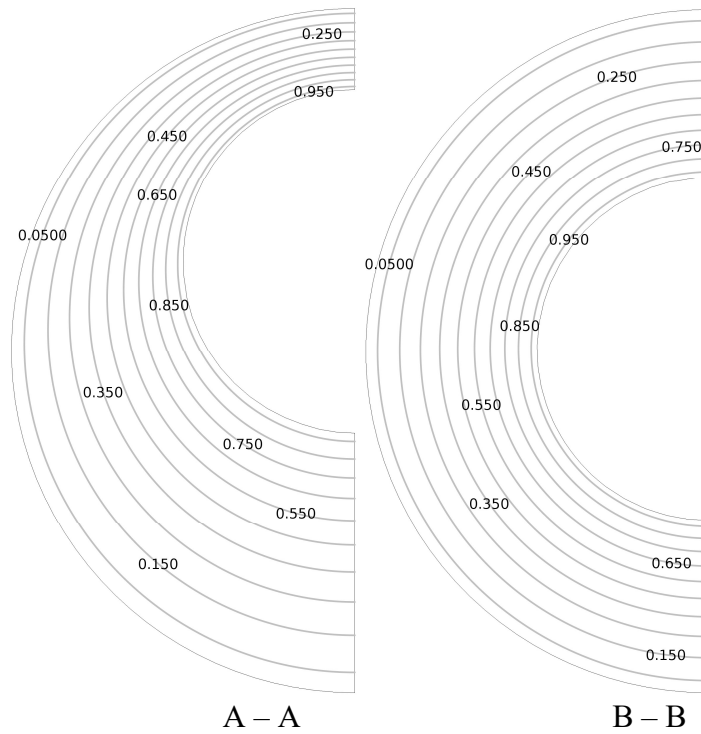


Figure 4. 3 The illustration of the electrical potential contours (normalized with the voltage applied on the inner rod) located at the middle location of the classification channel of a cylindrical DMC having the outer and inner cylinder radii of 1 and 2 cm, respectively, a 12 cm in classification length, and a 50% inner rod tilt.

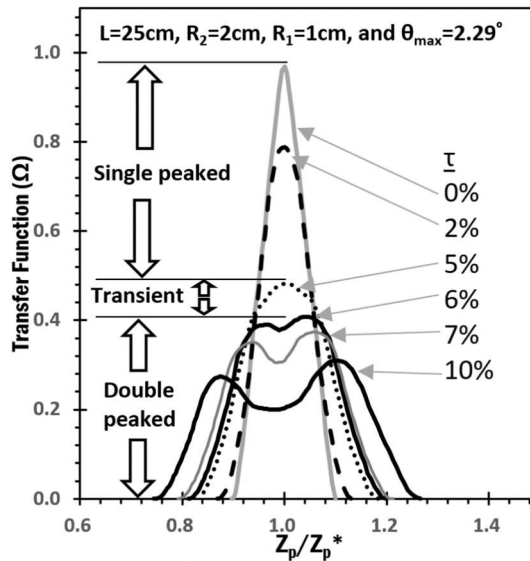


Figure 4. 4 The variation of the non-diffusive transfer function of tilted cylindrical DMCs having the inner and outer radii of 10 and 20 mm, and classification length of 5 cm as the function of inner rod tilting. The aerosol and sheath flow rates of DMCs were 1 and 10 lpm, respectively;



Figure 4.5 shows the particle fate near the exit slit of a DMC with a tilted inner rod after particles were released from the particle entrance slit. The abscissa of figure 4.5 is from 0 (for the narrowest gap in the DMC classification channel) to  $\pi$  (for the widest gaps), and reaching to  $2\pi$  which periodically returning to the same coordinate point of 0. Because of the variation of particle traveling distance after entering the classification channel, the particle position when moving close to the classified particle exit slit was varied at different angles. Only particles reaching the region nearby the particle exit slit (between two solid lines plotted in the figure) are expected to exit the classification channel. As shown in figure 4.5, the location variation of particles in the neighborhood of the exit slit was increased with the increase of inner rod tilting, resulting in the increase of particle loss in the classification channel. The variation status of particle position nearby the classified particle exit slit also depended on the electrical mobility of particles: less variation for particles with high electrical mobility compared to that for ones with low electrical mobility. It is why the peak in the low mobility range is lower than that in the high mobility range once the peak of the transfer function is split.

It is believed that both the flow and electrical field distortion in the particle classification channel of a DMC with tilted inner rod contributed to the deterioration of the transfer function. In this part of the study, we would like to identify the dominant factor influencing the shape of the DMC transfer function. Figure 4.6 shows the transfer functions calculated with the assumptions of uniform velocity profiles at the sheath flow entrance only and in the entire classification channel for a cylindrical DMC with the relative tilting of 5%

and 10%, operated at the aerosol and sheath flow rates of 1 and 10 lpm, respectively. The particle classification length of studied DMCs was 5 cm and the particle size was 160 nm. The difference between the two calculated transfer functions could be attributed to the effect of flow field distortion. By comparison, it is found that the shape and peak split of the transfer function for a DMC with a tilted inner rod is primarily due to the distortion of the electrical field. The distortion of the flow field makes the width of the transfer function broader.

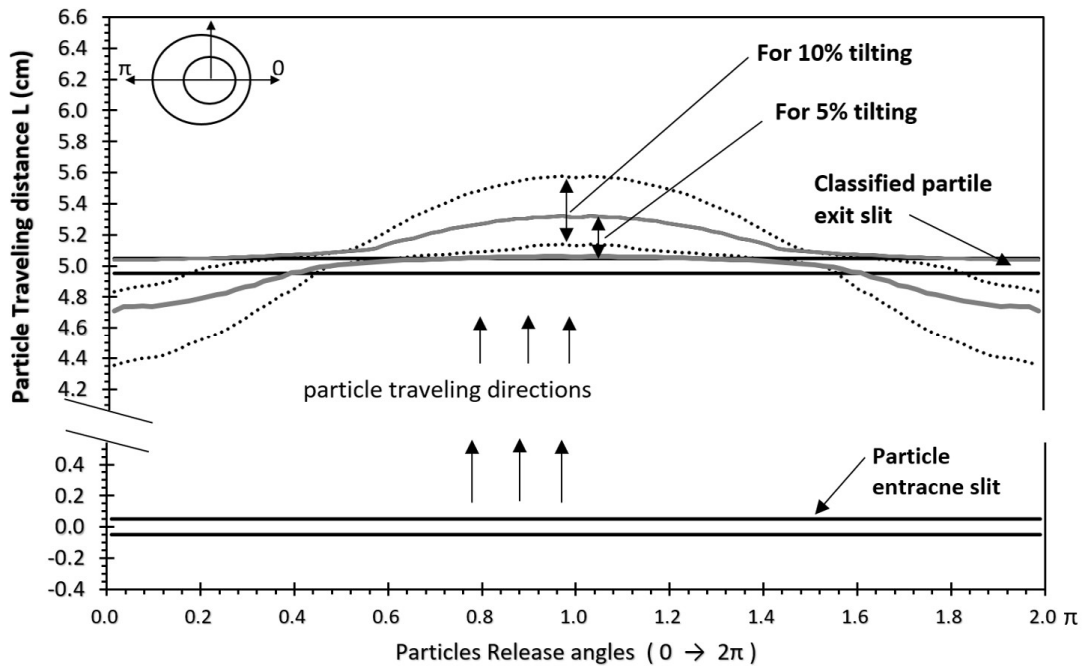


Figure 4. 5 The position of particles in the neighborhood of classified particle exit slit after they were released from the particle entrance slit of the DMCs with 5% and 10% inner rod tilting. The DMCs have the classification length of 5 cm, and inner rod and outer cylinder radii of 1 and 2 cm, respectively (operated at the aerosol and sheath flow rates of 1 and 10 lpm, respectively).

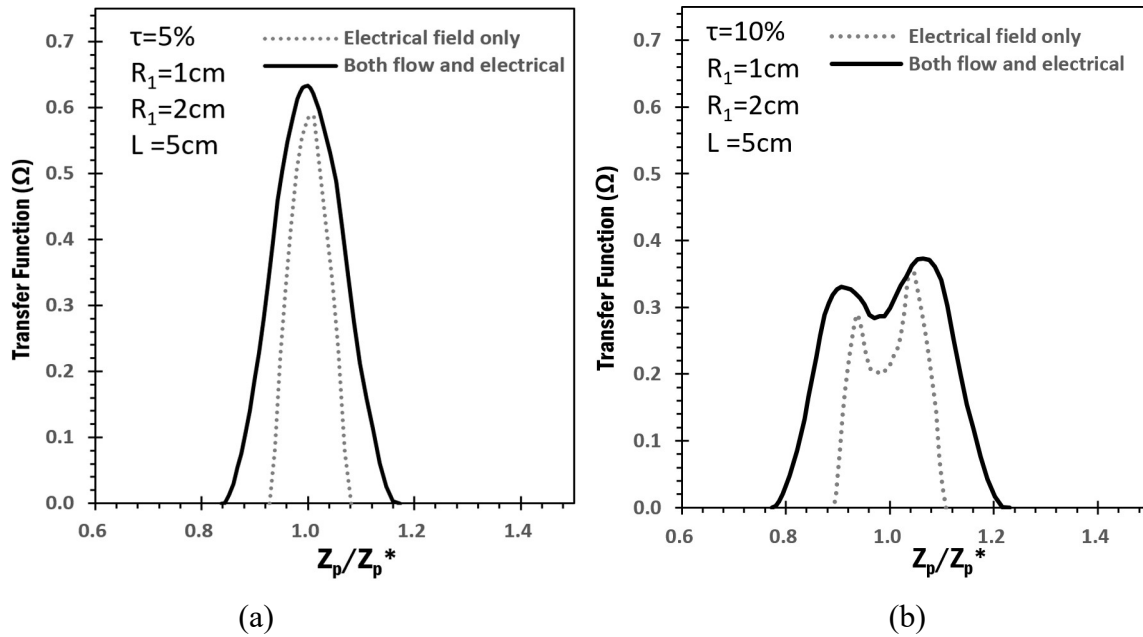


Figure 4. 6 The effect of the electrical field vs. the combined effects of flow and electrical field for the DMC numerical transfer function having the inner and outer cylinder radii of 10 and 20 mm, respectively, and the classification length of 5 cm. The aerosol and sheath flow rates of studied DMCs were 1 and 10 lpm, respectively: (a) for the 5% inner rod tilting, and (b) for the 10% tilting.

### 4.3.3 Tilted DMC transfer function at different sheath-to-aerosol flow rate ratios and total flow rates

The effect of sheath-to-aerosol flow rate ratio ( $\beta$ ) on the transfer function of a DMC having a tilted inner rod was investigated. The studied DMC with the 10% tilting has the classification length of 25 cm, and the inner and outer cylinder radii of 10 and 20 mm, respectively. [Figure 4.7a](#) shows the numerical transfer functions of studied DMCs, operated at  $\beta = 5, 10$  and 20. It is noticed that the effect of inner rod tilting on the transfer function of a DMC is more pronounced when operated at a high sheath-to-aerosol flow rate ratio (i.e., at high sizing resolution power) as compared with that at low  $\beta$ .

Figure 4.7b shows the numerical transfer function of a cylindrical DMC with the 10% inner rod tilting and the particle classification length of 25 cm (operated at the sheath-to-aerosol flow rate ratio of 5 under different total flow rates). It is found that the reduction of total flow rate, while keeping the sheath-to-aerosol flow rate ratio constant, increased in the particle loss, resulting in the reduction of the transfer function. It is because of flow velocity reduction at the classified particle exit slit (to overcome the electric force for exiting).

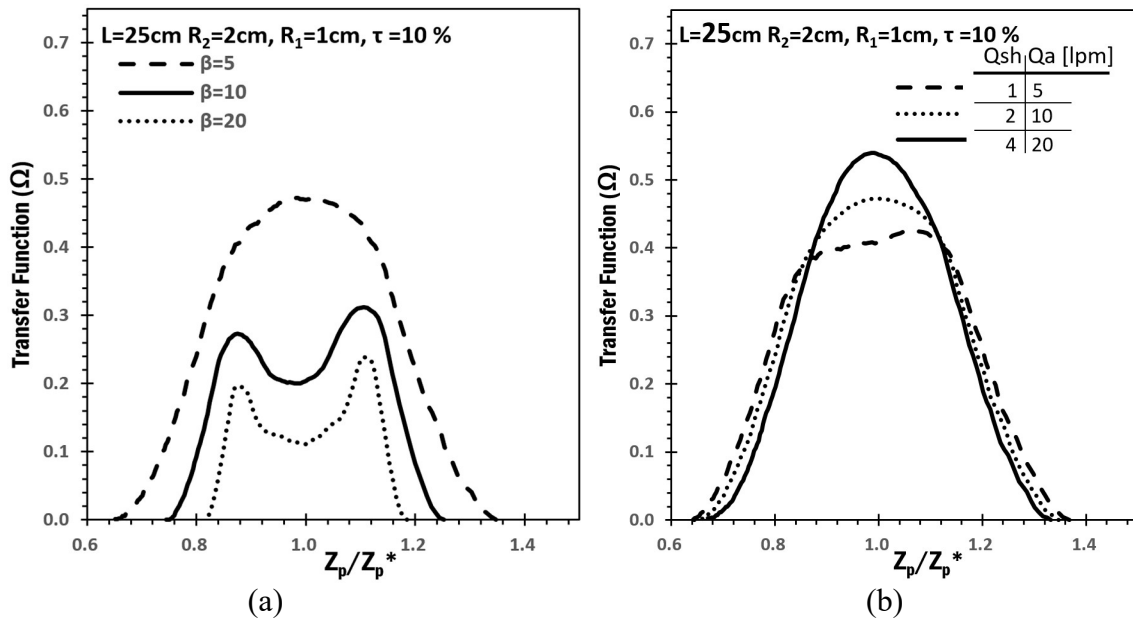


Figure 4. 7 Tilted DMC transfer function at different flow rate ratios and total flow rates (a) The variation of transfer function of a DMC with 10% inner rod tilting at the sheath-to-aerosol flow rate ratios,  $\beta$ , of 5, 10, 20 (for sheath flow rate of 10 lpm and particle flow rate of 2, 1, and 0.5, respectively); (b) The variation of transfer function of the above DMC operated at different total flow rates while keeping the  $\beta$  value at 5.

#### 4.3.4 Effect of the geometrical parameters of classification channel on tilted DMC transfer function

The classification channel of a cylindrical DMC can be characterized by the inner rod and outer cylinder radii of  $R_1$  and  $R_2$ , respectively, and the length,  $L$ . It is beneficial to generalize our results by studying the effect of two dimensionless factors, i.e., the ratio of outer cylinder to the inner rod radii,  $R_2/R_1$ , and the aspect ratio of the inner rod,  $L/R_1$  on the tilted DMC transfer function. Note that the selection of the above two parameters was because they define the maximal tilting in a DMC having a tilted inner rod (given in appendix D).

Figure 4.8a gives the numerical transfer functions for the DMCs with 10% inner rod tilting, the particle classification length of 5 cm, and radii ratios of 2, 3, and 4 (for the radii ratios  $R_2/R_1$  of 2:1, 3:1 and 4:1 cm, respectively). The particle and sheath flow rates applied in the studied DMC were 1 and 10 lpm. It is evidenced that, for the same tilting, the increase of the radii ratio (leading to the increase of the cross-sectional area of classification channel and actual tilting angle) decreased the height of tilted DMC transfer function. Figure 4.8b presents the calculated transfer functions of DMCs with the 10% tilting, particle classification length of 5 cm, and radii ratio of 2 while varying the rod aspect ratios (i.e., 2.5, 5, 7.5, and 10). It is found that the effect of the rod aspect ratio on the tilted DMC transfer function was negligible at the rod aspect ratio higher than 5 for given flow rates. However, at the low rod aspect ratio of 2.5, the height of the transfer function is significantly lower than those at higher aspect ratios. It is because, at the low rod aspect ratio, the actual inner

rod tilting angle was larger than those at high rod aspect ratio for the same tilting defined herein.

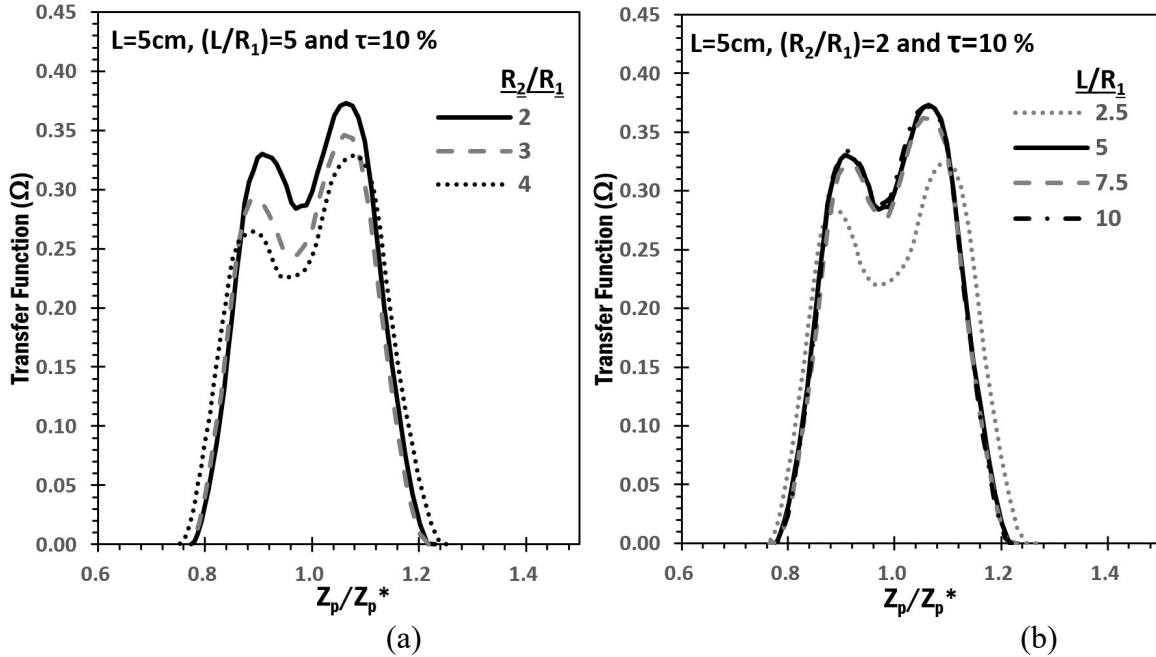


Figure 4. 8 The effect of DMC geometrical parameters on the transfer function of DMCs with 10% tilted inner rods while keeping the particle classification length of 5cm: (a) by varying the radii ratios,  $R_2/R_1$  of 2, 3 and 4) while keeping the rod aspect ratio,  $L/R_1$  of 5; (b) by changing the rod aspect ratio,  $L/R_1$  of 2.5, 5, 7.5 and 10 while keeping the radii ratio of 2. Studied DMCs were operated at the aerosol and sheath flow rates of 1 and 10 lpm.

#### 4.3.5 Effect of particle diffusivity on the tilted DMC transfer function

Figure 4.9 shows the transfer functions for DMCs with the 10% tilting for particles in the sizes of 5, 10, and 50 nm. The DMCs with the particle classification length of 5 cm were operated at the aerosol and sheath flow rates of 1 and 10 lpm. For each particle size, the tilted DMC transfer functions with and without the consideration of particle diffusivity were calculated. It is clearly shown that the increase of particle diffusivity further reduced the peak and broadened the full width at half maximum (FWHM) of the tilted DMC transfer

functions. Moreover, the particle diffusivity smeared out the peak splitting of the DMC transfer function.

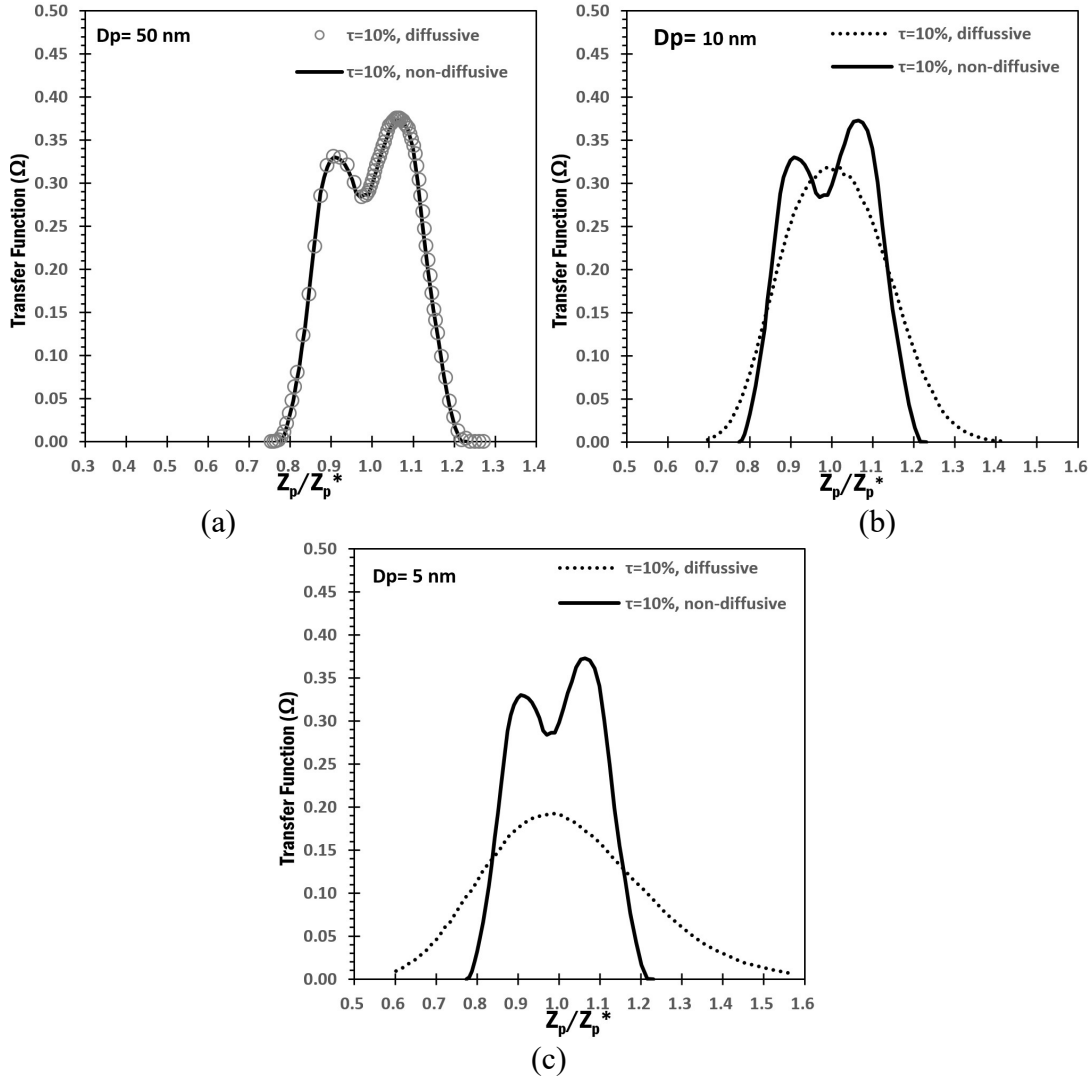


Figure 4.9 Comparison of non-diffusive and diffusive transfer functions for the 10% rod-tilted DMC. The DMC operated at the sheath and aerosols flow of 10 and 1 lpm respectively, has a classification length of 5cm,  $R_1$  of 1 cm and  $R_2$  of 2cm.

#### 4.3.6 Classification of the tilted DMC transfer function

For a given DMC operated at the fixed rates of particle and sheath flows, the shape of the transfer function is varied as the inner rod axis tilting is increased (as shown in figure 4.4). The shape variation of the DMC transfer function depends on both the sheath-to-aerosol

flow rate ratio and the length of the classification channel. Accordingly, the evolution of transfer function shape for a cylindrical DMC due to the inner rod tilting could be classified into three regions: single-peaked, transient, and double-peaked. Figure 4.10a shows the change of the single-peaked, transient and double-peaked transfer function regions as the function of classification channel length for a DMC operated at the  $\beta$  value of 10. Figure 4.10b shows the change of the aforementioned transfer function regions as the function of the sheath-to-aerosol flow rate ratio,  $\beta$ , for a DMC with the classification length of 25 cm. Note that the studied DMC has the inner rod and outer cylinder radii of 10 and 20 mm. It is evidenced in figure 4.10 that the tilting of the inner rod shall be tightly controlled for a cylindrical DMC having a long classification channel length and operated at a high sheath-to-aerosol flow rate ratio (for high sizing resolution).

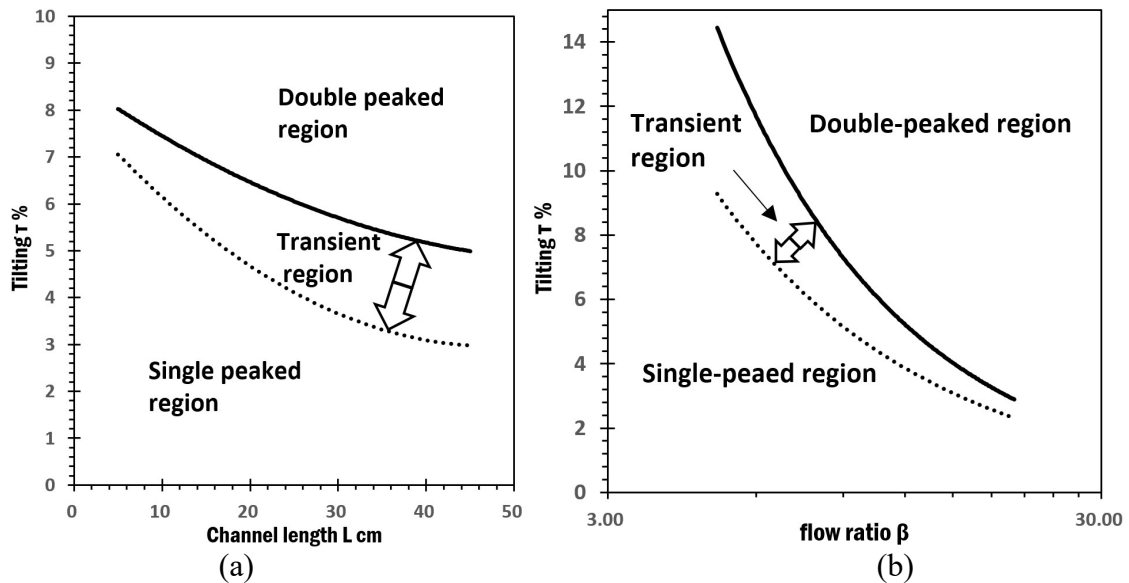


Figure 4. 10 The rods tilted DMCs transfer functions peaks regions with: (a) mapped on the tilting vs. classification length,  $L$  domain for DMCs, operated at the  $\beta$  value of 10; and (b) mapped on the tilting vs. sheath-to-aerosol flow rate ratio,  $\beta$ ., domain for DMCs with the classification length of 25 cm. All the studied DMCs have the inner rod and outer cylinder radii of 10 and 20 mm, respectively.



## CHAPTER 5 Parallel Plates Differential Mobility Classifier <sup>8</sup>

### 5.1 Introduction

Differential mobility classifiers (DMCs) have been used in the aerosol community to size and classify fine and ultrafine aerosol particles in a narrow size range (Flagan, 1998). A typical DMC has two inlets for polydisperse aerosol stream and clean sheath flow and two outlets for classified aerosol stream and excess flow. The performance of DMCs is characterized by the transfer function, defined as the probability of particles, with certain electrical mobility, passing through the device. DMCs are mostly designed either in the cylindrical, radial or parallel-plate configurations. The design of an early DMC is in fact in the parallel-plate configuration (Erikson, 1921). The focus of the DMC design later shifted to the cylindrical configuration to avoid the undesired side-wall effect encountered in parallel-plate DMCs (Hewitt, 1957; E. O. Knutson & Whitby, 1975). The development of parallel-plate DMCs had not made significant progress since the commercialization of the cylindrical DMC, originally designed by Particle Technology Laboratory, University of Minnesota (Intra & Tippayawong, 2008; Whitby & Clark, 1966). The cylindrical DMC has become the standard instrument for sizing and classifying particles in the sub-micrometer and nanometer size range. Recently, parallel-plate DMCs have regained the attention of

---

<sup>8</sup> The material of this chapter is taken from the publication-Alsharifi, T., & Chen, D.-R, (2018) "On the Design of Miniature Parallel-Plate Differential Mobility Classifiers," *Journal of Aerosol Science*, Published online on Volume 121, July 2018, Pages 1-11: <https://doi.org/10.1016/j.jaerosci.2018.04.003>

aerosol scientists in the characterization of ions, macromolecules or single-digit nanoparticles by coupling them with atmospheric pressure ionization (API)-mass spectrometers (MS) or molecular analyzers (de la Mora, et al, 2006). This because of the uniform electric field in the particle-sizing zone of a parallel-plate DMC and its low manufacturing cost compares to the cylindrical DMC design. The uniform electric field in the classification zone is believed to result in less broadening on the DMC transfer function due to the particle diffusivity (Alonso & Endo, 2001). The performance of a high-resolution parallel-plate DMC has been investigated both experimentally and theoretically (Santos, Hontañón, Ramiro, & Alonso, 2009). A parallel-plate DMC has also be applied to measure air ions generated by corona discharge and  $^{241}\text{Am}$  radiation source (Alonso, et al, 2009). Various parallel-plate DMCs had been proposed to couple with commercial API-MS (atmospheric pressure ionization mass spectrometers) for nanoparticle sizing, ion spectra measurement, and detecting of VOC (volatile organic compound) molecule (Pomareda et al., 2013; Rus et al., 2010). A parallel plate DMC with multiple electrometers (instead of having a classified particle exit), named as cross-flow ion mobility spectrometer, had been evaluated to characterize atmospheric ions (M. Zhang & Wexler, 2006). Notice that relatively high sheath flow rates (typically above 1000 lpm) were used in these developed DMCs. For example, the sheath flow rates of above 1000 lpm were used in the DMCs, described in the work of Rus et al (2010), with the flow channel cross-section of 1-2  $\text{cm}^2$ . Another DMC with the flow channel cross-sectional area of 0.25  $\text{cm}^2$  was operated at a sheath flow rate of 100–800 lpm, reported by the study of Pomareda, et al.,(2013).

For their relatively low cost in manufacturing, compact/miniature parallel-plate DMCs have been designed and their performance experimentally evaluated cost-effective electrical-mobility-based ultrafine particle sizers (Q. Liu & Chen, 2016a, 2016b; Steer et al., 2014). Different from the high-flow rate parallel-plate DMCs, these compact/miniature parallel-plate DMCs were typically operated at much low sheath flow rates (usually less than 5.0 lpm). A compact multi-electrode parallel-plate DMC with the feature of ESP (electrostatic precipitation) has also been proposed for submicrometer particle characterization in the work of (Ranjan & Dhaniyala, 2008).

In addition to the hardware development, the 2-D theoretical models have been reported to estimate the performance of parallel-plate DMCs/EAAAs, i.e., transfer function, for non-diffusive or diffusive particles (Rus et al., 2010), and (Q. Liu & Chen, 2016b).

Although much work was carried out to develop parallel-plate DMCs, the general design guideline for compact/miniature ones, i.e., the effect of geometrical parameters on parallel-plate DMCs on the transfer functions, has not been established yet.

Although both experimental and theoretical work has been carried out for parallel-plate DMCs, the general design guideline for compact/miniature parallel-plate DMCs has not been established yet. The understanding of the effect of design parameters of particle classification channel on the transfer function of compact parallel-plate DMCs, operated at a low sheath flow rate, will set up the foundation for the future design guideline.

Thus, the objective of this study is to investigate the effect of channel design variables on the performance of compact/miniature parallel-plate DMCs. Numerical modeling was applied to this work. Our modeling of the DMC performance was set up via

the combination of COMSOL Multiphysics 5.3<sup>®</sup> and MATLAB R2016a<sup>®</sup>. Prior to the parametric study, the modeling was verified by the comparison of numerical results with experimental data reported in the work of Liu and Chen (2016b). The studied design variables included the cross-sectional area and aspect ratio of particle classification channel, the opening percentages of aerosol inlet and exit slits (relative to the full width of classification channel), and aerosol injection angle. In the following sections, we will first present the modeling of parallel-plate DMCs and model validation. The effect of studied parameters on the DMC's transfer function will be shown in the section of Results and Discussion.

## 5.2 The Numerical Model

Both MATLAB R2016a<sup>®</sup> and COMSOL Multiphysics 5.3<sup>®</sup> were applied to set up the DMC modeling and to perform the parametric investigation. [Figure 5.1](#) shows the schematic diagram of the computational domain used to model a mini-plate DMC. [Figure 5.1a](#) and [5.1b](#) give both side and top views of the model, respectively. The cross-section of the DMC's particle classification channel is typically in the rectangular shape (as constructed by the top and bottom plates, and two side walls). Polydisperse aerosol flows into the particle classification channel from the top aerosol inlet slit and the classified aerosol particles leave the channel from the bottom exit slit. A clean sheath flow enters the classification channel from the left inlet and the excess flow exits it from the right outlet. A high voltage is applied on the bottom plate and the top plate is electrically ground. To minimize the side-wall effects on the DMC performance, the aerosol inlet and exit slits were typically partially opened relative to the full width of the DMC's classification channel.

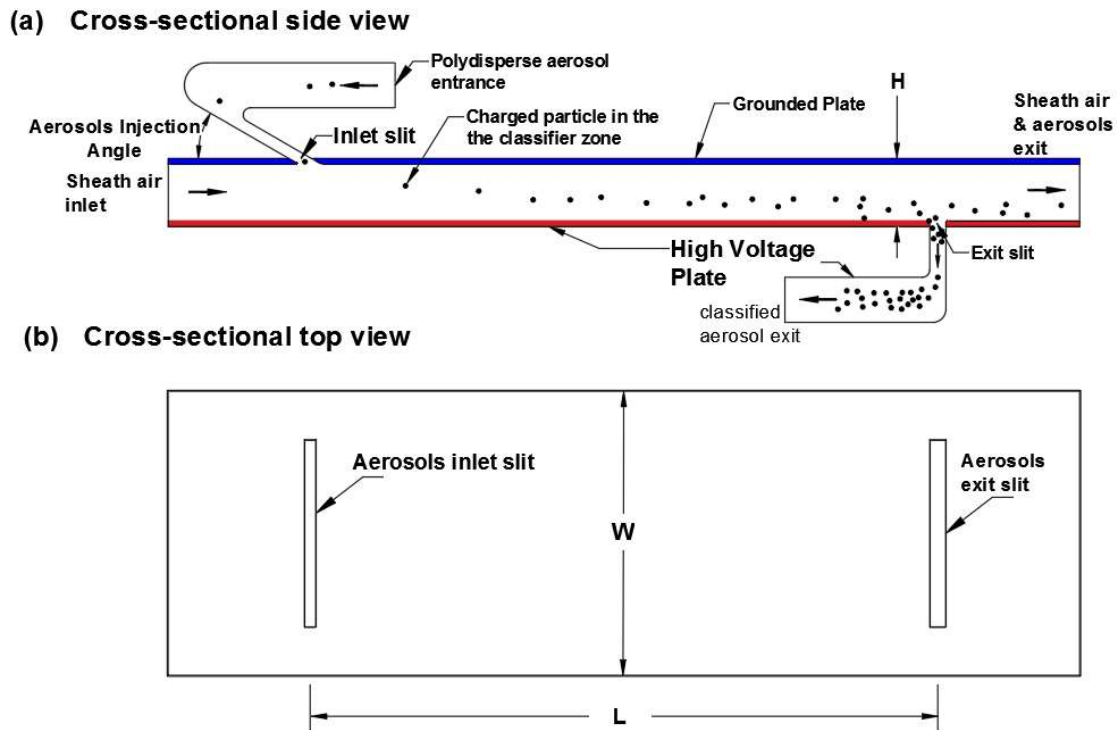


Figure 5. 1 The schematic diagram of the computational domain for the plates DMC modeling (a) side cross-sectional view (illustrating the particle movement in the classification channel); (b) top cross-sectional view.

Because all the DMCs are required to operate in the laminar flow condition, steady and incompressible Navier-Stokes and continuity equations were applied to calculate the flow field in the classification channel of a mini-plate DMC. The Laplace equation was used to calculate the electrical potential,  $\phi$ , in the DMC's particle classification channel. By knowing the electric potential in the classification, the electrical field,  $\vec{E}$ , was then derived by  $\vec{E} = -\nabla\phi$ .

As for the boundary conditions for the flow field calculation, uniform velocity profiles were assumed at both the polydisperse aerosol inlet and sheath flow entrances. A fully developed velocity profile was assumed at the classified aerosol and excess flow exits (Tanyeri et al., 2011). No-slip boundary conditions were applied to all the solid walls in

contact with fluid flow. For the electrical field, the bottom plate was at an elevated voltage, and the top plate was at the electrical ground.

The performance of a DMC is characterized by its transfer function, defined as the probability of a particle with given electrical mobility entering the DMC classification region and reaching the classified aerosol exit (Knutson & Whitby, 1975). To calculate the transfer function of a DMC for particles of a given size, we partitioned the cross-section of polydisperse aerosol entrance into meshes. A representative particle was released from the centroid of a mesh. Note that in the cases having a circular aerosol inlet, representative particles were released from the grids distributed based on the grid design scheme given in the works of Masset, Bruls, and Kerschen (2011) and Beckers and Beckers (2012). The trajectory of presentative particles was calculated and the fate of released particles was recorded. With the assumption of uniform particle concentration at the aerosol entrance, the transfer function of a DMC was calculated as

$$\Omega = \frac{\sum_1^m w_i A_i}{\sum_1^l w_i A_i} \quad (5.1)$$

where  $\Omega$  is the numerical transfer function of a DMC;  $l$  is the total number of particles released from the polydisperse aerosol entrance;  $m$  is the total number of particles reaching the classified particle exit;  $w_i$  is the gas flow velocity at the released particle location; and  $A_i$  is the mesh area associated with the released particle,  $i$ .

The trajectory of a singly-charged particle in a DMC is computed via Newton's second law.

$$\frac{d(m_p \vec{V}_p)}{dt} = \vec{F}_t \quad (5.2)$$

where  $m_p$  is the particle mass,  $\vec{V}_p$  is the particle velocity, and  $\vec{F}_t$  is the total force acting on the particle, including the flow drag and electrical forces

$$\vec{F}_t = \vec{F}_{Drag} + \vec{F}_{electric} \quad (5.2a)$$

$$\vec{F}_{Drag} = \frac{3\pi\mu D_p(\vec{V}_p - \vec{U})}{C_c} \quad (5.2b)$$

$$F_{electric} = en\vec{E} \quad (5.2c)$$

where  $\mu$  is air dynamic viscosity at room temperature,  $D_p$  is the particle diameter,  $\vec{V}_p$  is particle velocity,  $\vec{U}$  is air velocity,  $C_c$ : the Cunningham slip correction factor (Pramod et al., 2011),  $e$  is elementary charge, and  $n$  is the number of elementary charges on a released particle, which was assumed to be one in this work.

[Table 5.1](#) summarizes the values of the physical properties of gas and particles in our modeling. Particles of 100 nm in diameter were selected in this study because the objective of this work is to investigate the effect of channel design parameters on the performance of a compact parallel-plate DMC. The effect of particle diffusion on the DMC performance is not under consideration.

The studied channel design parameters include the aspect ratio (i.e., the ratio of channel width-to-height) and the total cross-sectional area of the DMC particle classification channel, the opening percentage of both aerosol inlet and exit slits (relative to the full channel width), the aerosol injection angle, and the sheath-to-aerosol flow rate ratio ( $\beta = Q_{sh}/Q_a$ ). For this investigation, the aspect ratio of the classification channel was varied from 1 to 20, and the opening percentages of aerosol inlet and exit slits were changed from 10% to 100%. Aerosol inlets in both rectangular and circular shapes were also considered. The

aerosol injection angle was varied from 5° to 90°. The sheath-to-aerosol flow rate ratio ( $\beta$ ) was selected in the range from 3.34 to 20.

For reference, the theoretical transfer function of a parallel-plate DMC for non-diffusive particles, under the assumption of perfect 2-D flow in the particle classification channel, is given as (Santos et al., 2009)

$$\Omega(k, \emptyset) = \begin{cases} 1 - \frac{Q_{sh}}{Q_a} \left| 1 - \frac{k}{k_c} \right| & \text{if } k_{min} \leq k \leq k_{max} , \\ 0 & \text{if } k < k_{min} \quad k > k_{max} \end{cases} \quad (5.3a)$$

where  $Q_{sh}$  is the sheath flow;  $Q_a$  is the aerosols flow;  $\emptyset$  is the voltage;  $k$  is particle mobility;  $k_c$  is the central voltage (the one associated with the max transferee function);  $k_{min}$ ,  $k_{max}$  are the minimal and maximal particle mobilities, respectively. The voltage for maximal penetration of particles with given electrical mobility is,

$$V_{2D} = \frac{Q_{sh}H}{WLZ_p} \quad (5.3b)$$

where H is the height of particle classification channel (i.e., the spacing between two parallel plates); W is the full width of the classification channel; L is the distance for the particle classification; and  $Z_p$  is the electrical mobility of singly charged particles in a given size.

Table 5. 1 Properties of the flow and particles used for parallel-plates DMC

CONSTANT	VALUE
Particle diameter, $D_p$	100 nm
Cunningham slip correction factor $C_c$	2.909
Particle mass density, $\rho$	1000 kg/m <sup>3</sup>
Air temperature, T	293.15 K
Air dynamic viscosity, $\mu$	18.5×10 <sup>-6</sup> N.s/m <sup>2</sup>
Air density	1.2047 kg/m <sup>3</sup>
Elementary charge e	1.602×10 <sup>-19</sup> C
Aerosols inlet and exit flow	0.3 l/min
Sheath flow rate range	1.0-6.0 l/min
Re <sub>aerosols</sub> range	31.6 - 260
Re <sub>sheath</sub> range	147.6 - 590.5



### 5.3. Modeling Results

#### 5.3.1 Validation of numerical modeling

The validation of the numerical modeling was accomplished by the comparison of the calculated transfer function and the voltage for the maximal probability of particles entering and exiting the particle-classification channel of mini-plate DMCs (miniature parallel-plate DMCs) to those measured in the experiments. Both mini-plate DMCs studied in the experimental work of Liu and Chen (2016a) were modeled in this validation. [Figure 5.2](#) shows the result of this comparison.

[Figure 5.2a](#) shows the comparison of the numerical transfer function with the experimental one for particles of 100 nm in diameter. The DMCs were operated at the aerosol and sheath flow rates of 0.3 and 3 lpm, respectively. Reasonable agreement was obtained between numerical and experimental transfer functions.

[Figure 5.2b](#) gives the comparison of the voltage correction factors ( $\eta$ ) obtained in the modeling and in the work of Liu and Chen (2016a) for particles with 100 nm in the diameter when mini-plate DMCs were operated at the aerosol flow rate of 0.3 lpm and sheath flow rates were varied from 1 to 6 lpm. The voltage correction factor,  $\eta$ , defined in the work of Liu and Chen (2016a), is the ratio of the measured voltage for the maximal particle penetration through a DMC to the predicted via the 2-D model for a parallel-plate DMC. Following a similar definition, we calculated the numerical correction factor,  $\eta$ , by taking the ratio of the central voltage obtained in the numerical modeling to that calculated by Eq. (5.3b). As evidenced in [figure 5.2b](#), a reasonable agreement was also achieved between the measured and modeled voltage correction factors.

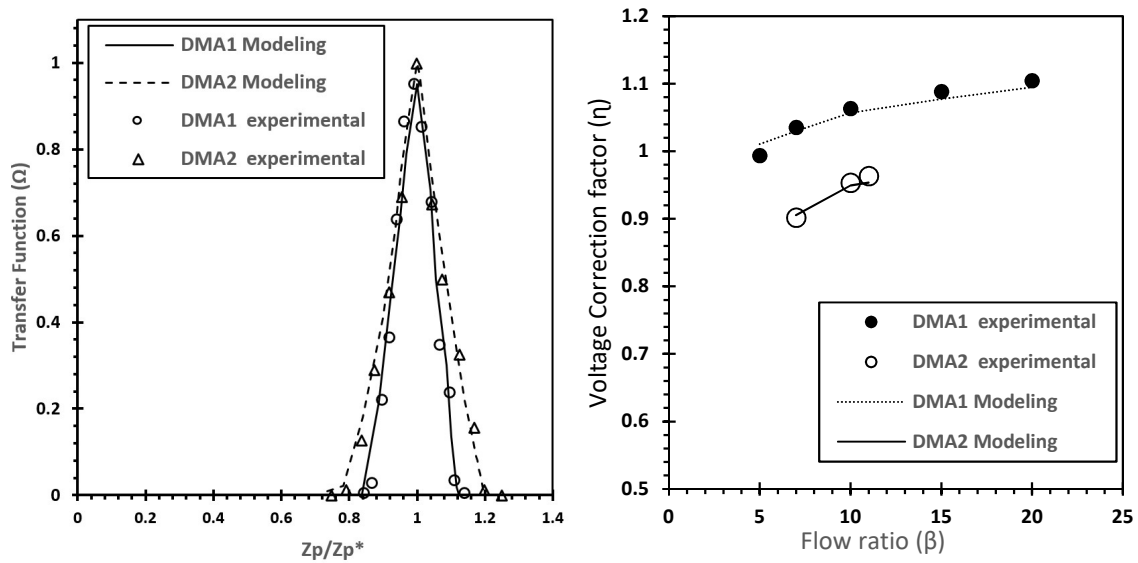


Figure 5. 2 Comparison of numerical results with the measured data given in the work of Liu and Chen (2016a) for (a) transfer functions (b) correction factor,  $\eta$ , of two mini-plate DMCs.

### 5.3.2 Effect of the classification-channel aspect ratio (CAR)

A parallel-plate DMC typically has a rectangular cross-section in the particle classification channel. The ratio of the channel width to the height (i.e., the plate-to-plate spacing) is defined herein as the channel aspect ratio (CAR) of the DMC particle classification channel. To investigate the CAR effect on the DMC transfer function, DMCs with the constant channel-cross-sectional area of  $80 \text{ mm}^2$  were studied. The selection of the cross-sectional area is because our modeling was started as the counterpart to the experimental work of (Q. Liu & Chen, 2016b). The CAR values of 1.0, 2.0, 3.0, 5.0, 8.0, 10.0, 15.0 and 20.0 were selected for this part of investigation. The aerosol flow rate of studied DMCs was kept at 0.3 lpm. Table 5.2 lists the dimensions of channel width and height for each studied DMC.

Table 5. 2 List of geometrical variables of miniature parallel-plate DMCs with the channel cross-section area of 80 mm<sup>2</sup> for studying the effects of channel aspect ratio (CAR) on the transfer function and the voltage for maximal particle penetration through the classification channel.

<b>Channel Aspect Ratio</b>	<b>Classification Channel dimensions (mm)</b>		
	<b>Height (h)</b>	<b>Width (W)</b>	<b>Length (L)</b>
1	8.94	8.94	52.39
2	12.64	6.32	
3	15.49	5.16	
4	17.88	4.47	
5	4.00	20.00	
8	25.29	3.16	
10	2.82	28.28	
20	2.00	40.00	

Figure 5.3 shows the transfer functions of mini-plate DMCs with the CARs of 1, 2, 3, 4, 5, 10, 15 and 20, and aerosol slit opening percentages of 90% (a), 75% (b) and 50% (c), respectively. The sheath-to-aerosol flow ratio,  $\beta$ , for these cases was fixed at 10. It is found that, for the DMCs with the 50%, 75% and 90% aerosol slit openings, the DMC sizing resolution (determined by the full width at the half-maximal height, FWHM, of the numerical transfer function) is in general not affected when the CAR is greater than 8. The peak of the DMC transfer function reduced as the CAR reduced to a value of less than 10. An obvious tail was observed on the left-hand side of the transfer function in the cases of DMCs with the 90% slit opening when the CAR reduces to 5 or less, dramatically increasing the skewness of the DMC transfer function. The above observation is apparently attributed to the presence of sidewalls required to construct the rectangular particle classification channel of a mini-plate DMC. As the DMC's CAR is reduced, the distance from a sidewall to the central line of the classification channel is also reduced. The viscosity effect from both sidewalls results in the slowdown of the maximal flow and particle velocities in the central

regime of the classification channel. Some particles are either deposited on the sidewalls (shown as the peak reduction) or they reach the classified aerosol exit slit at a reduced voltage (shown as the long-tail). The skewness of the DMC transfer function was less obvious for the DMCs with the 75% aerosol slit opening and was least obvious for the DMCs with the 50% opening. This is because introduced particles were kept away from the sidewalls in the DMCs with less aerosol slit opening, thus having fewer chances for particles entering the low-velocity region nearby the sidewalls. Once particles entered the low-velocity region of the classification channel, they either deposit on the channel sidewalls or require longer travel time to reach the aerosol exit slit.

Figure 5.4 shows the voltage correction factors, i.e.,  $\eta$ , for the maximal probability of particles in a given size entering and passing the classification channel of a mini-plate DMC (as the function of CAR for figure 5.4a and sheath-to-aerosol flow rate ratio,  $\beta$ , for Figure 5.4b). Figure 5.4a shows the variation of  $\eta$  as a function of CAR at the sheath-to-aerosol flow rate ratio,  $\beta$ , of 10 for DMCs having the slit opening percentages of 50%, 75% and 90% for both aerosol inlet and exit. Particles of 100 nm in size were again selected in this calculation. It is found that the value of the voltage correction factor,  $\eta$ , increased as the CAR value increased and eventually reached a constant value as the CAR value was higher than 10 for each studied DMC. The above finding is because of the sidewall effect on the velocity profile in the DMC classification channel. Also shown in figure 5.4 is that the DMC with the 50% aerosol slit opening has higher  $\eta$  values compared with those with the 75% and 90% opening. It is because particles were primarily staying in the central region of the

flow channel where the velocity is higher than that in the region near the sidewalls, thus requiring increased voltage to drive them across the sheath flow and exit the channel (compared with that calculated by an ideal 2-D flow model). The effect of sheath-to-aerosol flow rate ratio,  $\beta$ , on the  $\eta$  is given in figure 5.4b. Our modeling shows that the effect of  $\beta$  on the  $\eta$  is negligible for DMCs with a CAR value greater than 5.

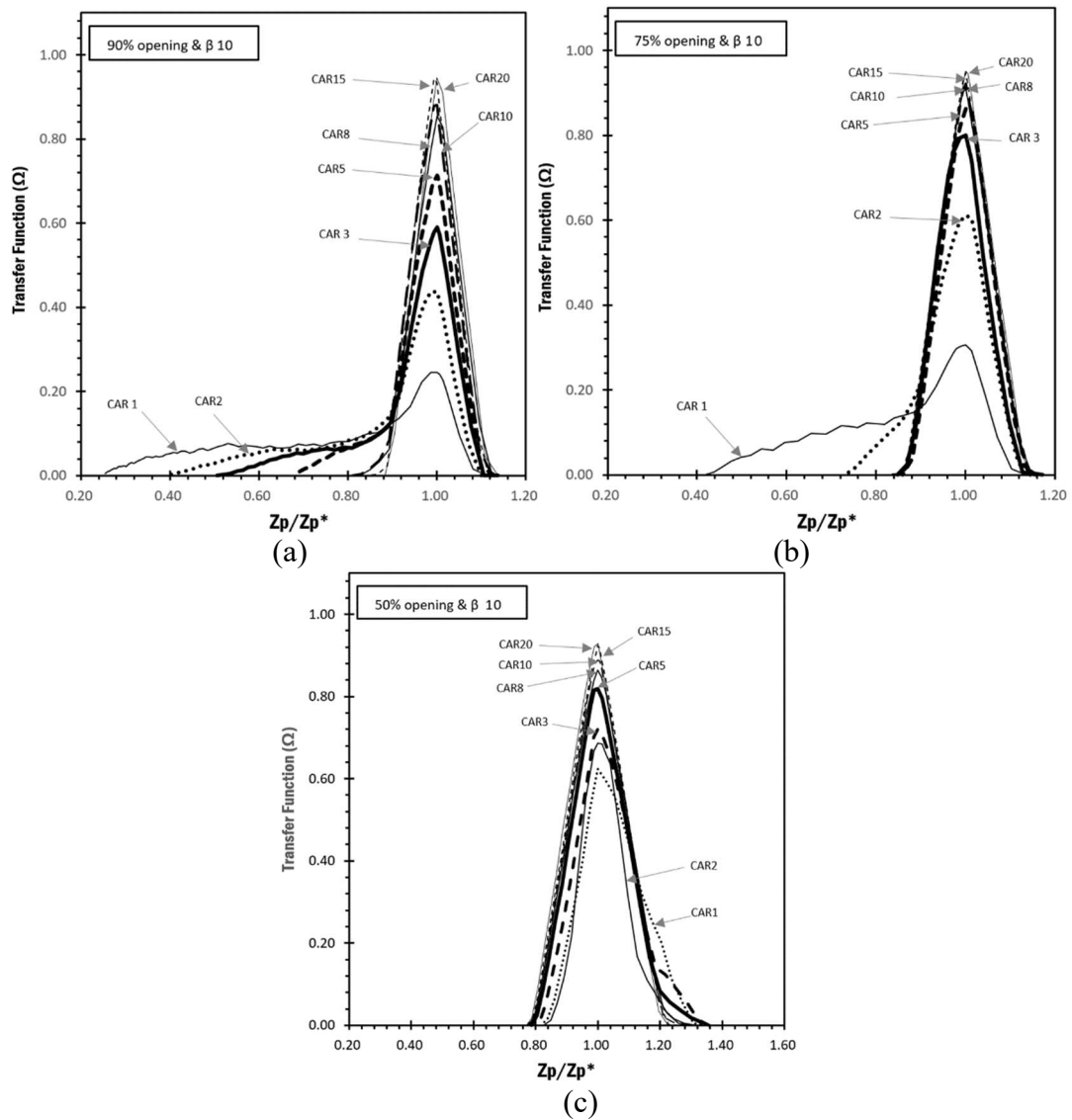


Figure 5. 3 DMC transfer functions at various channel aspect ratios, CARs for particles with the size of 100 nm. The sheath-to-aerosol flow rate ratio,  $\beta$ , is 10 and the aerosol flow rate is 0.3 lpm at (a) 90% opening, (b) 75% opening, and (c) 50%.

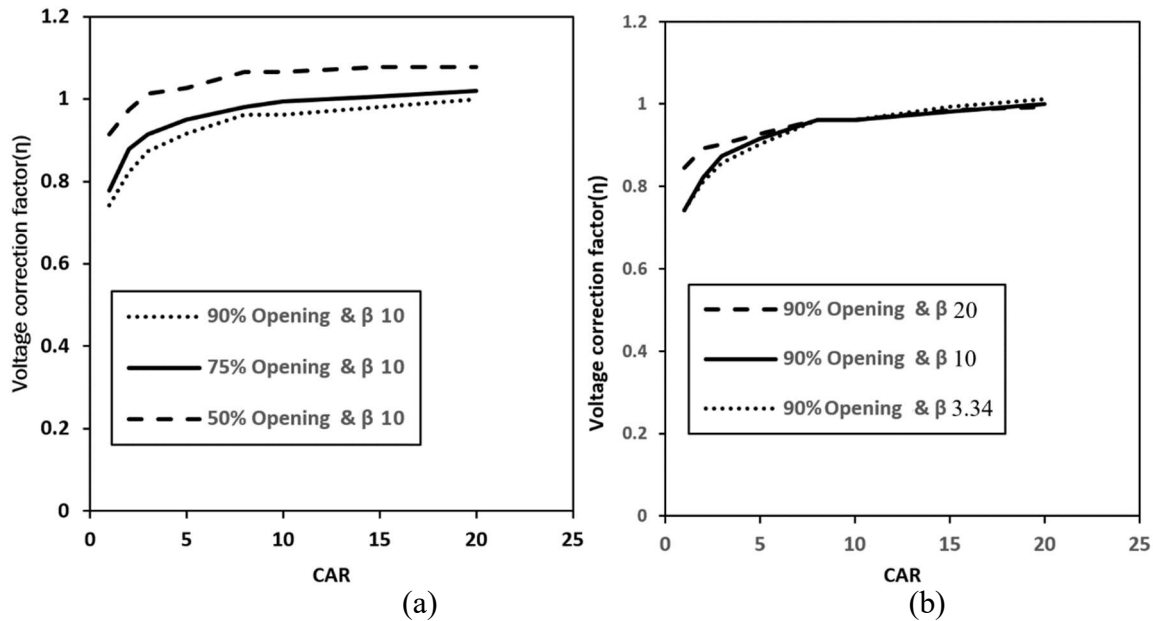


Figure 5. 4 The central voltage correction factor as a function of channel aspect ratio The central voltage correction factor as a function of channel aspect ratio for (a) various slit opening percentage (i.e., 50%, 75% and 90%) when the sheath-to-aerosol flow rate ratio,  $\beta$ , is 10; (b) different  $\beta = 20, 10$ , and 3.34 when the slit opening percentage is 90%.

### 5.3.3 Effect of the aerosol slit opening

Since the aerosol slit opening for a parallel-plate DMC typically does not cover the full width of the classification channel, the percentage of aerosol slit opening, defined as the ratio of slit opening length to the full width of DMC classification channel, is used in this study as the index to describe the slit opening condition in a parallel-plate DMC.

#### (a) For the cases having the same opening percentage for aerosol inlet and exit

Figure 5.5 shows the numerical transfer functions of studied DMCs with the slit opening percentages of 25%, 35%, 50%, 75%, 90%, and 100%. In this part of the investigation, the area of the slit openings was kept the same in all the studied cases. These DMCs operated at the sheath-to-aerosol flow rate ratio,  $\beta$ , of 10 had the CAR of 15. It is observed that the sizing resolution of mini-plate DMCs in general reduced as the slit opening

percentage decreased. Minor tail on the right-hand side of the transfer function peak was shown in the cases where the DMCs had a 25% slit opening. This is due to the fact that the shape of slit openings for aerosol inlet and exit became elongated in the flow direction (because we kept the opening area the same in this part of the study). Consequently, a very small percentage of particles in high electrical mobility was deposited in the neighborhood of the exit slit. A long tail was also shown on the left-hand side of the transfer function for a DMC with a 100% slit opening because of the sidewall effect.

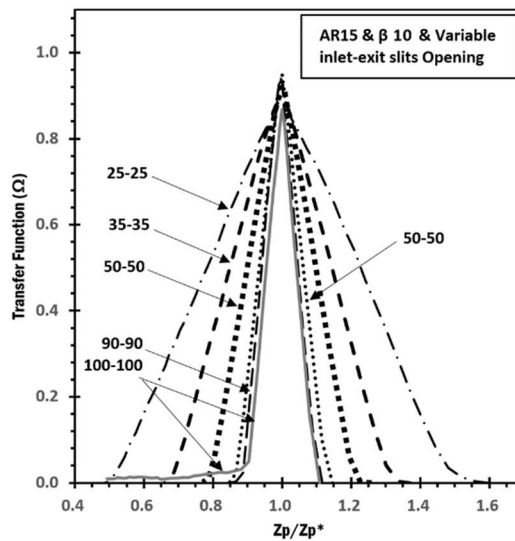


Figure 5. 5 The transfer functions of studied DMCs with different slit opening percentages . The studied DMCs has the CAR value of 15 and the opening percentages for aerosol inlet and exit slits are kept the same.

Note that the concept of effective (or working) sheath flow rate was introduced in the work of (Q. Liu & Chen, 2016b). It was believed that, because of the partial slit opening (relative to the full classification channel width), the effective sheath flow should be the portion of total sheath flow rate underneath the slit opening and the remaining sheath flow should be merely for keeping particles away from the DMC's sidewalls. To verify the above hypothesis, the comparison of numerical transfer FWHM and the 2-D theoretical FWHMs

of both total and effective sheath flow rates as a function of slit opening percentage is given in figure 5.6. Reasonable agreement between the FWHMs calculated using the effective sheath flow rate and numerical FWHM evidences the hypothesis, particularly for the cases of parallel-plate DMCs with a slit opening percentage greater than 50%. For the cases of DMCs with a slit opening less than 50%, FWHMs, based on the effective sheath flow hypothesis, are in value less than numerical FWHMs. This is probably because of much wider opening slits in the cases with the opening percentage of less than 50% when compared with those in the cases with the percentages greater than 50%. It is due to the fact that the opening areas of both aerosol entrance and exit slits were kept the same in the studied DMCs. As a result, the classification length for particles in the DMCs having the slit opening less than 50% were more varied when compared with that for DMCs with the greater-than-50% opening slits.

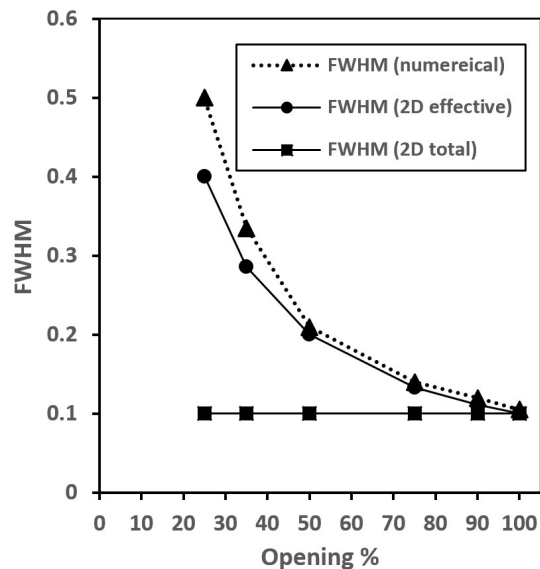


Figure 5. 6 The comparison of numerical FWHMs with FWHMs calculated via the 2-D model and the assumption of total sheath and effective sheath flow rates (as a function of the aerosol slit opening percentages). Note that FWHM is the Full Width at Half Maximum of the transfer function.



**(b) For the cases with different inlet and exit opening percentages**

In the previous investigation, we assumed that all the studied DMCs have the same slit opening percentage for aerosol in as that of aerosol out of the classification channel. In this part of the study, we considered DMCs having different slit opening percentages for exit slits while keeping the 90% opening for aerosol inlet slit. The studied DMCs again had the CAR of 15 and operated at the sheath-to-aerosol flow rate ratio,  $\beta$ , of 10 (with the aerosol flow rate kept at 0.3 lpm). In addition, we also studied the case with a DMC having a round exit opening instead of a rectangular exit opening. Note that the opening area of the aerosol exit slit was kept the same as that of the aerosol inlet slit.

Figure 5.7 shows the numerical transfer functions of DMCs with the aerosol exit slit opening percentages of 10%, 25%, 50%, 75%, and 90%. The transfer function of a DMC with a round exit is also included in the same figure. It is found that the peak and FWHM of the transfer functions deteriorated as the exit slit opening percentage reduced. The worst scenario was observed in the case with a round exit. By keeping the slit opening area and aerosol flow rate constant, the average flow velocity at all the exits remained the same. In other words, the flow suction power for particles near the channel exit was kept the same in all studied cases. Because the aerosol inlet has the 90% percentage opening, some particles move in the region close to the channel sidewalls. When the exit slit percentage reduced, particles moving in the close-to-sidewall regions would have less chance to flow out at the exit. As a result, the peak of the numerical transfer function was reduced as the exit slit opening percentage was reduced. It is further observed that the long tail on the left-hand side of the numerical transfer function in the cases with the exit slit openings less than 50%. It is

because of the strong local flow velocity at the exit slit interrupting the function of sheath flow.

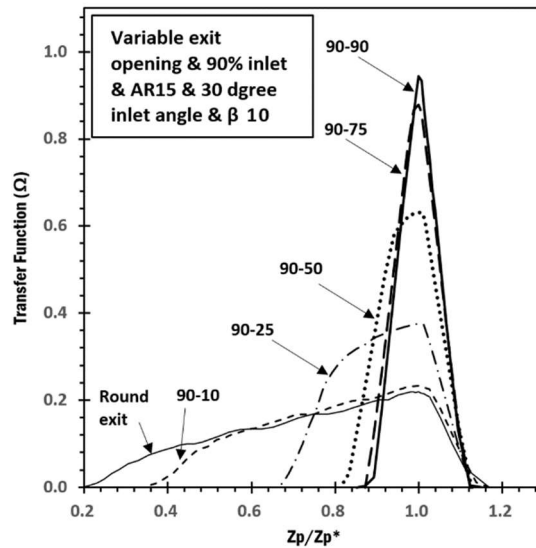


Figure 5. 7 The effect of varying the exit slit size on the transfer function of DMCs having a fixed aerosol inlet silt percentage of 90% and different exit slit opening percentages (i.e., 10%, 25%, 50%, 75%, and 90%). The transfer function of the DMC with the exit in the round shape is also included. All the studied DMCs have the CAR value of 15 and operate at the sheath-to-aerosol flow rate ratio of 10.

### 5.3.4 Effects of cross-sectional area and aerosol injection angle of the particle classification channel

The effect of the cross-section area of the particle classification channel on the DMC transfer function was also investigated. For this part of the study, we calculated the transfer function of mini-plate DMCs having the channel cross-sectional areas of 160 and 40 mm<sup>2</sup> (i.e., a factor of 2 and 0.5 of the area studied in the above investigation, respectively). Studied DMCs had CAR of 15. They were assumed to operate at the sheath-to-aerosol flow rate ratio,  $\beta$ , of 10 with the aerosol flow rate of 0.3 lpm. As shown in [Figure 5.8a](#), the effect of channel cross-section area was negligible on the numerical DMC transfer function.

Figure 5.8b shows the calculated transfer functions of the DMCs having the aerosols injection angle of 5°, 30°, 60° and 90°. Studied DMCs operated at the sheath-to-aerosol flow ratio,  $\beta$ , of 10 had the CAR of 15, and both aerosol inlet and exit slit opening percentages of 90%. A negligible effect on the obtained DMC transfer functions was observed in figure 5.8b. The above result is most likely because of the laminar flow assumption in our numerical modeling, limiting the modeling's capability of identifying the potential occurrence of turbulent flow condition (as long as the converged flow field solution is obtained).

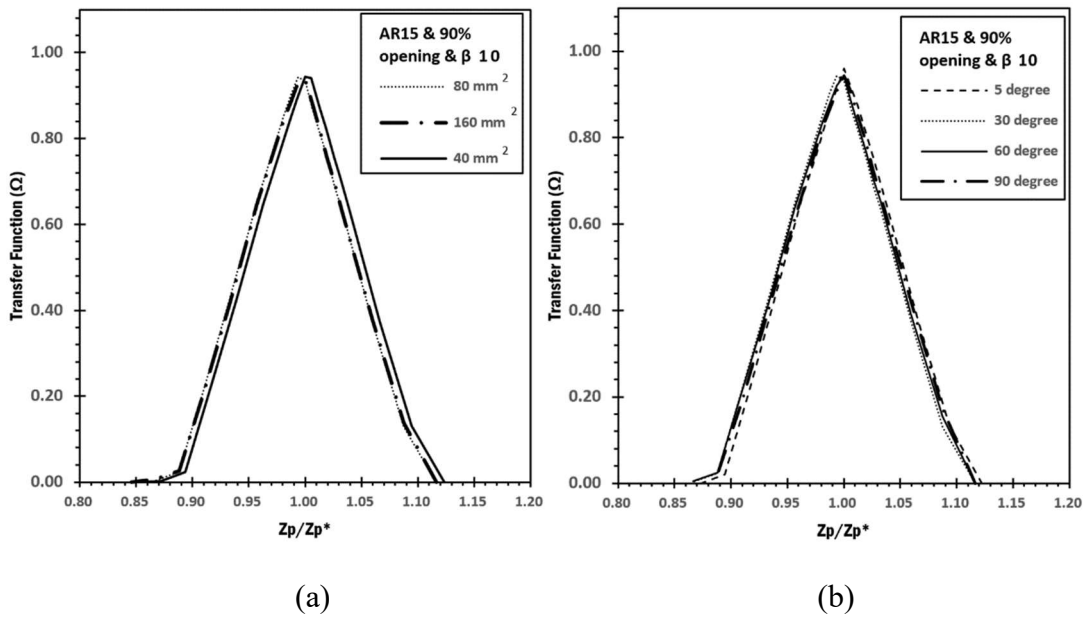


Figure 5. 8 The effect of channel cross-section areas (a) and aerosol injection angles (b) on the DMC transfer function. Studied DMCs have the CAR value of 15% and 90% opening percentages for aerosol slits. The sheath-to-aerosol flow rate ratio is 10.

## CHAPTER 6 Plates Tilting/ Parallel Plates Differential Mobility Classifier<sup>9</sup>

### 6.1 Introduction

Differential mobility classifiers, DMC, have been developed for aerosol applications to characterize nanoscale particles in nanoscale size range (Intra & Tippayawong, 2008). A majority of existed DMCs are designed in the cylindrical, radial or parallel-plate configurations. Among them, parallel-plate DMC has recently attracted much attention in the development of miniature DMCs. This is because of its low manufacture cost and uniform electric field in the particle classification zone, resulting in less particle diffusional broadening of the DMC transfer function (Alonso & Endo, 2001; Steer et al., 2014).

Parallel plate design configuration has been utilized to classify large particles as a separator. It designed to characterize PM<sub>2.5</sub> particles based on particle charging states (Lenggoro et al., 2015; Yonemichi et al., 2019). It is also used to classify/precipitate submicron particle which is name the electrostatic classifier (or analyzer) (Giacomelli Maltoni et al., 1973; Langer & Radnik, 1961; Liu & Chen, 2016a; Wen et al., 2016). The electrostatic classifier was the best technique to collect a specific cut off size of nanoscale particles by taking advantage of the electrical mobility of these small particles. The more

---

<sup>9</sup> The material of this chapter is taken from the publication-Alsharifi, T., & Chen, D.-R, (2019) "The influence of plate tilt on the transfer function of small plate differential mobility analyzers," *Journal of Aerosol Science*, Volume 136, October 2019, Pages 48-59: <https://doi.org/10.1016/j.jaerosci.2019.06.006>.

advanced version of the parallel-plates classifier is used to collect a selective size of nanoscale particles. It is named as the parallel-plates differential mobility classifier (or analyzer) DMC (or DMA as mentioned in the literature) (Alsharifi & Chen, 2018; Q. Liu & Chen, 2016b; Rus et al., 2010).

The parallel plate DMC consist of two opposite plates forming a perfect rectangular cross-section channel/duct. Clean sheath air is flowing in the channel while charged poly-disperse aerosols introduced from the upper plate toward the lower plate while it is drifting toward the end of the classification channel. While the electrical field applied between the plates (the upper plate is ground and lower has electrical potential). A selective mono-disperse particles with a specific mobility exit through the aerosol exit slit at lower plate. The remaining aerosols will either deposit on the lower plate or exit from the main channel excess flow. Therefore, DMC has two inlets (for sheath clean air and aerosol) and two exits (for classified aerosols and excess air). The sheath air is flowing rectangular cross-section while aerosols introduced from the aerosol entrance slit at the upper plate. However, this will not be the case especially in the case of the geometrical manufacturing tolerance in the spacing between the plates.

Since first the parallel plate classifier design found by Erikson (1921), there were a few attempts to improve the performance of the parallel-plate DMC. Besides recent improvement of the flow laminar by Amo-González & Pérez (2018), thereby enable the classifier to reach a high flow velocity, there was not much work that has been done to further enhance the performance of the parallel plate DMC. To the authors' knowledge, the effect plates alignment on the performance of parallel-plate DMCs, i.e., transfer functions, has not been

numerically or experimentally being studied before, especially the effect of geometrical design parameters on the DMC's transfer functions.

It is very likable and depending on the parallel plate tolerance type, the plates tend to be misaligned by either rotate around the streamwise direction or around diagonal of the plate. In this chapter, we decided/studied/considered the plate tilting into the side direction (rotation around the streamwise direction), and the front point and back point tilting (rotating around the plate diagonal in both directions). While plate rotation around the stream spanwise direction is not considered as imprecation because it does not affect particle traveling distance, moreover, it is also one of the designs that considered by Rus et al., (2010).

Therefore, the objective of this study is thus to numerically model the performance of parallel-plate DMCs and to systematically investigate the effect of plates parallelism and alignment on the DMC transfer function. COMSOL Multiphysics 5.4<sup>®</sup> and MATLAB R2018a<sup>®</sup> were used to set up the numerical model. The model was further verified through our previous work, chapter 5, for perfect parallel-plates DMC (Alsharifi & Chen, 2018) with the experimental data collected in the work of Liu and Chen (2016). A parametric study was then performed to investigate the effect of tilting on the geometrical design variables on the transfer function of parallel-plate DMCs. The studied design parameters include the cross-section area and aspect ratio and the length of particle classification zone, aerosol inlet and exit slit openings. Other operational parameters like sheath-to-aerosol flow ratio and the total flow rate were also investigated. In the following sections, we will first present the modeling

of parallel-plate DMCs. The model verification and the effect of studied design parameters on the DMC's transfer fraction are given the section of Results and Discussion.

## 6.2 Numerical Modeling of the Tilted-plate DMCs

Both MATLAB R2018a<sup>®</sup> and COMSOL Multiphysics 5.4<sup>®</sup> has used to set up the model and to perform the investigation. Because the DMCs are required to operate in the laminar flow condition, steady incompressible Navier-Stokes equations are applied to calculate the flow field in a DMC. However, the flow profile continuously changes through the DMC channel due to the continuous variation of channel cross-section. The Laplace equation is used to calculate the electrical potential,  $\phi$ , in the particle classification zone. The electrical field,  $\vec{E}$ , is then derived from the following equation  $\vec{E} = -\nabla\phi$ . A typical computational domain for modeling a parallel-plate DMC is shown in [Figure 1](#) ([a](#) is the side view; [b](#) is the top view of perfect parallel plate DMC, and [c](#) are three selected cases for tilting between the plates in the classifying chamber).

In this study, we define the relative tilting percentage,  $\tau$ , for the plate DMC as the ratio of the reduction in the spacing between the plates in the case of tilting,  $h$ , to the typical spacing (distance) between the plates  $H$ . The possible tilting (parallelism misalignment between the plates) are studied and illustrated in [Figure 1c](#). The side tilting  $\tau_s$  proposed by assuming the upper plate tilted in the spanwise of the flow direction. The DMC channel cross-section is fixed right trapezoid. The other kind of tilting is point tilting which accrues due to change in spacing in at two points in the diagonal of the classifying channel. Point tilting can be classified into: front tilting  $\tau_{pf}$  and back tilting  $\tau_{pb}$ . Both the front and back tilting has trapezoid cross-section, however, the cross-section spacing between the plates for

the front is converging via height reduction while for the back tilting is diverging via increased in spacing between the plates as moving downstream the classifying channel.

For the flow field calculation, the flow velocity profiles at both the polydisperse aerosol and sheath flow inlets are assumed uniform. The flow velocity at classified aerosol exit is assumed uniform. No-slip boundary conditions are applied to all the solid walls. For the electrical field, the lower plate is at elevated voltage and the upper plate is at the electrically ground.

The performance of a DMC is characterized by its transfer function, which defined as the probability of a particle with given electric mobility ( $Z_p$ ), entering the DMC classification region and reaching the classified aerosol exit (Knutson & Whitby, 1975). The calculation of the transfer function of a DMC for singly charged particles of a given size was based on the particle flux. The detail can be found in the work of (Alsharifi & Chen, 2018). [Table 6.1](#) summarizes the values of the physical properties of gas and particles used in our modeling. The effect of side and point (front and back) tilting on the performance of a cylindrical DMC was investigated for particles sizes of 5, 20 and 80 nm and under the condition of different sheath-to-aerosol flow rate ratios,  $\beta$ , of 5, 10 and 20 (i.e., sheath flow rates were varied in 1.5-6 lpm), and also (both sheath and aerosols flow was scale in 1-9 lpm and 0.1-0.9 lpm, respectively). Both aerosols inlet and exit slits opening percentage  $\eta$  were investigated ( $\eta = \frac{\ell}{W}$ ,  $\ell$ : is slit length, and  $W$  : is channel width). The particle diffusivity was considered for particles with sizes less than 50 nm. [Table 6.2](#) summarizes the ranges of DMC dimensions studied.



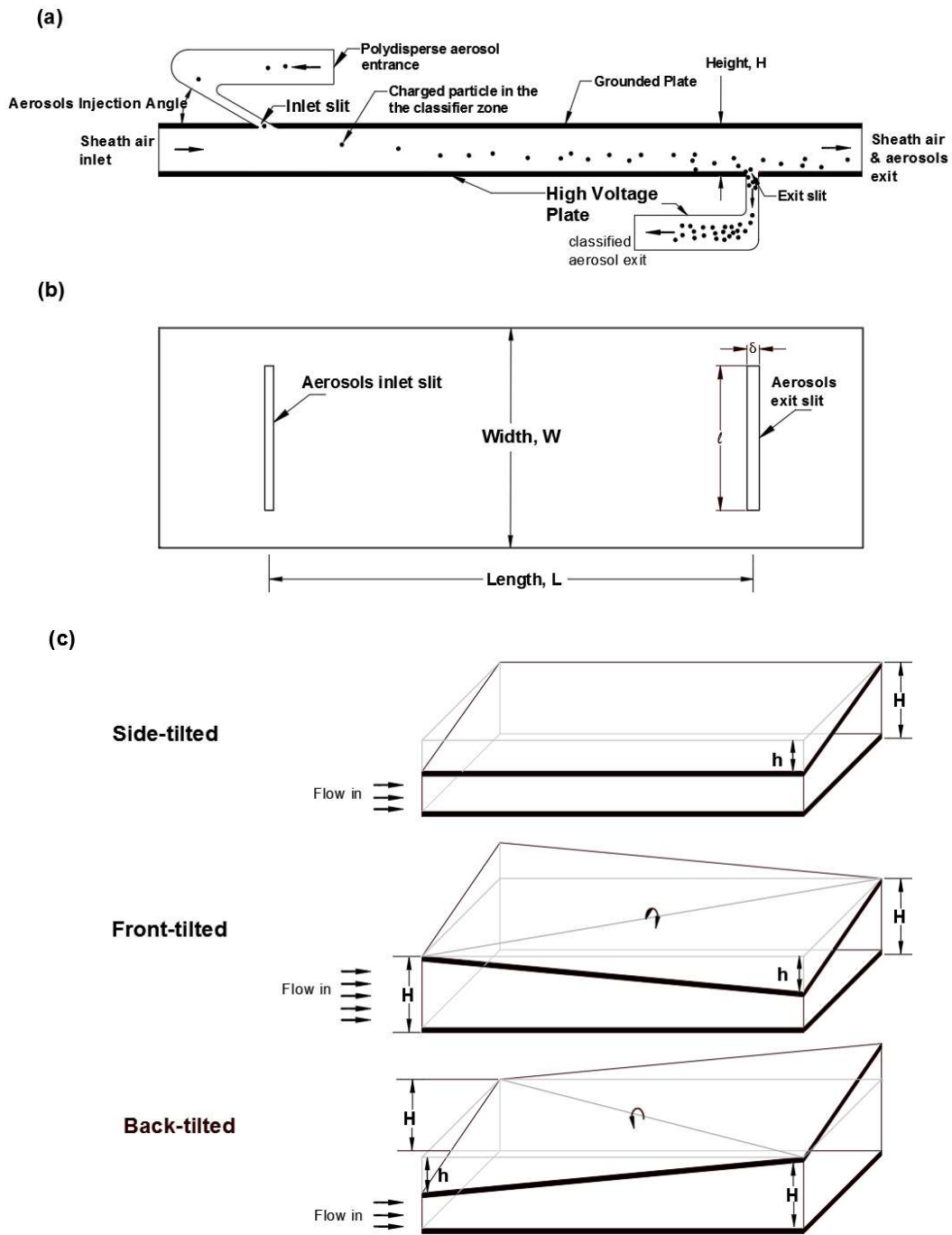


Figure 6. 1 The schematic diagram of the plates tiled DMC showing the computational domain used in the modeling: (a) side view (with the illustration of the particle movement in the classification channel); (b) the top view; (c) the three types of imperfect classifying channel under study (side tilting, point tilting (front, and back)).

Table 6. 1 Constants and physical properties inside the plates-tilted DMC.

	<b>CONSTANT</b>	<b>VALUES AND FORMULAS</b>
<b>PARTICL</b>	Diameter, $dp$	5, 20, 80 nm
	Mass density, $\rho_p$	1000 kg/m <sup>3</sup>
	Slip correction factor $C_c$	$C_c = 1 + Kn \left( 1.155 + 0.471 e^{-\frac{0.596}{Kn}} \right)$
	Elementary charge e	$1.602 \times 10^{-19}$ C
<b>AIR</b>	temperature, t	293.15 K
	dynamic viscosity, $\mu$	$18.5 \times 10^{-6}$ N.s/m <sup>2</sup>
	density, $\rho$	1.2047 kg/m <sup>3</sup>
	mean free path $\lambda$	0.066 [um]
	Boltzmann constant	$1.38064852e-23$ [J/K]
<b>FLOW</b>	Aerosols inlet and exit flow	0.1-0.9 lpm
	Sheath flow rate range	1-9 lpm
	Flow ratio $\beta$	5-20

Table 6. 2 The key dimensions for plates-tilted DMC.

<b>GEOMTRICAL PARAMETER</b>	<b>RANGE</b>
Channel width W	2.828-4.0 [cm]
Channel height H	0.2-0.282 [cm]
Channel length L	2.5-10 [cm]
Channel aspect ratio (AR=W/H)	10-20
Channel cross-section area (A=W*H)	0.8 [cm <sup>2</sup> ]
Slit opening percentage $\eta$	50-90%

### **6.3 Model verification**

Prior to proceed with the current numerical study/investigation, our model had been verified for the perfect parallel-plates DMC with the experimental work of Liu and Chen (2016). The comparison performed for the transfer function and voltage correction factors (define as the ratio of the measured voltage for the maximal particle penetration through a DMC to the predicted via the 2-D model for a parallel-plate DMC) and it is presented through chapter five and our previous work (Alsharifi & Chen, 2018). The comparison was for the particle sizes of 100 nm under operated at the aerosol flow rate of 0.3 and sheath flow range of 1 to 6 lpm. Good agreement between our numerical data and the experiment was obtained.

### **6.4 Modeling Result**

#### **6.4.1 Typical flow and electrical fields inside the tilted DMC classifying channel**

Figure 2 shows typical flow field inside the particle classification channel at a cross-section at the middle of the 5cm channel, for both perfect parallel plate and 10% side-tilted plates. Because of the plate tilting, the channel cross-section is not rectangular cross-section which affects the flow field. Figure 2a shows the streamwise flow velocity contours and Figure 3b shows the spanwise velocity vectors. The flow will be symmetric for the perfect parallel plates flow case with 0% tilting. The maximum value of stream will accrue at the center of the channel spacing while the spanwise velocities will flow from the side walls toward the width center of the maximum flow velocity. At 10% side tilted DMC channel, the maximum stream velocity will shift little to the wider spacing gap the walls. While the

spanwise velocity (secondary flow) will be asymmetric and increase from the narrow spacing toward wider spacing walls.

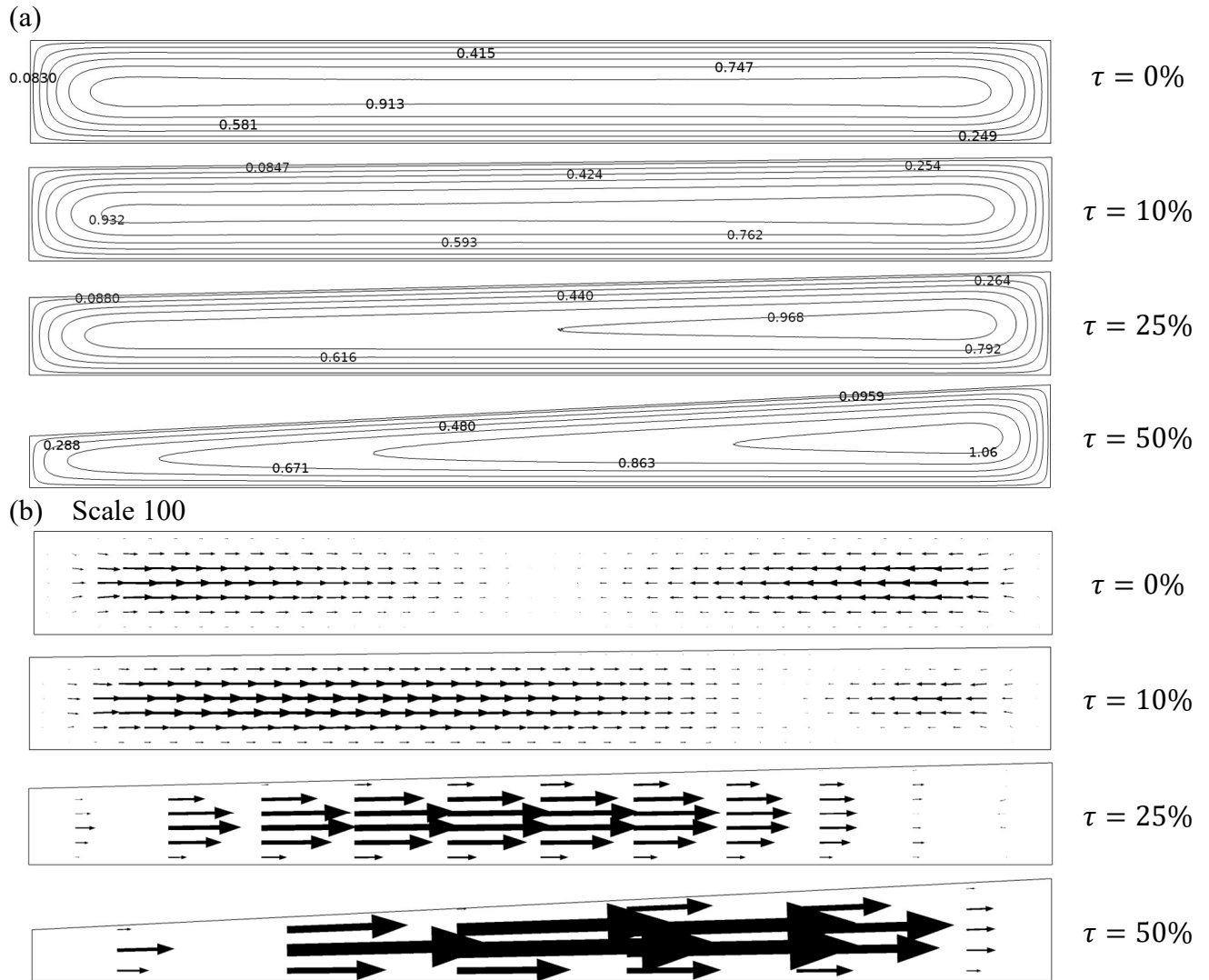


Figure 6. 2 The flow in the cross-section of the plate tilted DMC classification channel with side tilting of 0, 10,25, and 50%, AR=10 and sheath flow of 3 lpm (a) the counter of streamwise velocity m/s (b) the velocity in spanwise cross-section (scale 100), for the DMC channel.

On the other hand, the electrical field intensity is depended on the spacing gap between the DMC opposite electrodes (i.e. plates). Figure 6.3 shows the electrical potential at the DMC cross-sections with tilting of 0, 10, 25, and 50 respectively. The electrical field potential is intensified in the narrow gap compared to that in the wide gap. The plate tilting will change the gap between the plates along the classifier cross-section. This disturbs the electrical field at the cross-section of DMC classification channel and therefore it will be varied across the narrow spacing to the wider spacing because of the uneven gap.

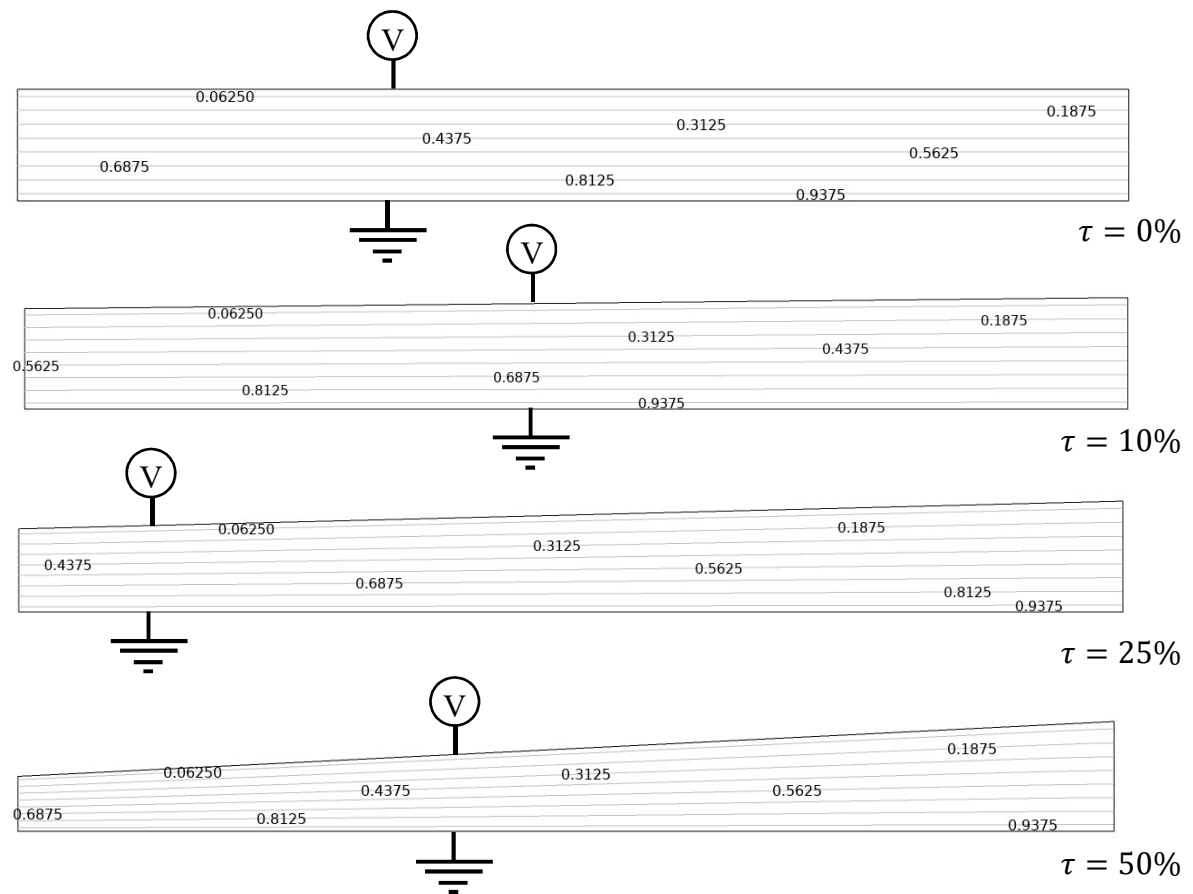


Figure 6. 3 The electrical field inside the cross-section of the plate tilted DMC classification channel with tilting of 0, 10,25, and 50%. The plot shows the normalized electrical potential contours with the maximum penetration voltage.

### 6.4.2 Side Tiled Transfer Function

Figure 6.4 shows the DMC transfer function for the tilting of 0, 5, 10, and 15 for channel aspect ratio 10 and 20, for aerosols slits opening  $\eta$  of 90%, and for sheath and aerosols flow of 3 and 0.3 lpm. The results show that the transfer function height decrease and width increase as the tiling increase; This due to the disturbance in both flow and electrical field. The tilting causes a variance in particle traveling distance along the width on the classifying channel (in the stream spanwise). This pushes the particles to travel in the stream span direction toward the wider gap zone, which leads to a higher concentration of particles that traveling faster in the streamwise direction of the channel. This unbalance of particle flow leads to divergence in particle location for the same entrance location. This leads to particle loss inside the DMC chamber and deterioration in the overall resolution.

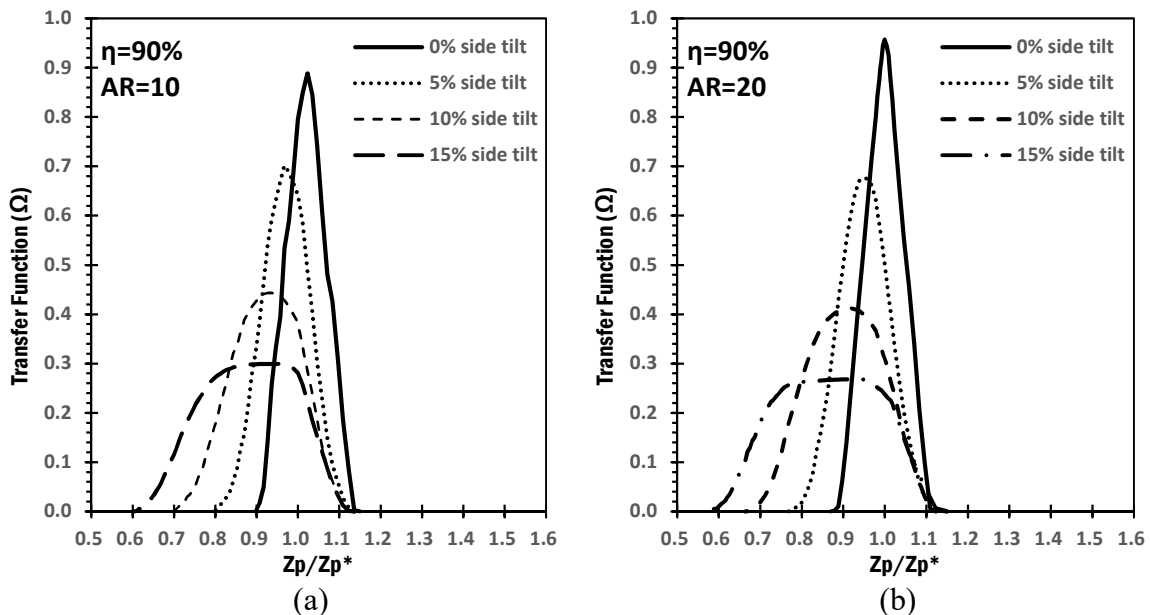


Figure 6. 4 The transfer function at relative tilting percentages of 0, 2, 5, 10, and 15% respectively, and slits opening of 90% DMC and channel length of 50 mm, and cross-section aspect ratio of 10.

It is believed that both the flow and electrical field distortion in the particle classification channel of a DMC with tilted plates contributed to the deterioration of the transfer function. In this part of the study, we would like to identify the dominant factor influencing the shape of the DMC transfer function. Figure 6.5 shows the transfer functions calculated with three different assumptions: 1) uniform sheath flow velocity profiles at the classifying channel only; 2) uniform electrical field only, and 3) tilted (distorted) flow and electrical field in the entire classification channel for a plate DMC with the side tilting of 10%, operated at the aerosol and sheath flow rates of 0.3 and 3 lpm, respectively. The particle classification length of studied DMCs was 5 cm, and particle size was 80 nm.

It has been noticed through the case of uniform flow with a distorted electrical field that the electrical field is the dominant factor to affect the transfer function. While the other case of uniform electrical field with distorted flow will result in a compatible (close value) transfer function to the case of combined tilted flow and electrical field.

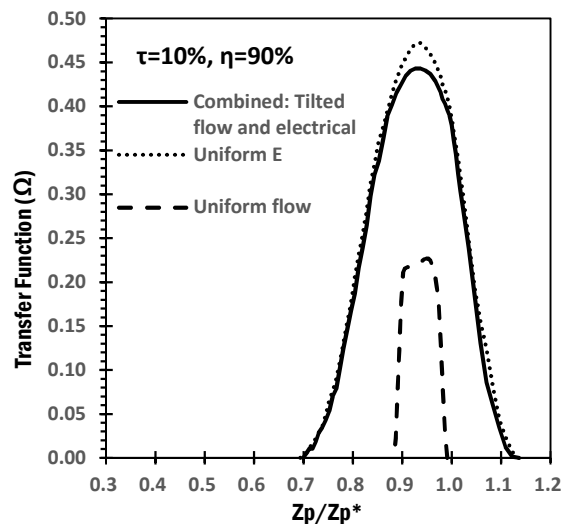


Figure 6. 5 Comparison between the combined effect and separate effect of flow and electrical field , for the differential mobility classifier transfer function for the case of aspect ratio of 10 and sheath to aerosols flow ratio of 10 and channel length of 50mm.

### 6.4.3 Channel Aspect Ratio (AR)

Through our previous work (Alsharifi & Chen, 2018), it has been concluded that the optimal parallel plated DMC channel aspect ratio will be above 8. However, technically for a mini plate DMC with a small dimension, the aspect ratio will not exceed 20. Therefore, this study focus on two aspect ratios with this range. [Figure 6.6a](#) illustrates the DMC transfer function for channel aspect ratios of 10 and 20, for side tilting of 10%, and both aerosols slits (entrance and exit) opening of 90%, and for sheath and aerosols flow of 3 and 0.3 lpm respectively. The results show that tilting at a higher aspect ratio of 20 is more distortive to the DMC transfer function than it at the aspect ratio of 10. This small difference in the transfer function is due to variance in the flow profile across the classifying channel.

[Figure 6.6b](#) shows the velocity profile at the mid-channel length and height line along the DMC width. The velocity is normalized with mean velocity profile for two aspect ratios of 10 and 20, and both have cross-sectional area of  $80 \text{ mm}^2$ , for sheath and aerosols flow rates of 3 and 0.3 lpm. The figure shows that the variance in the velocity profile for AR 10 is less than AR 20. This due to the relatively small gap spacing at the narrowest side of AR 20 compares to AR 10 that leads to build a bigger pressure drop based on (according to) the fluid mechanics' continuity equation.



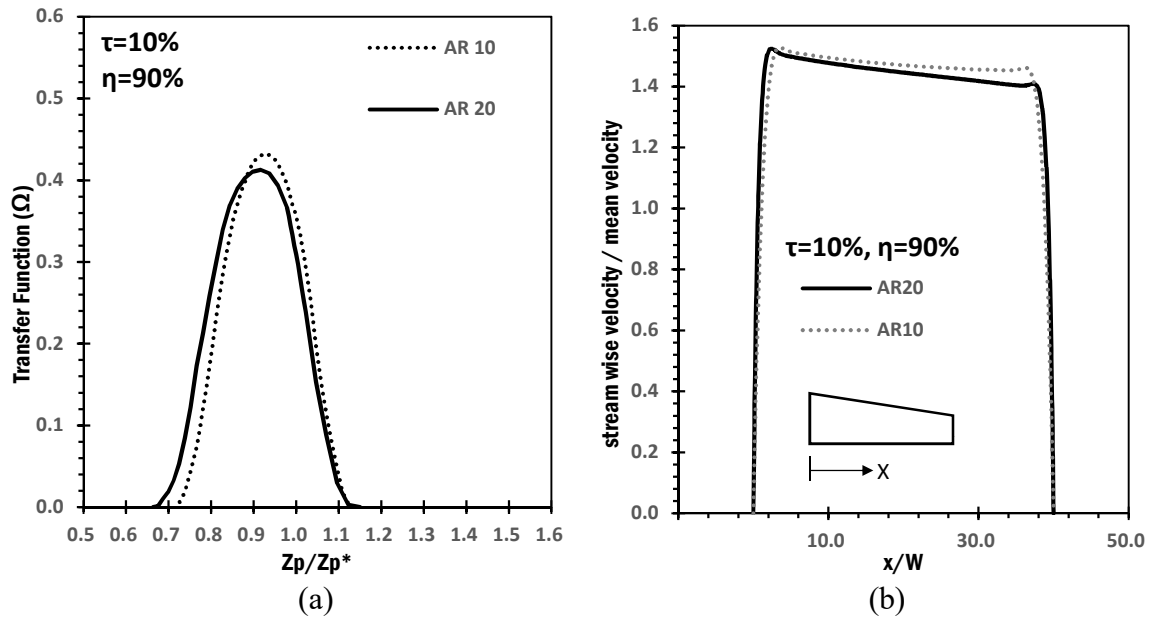


Figure 6.6 The transfer function with channel aspect ratio for the plates tilted DMC (a) for aspect ratios of 10, and 20 respectively, (b) the velocity profile at the mid-channel height normalized with mean velocity profile. Both (a) and (b) are for tilting percentage of 10% and slits opening of 90% and channel lengths of 50 mm.

#### 6.4.4 Channel Length

Figure 6.7 shows the DMC transfer function for different channel lengths of 25, 50, and 100 mm respectively, and tilting percentage  $\tau$  of 10%, and slits opening  $\eta$  of 90%. The results show that the DMC transfer function height is deteriorating as the classifying channel increased. The resolution of the transfer function is decreed (i.e. increase in the width of the transfer function) as the classifying channel of the DMC becomes longer. This due to increasing the impact on particle path inside the longer tilted classifying channel, which caused by the rise of the major electrical field effects combined with the minor flow effect for long DMCs.

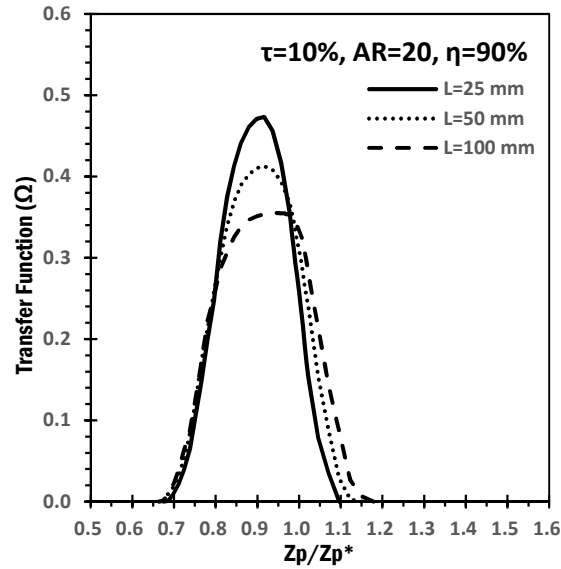


Figure 6. 7 The DMC transfer function for various particle residence time for side tilting percentage of 10% and slits opening of 90% and sheath-to-aerosols flow ratios to 10 and fixed the channel cross-section while varying the channel lengths of 25, 50, and 100 mm respectively.

#### 6.4.5 Flow Ratio $\beta$ and Total Flow

Figure 6.8a illustrates the effect of the flow field on the performance of the DMC classifying channel tilting  $\tau$  of 10%, and slits opening  $\eta$  90%, for cases of sheath to aerosols flow ratios  $\beta$  of 5, 10, and 20. The figure shows that a high flow ratio (high resolution) of 20 is having the lowest particle transfer function and very sensitive to the tilting compare to the low resolution at which it is not very sensitive to the tiling and has a higher tilted transfer function.

Figure 6.8b shows the case of scaling the total flow while fixing the flow ratio  $\beta$  to 10. The studied case of sheath-to- aerosols flow (9:0.9; 3:0.3; 1:0.1 lpm). The results show the higher flow ratio yields a better DMC performance with higher transfer function peak

and slightly superior resolution. This because for the same DMC configuration, the higher total flow had more (faster) effective particle suction at the monodisperse particle exit zone that the lower total flow.

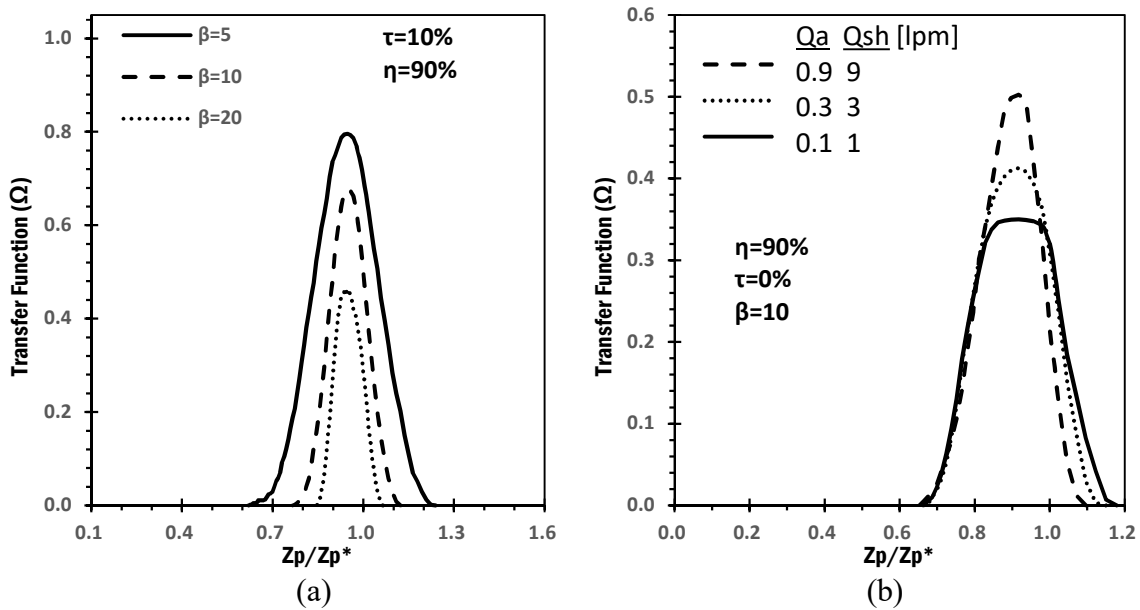


Figure 6. 8 The flow effect on the plate tilted DMC transfer function for 10 % tilting and 90% slits opening (a) for sheath-to-aerosols flow ratios of 5, 10, and 20 (b) different total flow for sheath-to-aerosols flow of 9: 0.9 , 3: 0.3 and 1: 0.1 lpm respectively

#### 6.4.6 Slits opening $\eta$

Figure 6.9 shows the 10% tilted plates DMC transfer function for aerosols slits openings  $\eta$  of 50, 75, and 90%, for the case of fixed flow ratio  $\beta$  of 10 (sheath-to- aerosols flow of 3:0.3 lpm). The results show the wider opening of 90 has the least value of transfer function. This due to the fact that at wider opening more particles will flow near the DMC side walls. And the velocity of particle near these walls (in the opposite sides of a narrow and wider gap between the plates) is varied, which leads to particle deviated from the designated destination which is the worst scenario at a wider opening.

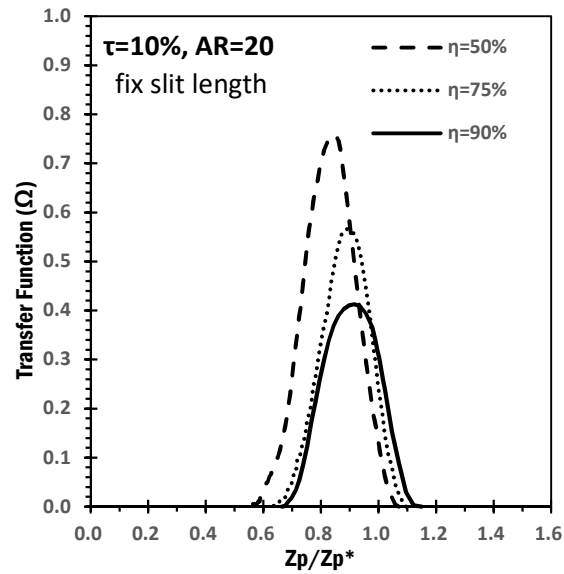


Figure 6. 9 The DMC transfer function with different slit openings of 50%, 75%, and 90% respectively, for 10% tilting percentage, and aspect ratio of 20 and channel length of 50mm.

#### 6.4.7 Particle Size/Diffusivity

Figure 6.10 shows the comparison between the diffusive and non-diffusive DMC transfer function. The studied case for 5, and 80 nm respectively, and for 90% opening and 10% tiling. The effect particle diffusivity is representing of loss in the transfer function height and increase width/resolution and this due to the particle loss at the classifying channel.

#### 6.4.8 Tilting Type

The three possible options for the plates tiling is studied. Figure 6.11a show the DMC transfer function of 10%tiling of the cases of (side tiling, point and). All three imperfection/tilted transfer functions is plotted with the perfect case for the case of 90% opening and flow ratio of 10. The results of all three tiltings show close values of transfer

function width and peak height. However, the tilted value is always less peak and more width (less resolution) when compared with the perfect case of 0% tilting.

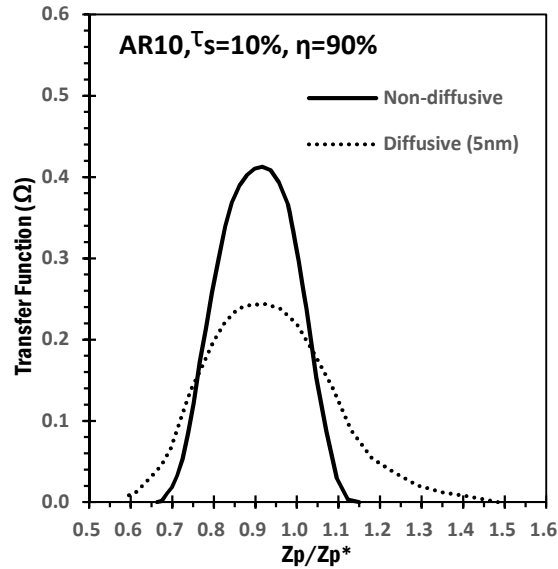


Figure 6. 10 Compare between the diffusive and non-diffusive DMC transfer function for channel aspect ratio of 10 and tilting of 10%.

Generally, the comparison between the three tilting yield a noticeable shifting in the transfer function curves. The side tilting transfer function had a higher amount for shifting to the left side. This due to the increase in the premature particle deposition on the exit slit region which is attributed to the high value of streamwise velocities in the wider spacing, and the spanwise velocities in the same direction. On the other hand, the front point tilting curve has the opposite behavior of transfer function shifting to the right. This because of the increase in particle velocity in the exit zone due to the point tiling at this location. Back tilting had the least value of peak shifting because the spacing is non-tilted at the exit cross-section location/zone and it is tilted at the particle entrance release cross-section zone. The imperfection in the DMC cross-section at particle entrance zone will be corrected as particle

travel in the streamwise direction which leads to a reduction in tilting effects (i.e. the premature and the mature particle deposition effects). However, the three kinds of tilting when it sits aside (compared) with the perfect DMC cases, it will show a difference in the peak and width of the transfer function curves. All three tilting case has less peak height and less resolution (more width) when it compared with non-tilted DMC transfer function.

Figure 6.11b shows the DMC transfer function peaks' position on the curve of the transfer function and normalize particle mobility. The three studied tilting cases are plotted with aerosols slits opening  $\eta$  for flow ratio  $\beta$  of 10 and aspect ratio of 20. All three kinds of tilting showed an increase in peak shifting (deviation of the peak position off the unity) as the aerosol opening reduces below 60%. This can be understood from the figure 6.9 at which the values for the transfer function peak improved (raised) and shifted to the left side off the unity as the slits opening reduced. This can be related to the particle deposition location around the exit slit for different cases of opening. The wider slits opening results in a huge variation in particle deposition location at which particle in the narrow spacing will travel slow and results in less transfer function shifting off the unity. On the other hand, the narrow slits' opening leading particles to travel in the faster flow zone and exit earlier from the DMC channel, which causes a huge amount of peak shifting at the small slit opening.

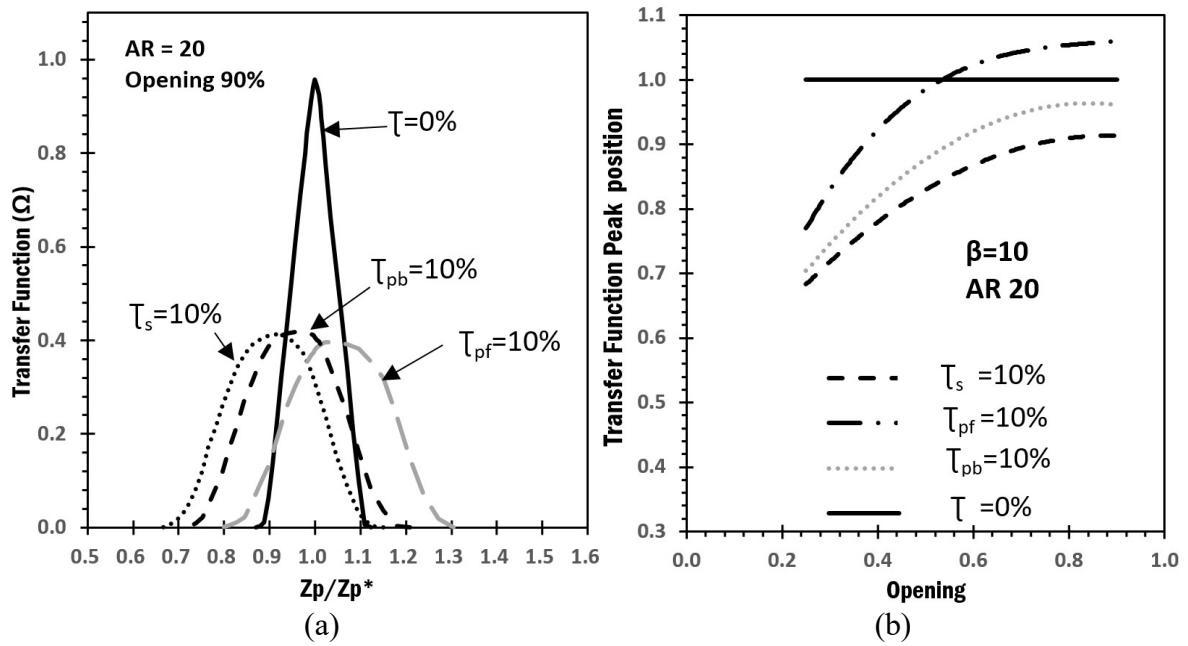


Figure 6. 11 Tilting type effect on the DMC transfer function

(a) Comparison between the DMC transfer functions under three studied imperfection tilting, (b) Peak position for the three tilting DMC transfer function, for DMC classifying channel length  $L=5\text{cm}$  and sheath flow  $Q=3\text{ lpm}$  and flow ration  $\beta=0.1$ .

## **CHAPTER 7 Dissertation Summary and Future Work**

### **7.1 Dissertation Summary**

The geometrical imperfection effects on the performance of both cylindrical and parallel-plate DMCs were investigated in this dissertation. COMSOL and MATLAB were used to build the numerical model and analyze the data. Prior to the study, the model was validated with the existing analytical and experimental data in the literature. For the cylindrical classifier, two major geometrical imperfections were studied: the eccentricity (i.e. shifting of both ends of the inner rod) and tilting of the inner cylinder. The main focus was to examine the impact of these imperfections on the DMC performance via the transfer function change. Whereas for the parallel-plate DMC, the major focus was to investigate the plate alignment. For both classifiers, parametric studies were performed with a wide range of dimensions and operating conditions. In the following sections, summaries of the dissertation's accomplishments are given.

#### **7.1.1 Eccentric Cylindrical Classifier**

The effect of axial eccentricity on the transfer function of a cylindrical differential mobility classifier (DMC) has been numerically investigated. Our modeling was validated by the comparison of the calculated transfer functions with the experimental and theoretical ones for concentric and eccentric DMCs reported in the literature.



The axial misalignment of the inner rod and outer cylinder in a cylindrical DMC distorts the flow and electrical fields in the annular particle classification channel of the DMC, resulting in the change of its transfer function. The eccentricity effect on the DMC transfer function was characterized by the decrease of peak and increase of the full width at half maximum (FWHM) in the DMC transfer function at the low axial eccentricity. As the eccentricity increased, the peak of the DMC transfer function was flattened and eventually split into two peaks (i.e., double-peaked transfer function with one in low mobility range lower than the other in high mobility range). Further study shows that the shape distortion of the transfer function of a cylindrical DMC was dominantly attributed to the distortion of the electrical field in the annular particle classification channel. The distortion of the flow field in an eccentric DMC made the width of the transfer function broader.

The sheath-to-aerosol flow rate ratio ( $\beta$ ) had a significant effect on the transfer function of an eccentric DMC. As the value of  $\beta$  increased, the shape change of the eccentric transfer function was increasingly sensitive to the axial eccentricity. In addition, the eccentric DMC transfer function was not the same when varying the total flow rate while keeping the sheath-to-aerosol flow rate ratio constant. This is because of the difference in the circumferential velocity component during the flow profile development from the uniform one at the sheath flow entrance to the fully developed one downstream of the classification channel.

The effect of the DMC classification channel length on the eccentric DMC transfer function is more obvious on a long DMC compared with that on a short DMC. This is due to the fact that the flow profile in the annular classification channel of a short DMC remains

mostly uniform (i.e., the effect of the circumferential velocity component on the particle motion is minor) in the short DMC. The radius ratio of a cylindrical DMC (i.e.,  $R_2/R_1$ ) has a minor effect on the performance of an eccentric DMC in the cases of assuming a fully developed velocity profile at the sheath flow entrance. Its effect on an eccentric DMC transfer function is, however, observable in the cases of assuming uniform velocity profile at the sheath flow entrance. The above observation is even more obvious in a long DMC. The effect of an aspect ratio of particle classification channel (length/spacing) on an eccentric transfer function is however negligible.

The peak height and sizing resolution of the eccentric DMC transfer function were reduced with the consideration of particle diffusivity. The particle diffusion made the effect of axial eccentricity less obvious on the eccentric DMC transfer function. The double-peaked transfer function of an eccentric DMC occurred at higher eccentricity when compared to that without considering the particle diffusivity.

### **7.1.2 Tilted Cylindrical Classifier**

The performance of a cylindrical differential mobility classifier (DMC) with a tilted inner rod has been numerically investigated. The knowledge learned in this study provides the basics on the control of axial tilting in the construction of a cylindrical DMC. It was found that the tilting of the inner rod in a cylindrical DMC distorted the flow field (resulting in the imbalance of axial flow velocity and development of circumferential velocity) and electrical field (resulting in asymmetrical intensity) in the particle classification channel. The rod tilting consequently led to peak reduction and width increase at half peak height (less

resolution) of the DMC transfer function. At the extreme tilt, the single peak of the transfer function was split into two (i.e., double-peaked). This is because of the increase in inner rod tilting that distorts the flow and electrical fields in the DMC classification channel. As a result, particles' position varied when moved in the region nearby the exit slit (up and down relative to the exit slit depending on the particle releasing position), causing more particles' loss in the classification channel. Further investigation identified that the distortion in the electrical field is the dominant factor influencing the shape of the DMC transfer function.

Our study also found that the effect of inner rod tilting on the DMC transfer function is more obvious when the DMC was operated at a high sheath-to-aerosol flow rate ratio (compared to that at low sheath-to-aerosol flow rate ratio). The increase of total flow rate and decrease of classification channel length minimized the adverse effects of tilting on the DMC transfer function. Regarding the geometrical parameters, the ratio of inner rod and outer cylinder radii affected the performance on the DMC under the same relative tilting condition. The change of the aspect ratio of the inner rod (i.e., channel length-to-inner rod radius) had an effect on the DMC transfer function only for the ratio less than 2.5. This is because of the increase of the absolute tilting angle of the inner rod (as the aspect ratio was reduced). The particle diffusivity tended to shadow the effect of inner rod tilting on the DMC transfer function.

To summarize the shape change of the DMC transfer function due to the variation of the relative inner rod tilting, we categorized the change into three different domains: single-peaked, transitional and double-peaked. The classification length and the sheath-to-aerosol flow rate ratio determined the shape of the domains. For a fixed classification channel length,

the single-peaked zone occurred at low relative tilting. As the relative tilting increased, the shape of the DMC transfer function was transitioned to the double-peaked zone. A similar observation was obtained in the case of sheath-to-aerosol flow ratio. However, the transitional range became broadened as the length of the classification channel increased while the increase of the sheath-to-aerosol flow ratio reduced the transitional range.

### **7.1.3 Parallel Plates Classifier**

The performance of a miniature parallel-plate differential mobility classifier, operating at low aerosol and sheath flow rates, has been numerically investigated with the study objective to establish a general guideline for the future design of compact DMCs of this type. The result of our modeling was first validated by the comparison of the numerical and experimental transfer functions of the mini-plate DMCs evaluated in the work of Liu and Chen (2016a). The calculated and measured voltages of the maximal penetration of 100 nm particles through the classification channel of mini-plate DMCs as a function of the sheath-to-aerosol flow rate ratio,  $\beta$ , were also compared in the model validation. The agreements between the calculated and measured data validated our modeling was good. A systematic study was then performed to investigate the effect of geometrical parameters of the mini-plate DMC's classification channel on the transfer function. The channel design parameters under consideration are the aspect ratio and the total cross-sectional area of particle classification channel, the percentages of slit opening for aerosol inlet and exit slits, and the angle of aerosol injection. The effect of the sheath-to-aerosol flow rate ratio on the DMC transfer function was also considered. It is found that both the channel aspect ratio

(CAR) and the slit opening percentage have significant effects on the performance of mini-plate DMCs (i.e., the transfer function and the voltage for maximal particle penetration through the classification channel). In reference to the 2-D transfer function in which the total sheath flow rate is contributed to the sizing resolution of a DMC, the plate DMC shall have the CAR greater than 10 and the opening percentage of 75–90% for both the aerosol inlet and exit slits. The peak of DMC transfer function deteriorated when mini-plate DMCs had a CAR less than 8.0. To obtain a good performance of a mini-plate DMC, the opening percentages for aerosol inlet and exit slits shall be kept the same. In the cases where the aerosol slit opening percentage is the same as that of the aerosol exit slit, the effect of slit opening percentage less than 35% was very minor on the transfer function of DMCs. In the cases where the aerosol inlet slit percentage is fixed while varying the aerosol exit slit percentage, the worst mini-plate DMC performance was found in the case of DMCs with a round aerosol exit. The effects of the aerosol injection angle and the total cross-sectional area of particle classification channel on the transfer function of mini-plate DMCs were found negligible. Note that the observation of the negligible aerosol injection angle effect on the DMC transfer function is due to the laminar flow assumption of our numerical modeling. Finally, the concept of effective sheath flow, proposed in the work of Liu and Chen (2016a), was confirmed in this study, especially for DMCs with the slit opening percentage greater than 50%.

#### **7.1.4 Parallelism of the Parallel Plates Classifier**

The performance of a small plate differential mobility classifier transfer function, having the issue of plate incline (potentially due to the improper practice in the DMC re-assembly, required after cleaning the device), has been investigated in this study. Three basic types of plate incline were included in this study: plate sided-incline, and plate pointed-incline (front and back points). Similar to the geometrical imperfection on the cylindrical DC, the plate incline in a plate DMC, in general, resulted in the reduction of peak height, the broadening of width at half peak height, and the drifting of peak electrical mobility of the transfer function. This is because the plate incline distorts the flow and electrical fields in the DMC classification channel, causing increased spatial variation of particle motion in the region nearby the classified particle exit slit. More particles are thus lost on the walls nearby the particle exit slit (compared to the ideal case i.e., for ideal plate DMCs). The distortion of the electrical field in the DMC classification channel was identified as the primary contributor to the degradation of the transfer function.

Our study also found that the adverse effect of plate incline on the transfer function is enhanced when the plate DMC was operated at a high sheath-to-aerosol flow rate ratio. The increase of total flow rate and decrease of classification channel length minimized the negative impact of plate incline on the DMC transfer function. The incline effect on the DMC transfer function was further affected by the variation of the classification channel aspect ratio under the same plate incline condition. The classification channel with a high aspect ratio tends to be more subjected to the plate incline because of the greater reduction

of the plate-to-plate spacing for the same plate incline (as the channel aspect ratio was increased).

The peak electrical mobility of the side-inclined plate DMC transfer function was shifted to the lesser mobility range. Compared to the case of side-incline, the peak mobility in the case of back-pointed incline was less shifted. The peak mobility of transfer function in the case of a plate DMC with the plate front-pointed incline was further drifted into the high mobility regime. It is due to the change of the flow in the particle classification channel that leads to the observed variance in the transfer function peak shifting.

## **7.2 Recommendations for Future Research**

The study of the geometrical imperfections is a challenge that needs continuous attention for all types of instruments, especially nanoparticle classifiers. The knowledge of these imperfections helps to set the machining tolerance limits when building these instruments. The importance of these geometrical tolerance limits comes from the direct relation between the geometry and both the flow and electrical fields. Still, there is much research to be done to set all possible machining tolerances for manufacturers. Furthermore, the numerical procedure and the methodology of this thesis can be applied to most aerosol measuring instruments like the electrostatic precipitators, aerosols mass analyzers, etc.

The geometrical imperfections of both cylindrical and parallel-plates DMCs were investigated via numerical modeling techniques. The challenge of using and verifying the models for imperfect geometries can always be improved. It would be useful to summarize

and assemble all the geometrical imperfections of cylindrical and parallel-plates DMCs via driving an analytical solution for all possible types of classifier imperfections.

Furthermore, the advantage of using the numerical method made it easy to investigate various cases of imperfection. However, it was unfortunate that utilizing two different classifiers in a tandem setup was not thoroughly considered. The skewness in the numerical tandem DMC transfer function's curve will be a good indicator to its experimental counterpart and is useful for DMC calibration.

The focus in modeling the two main types of DMCs (the cylindrical and parallel plate) was a good start to this field of research. Therefore, it would be reasonable to extend it to investigate the other types of DMCs like the disk and circular shape designs. Despite the fact that these two types are not yet commercialized, investigating the tolerance limitations will encourage designers and companies to invest in building and commercializing them.

The numerical modeling methodology and the procedure that was applied here will encourage further expansion of this research by investigating DMC aerosol measurement at high temperatures and high concentrations. It will be more useful to isolate these parameters (temperature and concentration) numerically than performing the experiments. This can be achieved by considering the thermophoresis effects and space charge effects. Finally, extend the study and include gravity and the inertial forces for large particles is a good idea needs to be considered in future studies.



## **Literature Cited**

## Literature Cited

- Aganval, J. K., and Sem, G. J. (1978). Generating Submicron Monodispersc Aerosol for Instrument Calibration. *TSI Quarterly, May/June*, 3–8.
- Allen, M. D., & Raabe, O. G. (1982). Re-evaluation of millikan’s oil drop data for the motion of small particles in air. *Journal of Aerosol Science*, *13*(6), 537–547. [https://doi.org/10.1016/0021-8502\(82\)90019-2](https://doi.org/10.1016/0021-8502(82)90019-2)
- Allen, Michael D., & Raabe, O. G. (1985). Slip Correction Measurements of Spherical Solid Aerosol Particles in an Improved Millikan Apparatus. *Aerosol Science and Technology*, *4*(3), 269–286. <https://doi.org/10.1080/02786828508959055>
- Alonso, M., & Endo, Y. (2001). Dispersion of aerosol particles undergoing Brownian motion. *Journal of Physics A: Mathematical and General*, *34*(49), 10745–10755. <https://doi.org/10.1088/0305-4470/34/49/301>
- Alonso, M., Santos, J. P., Hontañón, E., & Ramiro, E. (2009). First differential mobility analysis (DMA) measurements of air ions produced by radioactive source and corona. *Aerosol and Air Quality Research*, *9*(4), 453–457. <https://doi.org/10.4209/aaqr.2009.05.0033>
- Alsharif, T., & Chen, D.-R. (2018). On the Design of Miniature Parallel-Plate Differential Mobility Classifiers. *Journal of Aerosol Science*. <https://doi.org/10.1016/j.jaerosci.-2018.04.003>
- Amo-González, M., & Pérez, S. (2018). Planar Differential Mobility Analyzer with a Resolving Power of 110. *Analytical Chemistry*, *90*(11), 6735–6741. <https://doi.org/10.1021/acs.analchem.8b00579>
- AMS. (2012). Differential mobility analyzer - AMS Glossary. Retrieved July 15, 2018, from [http://glossary.ametsoc.org/wiki/Differential\\_mobility\\_analyzer](http://glossary.ametsoc.org/wiki/Differential_mobility_analyzer)
- Azarmi, S., Roa, W. H., & Löbenberg, R. (2008). Targeted delivery of nanoparticles for the treatment of lung diseases. *Advanced Drug Delivery Reviews*, *60*(8), 863–875. <https://doi.org/10.1016/j.addr.2008.06.003>

doi.org/10.1016/j.addr.2007.11.006

- Beckers, B., & Beckers, P. (2012). A general rule for disk and hemisphere partition into equal-area cells. *Computational Geometry: Theory and Applications*, 45(7), 275–283. <https://doi.org/10.1016/j.comgeo.2012.01.011>
- Brunelli, N. A., Flagan, R. C., & Giapis, K. P. (2009). Radial differential mobility analyzer for one nanometer particle classification. *Aerosol Science and Technology*, 43(1), 53–59. <https://doi.org/10.1080/02786820802464302>
- Chen, B. T., Schwegler-Berry, D., Cumpston, A., Cumpston, J., Friend, S., Stone, S., & Keane, M. (2016). Performance of a scanning mobility particle sizer in measuring diverse types of airborne nanoparticles: Multi-walled carbon nanotubes, welding fumes, and titanium dioxide spray. *Journal of Occupational and Environmental Hygiene*, 13(7), 501–518. <https://doi.org/10.1080/15459624.2016.1148267>
- Chen, D. (1996). *Nanometer aerosol generation and measurement*. University of Minnesota.
- CHEN, D., & LIU, Q. (2019). *CURVED CLASSIFIERS AND CLASSIFICATION METHODS* (No. 15 / 768 , 574). United States Patent Application Publication, USA.
- Chen, D. R., Pui, D. Y. H., Hummes, D., Fissan, H., Quant, F. R., & Sem, G. J. (1998a). Design and evaluation of a nanometer aerosol differential mobility analyzer (NanoDMA). *Journal of Aerosol Science*, 29(5–6), 497–509. [https://doi.org/10.1016/S0021-8502\(97\)10018-0](https://doi.org/10.1016/S0021-8502(97)10018-0)
- Chen, D. R., Pui, D. Y. H., Hummes, D., Fissan, H., Quant, F. R., & Sem, G. J. (1998b). Design and evaluation of a nanometer aerosol differential mobility analyzer (NanoDMA). *Journal of Aerosol Science*, 29(5/6), 497–509. [https://doi.org/10.1016/S0021-8502\(97\)10018-0](https://doi.org/10.1016/S0021-8502(97)10018-0)
- Choi, H. S., Ashitate, Y., Lee, J. H., Kim, S. H., Matsui, A., Insin, N., ... Tsuda, A. (2010). Rapid translocation of nanoparticles from the lung airspaces to the body. *Nature Biotechnology*, 28(12), 1300–1303. <https://doi.org/10.1038/nbt.1696>
- Cummings, C. A. (1998). *A theoretical study of the flow of slightly compressible non-Newtonian fluids in eccentric annuli with entrance effects*. University of Oklahoma. Retrieved from <https://search-proquest-com.proxy.mul.missouri.edu/docview/30437->

0221/previewPDF/48F2E28EC13C424DPQ/1?accountid=14576

- Dahl, R., & Mygind, N. (1998). Anatomy, physiology and function of the nasal cavities in health and disease. *Advanced Drug Delivery Reviews*, 29(1–2), 3–12. Retrieved from <http://eutils.ncbi.nlm.nih.gov/entrez/eutils/elink.fcgi?dbfrom=pubmed&id=10837577&retmode=ref&cmd=prlinks>
- de la Mora, J. F., Ude, S., & Thomson, B. A. (2006). The potential of differential mobility analysis coupled to MS for the study of very large singly and multiply charged proteins and protein complexes in the gas phase. *Biotechnology Journal*, 1(9), 988–997. <https://doi.org/10.1002/biot.200600070>
- Donaldson, K., Brown, D., Clouter, A., Duffin, R., MacNee, W., Renwick, L., ... Stone, V. (2002). The Pulmonary Toxicology of Ultrafine Particles. *Journal of Aerosol Medicine*, 15(2), 213–220. <https://doi.org/10.1089/089426802320282338>
- Erikson, H. A. (1921). The change of mobility of the positive ions with age in oxygen and nitrogen. *Physical Review A*, 55(6), 4015–4018.
- Fissan, H., Hummes, D., Stratmann, F., Büscher, P., Neumann, S., Pui, D. Y. H., & Chen, D. (1996). Experimental comparison of four differential mobility analyzers for nanometer aerosol measurements. *Aerosol Science and Technology*, 24(1), 1–13. <https://doi.org/10.1080/02786829608965347>
- Flagan, R. C. (1998). History of Electrical Aerosol Measurements. *Aerosol Science and Technology*, 28(4), 301–380. <https://doi.org/10.1080/02786829808965530>
- Geiser, M., Rothen-Rutishauser, B., Kapp, N., Schürch, S., Kreyling, W., Schulz, H., Gehr, P. (2005). Ultrafine particles cross cellular membranes by nonphagocytic mechanisms in lungs and in cultured cells. *Environmental Health Perspectives*, 113(11), 1555–1560. <https://doi.org/10.1289/ehp.8006>
- Giacomelli Maltoni, G., Melandri, C., Prodi, V., Tarroni, G., Zaiacomo, A. De, Bompane, G. F., & Formignani, M. (1973). An improved parallel plate mobility analyzer for aerosol particles. *Journal of Aerosol Science*, 4(6). [https://doi.org/10.1016/0021-8502\(73\)90136-5](https://doi.org/10.1016/0021-8502(73)90136-5)
- Grassin-Delyle, S., Buenestado, A., Naline, E., Faisy, C., Blouquit-Laye, S., Couderc, L. J.,

- Devillier, P. (2012). Intranasal drug delivery: An efficient and non-invasive route for systemic administration - Focus on opioids. *Pharmacology and Therapeutics*, *134*(3), 366–379. <https://doi.org/10.1016/j.pharmthera.2012.03.003>
- Gysel, M., McFiggans, G. B., & Coe, H. (2009). Inversion of tandem differential mobility analyser (TDMA) measurements. *Journal of Aerosol Science*, *40*(2), 134–151. <https://doi.org/10.1016/j.jaerosci.2008.07.013>
- Hagwood, C., Sivathanu, Y., & Mulholland, G. (1999). The DMA Transfer Function with Brownian Motion a Trajectory/Monte-Carlo Approach. *Aerosol Science and Technology*, *30*(1), 40–61. <https://doi.org/10.1080/027868299304877>
- Hattori, K., Nakadate, K., Morii, A., Noguchi, T., Ogasawara, Y., & Ishii, K. (2017). Exposure to nano-size titanium dioxide causes oxidative damages in human mesothelial cells: The crystal form rather than size of particle contributes to cytotoxicity. *Biochemical and Biophysical Research Communications*, *492*(2), 218–223. <https://doi.org/10.1016/j.bbrc.2017.08.054>
- Herbarth, O., Fritz, G., Krumbiegel, P., Diez, U., Franck, U., & Richter, M. (2001). Effect of sulfur dioxide and particulate pollutants on bronchitis in children - A risk analysis. *Environmental Toxicology*, *16*(3), 269–276. <https://doi.org/10.1002/tox.1033>
- Hewitt, G. W. (1957). The charging of small particles for electrostatic precipitation. *American Institute of Electrical Engineers, Part I: Communication and Electronics, Transactions of The*, *76*(3), 300–306. <https://doi.org/10.1109/TCE.1957.6372672>
- Hinds, W. C. (1999). *Aerosol Technology: Properties, Behavior, and Measurement of Airborne Particles*, 2nd Edition. Wiley.
- Hinds, W. C. (2011). Physical and Chemical Processes in Aerosol Systems. *Aerosol Measurement: Principles, Techniques, and Applications: Third Edition*, 31–40. <https://doi.org/10.1002/9781118001684.ch3>
- Intra, P., & Tippayawong, N. (2008). An overview of differential mobility analyzers for size classification of nanometer-sized aerosol particles. *Songklanakarinn Journal of Science and Technology*, *30*(2), 243–256.
- Karlsson, H. L., Gustafsson, J., Cronholm, P., & Möller, L. (2009). Size-dependent toxicity

- of metal oxide particles-A comparison between nano- and micrometer size. *Toxicology Letters*, 188(2), 112–118. <https://doi.org/10.1016/j.toxlet.2009.03.014>
- Kinney, P., Pui, D., Mulliolland, G., & Bryner, N. (1991). Use of the Electrostatic Classification Method to Size 0.1  $\mu\text{m}$  SRM Particles - A Feasibility Study. *Journal of Research of the National Institute of Standards and Technology*, 96(2), 147–176.
- Knutson, E. O., & Whitby, K. T. (1975). Aerosol classification by electric mobility: apparatus, theory, and applications. *Journal of Aerosol Science*, 6(6), 443–451. [https://doi.org/10.1016/0021-8502\(75\)90060-9](https://doi.org/10.1016/0021-8502(75)90060-9)
- Knutson, Earl Owen. (1972). The distribution of electric charge among the particles of an artificially charged aerosol. *Mechanical Engineering, Ph. D.*
- Kousaka, Y., Okuyama, K., & Adachi, M. (1985). Determination of Particle Size Distribution of Ultra-Fine Aerosols Using a Differential Mobility Analyzer. *Aerosol Science and Technology*, 4(2), 209–225. <https://doi.org/10.1080/02786828508959049>
- Kousaka, Yasuo, Okuyama, K., Adachi, M., & Mimura, T. (1986). Effect Of Brownian Diffusion On Electrical Classification Of Ultrafine Aerosol Particles In Differential Mobility Analyzer. *Journal of Chemical Engineering of Japan*, 19(5), 401–407. <https://doi.org/10.1252/jcej.19.401>
- Kozlowski, J., & Ferna, J. (2013). Hand-held differential mobility analyzers of high resolution for 1 – 30 nm particles : Design and fabrication considerations, 57, 45–53. <https://doi.org/10.1016/j.jaerosci.2012.10.009>
- Kulkarni, P., Baron, P. A., & Willeke, K. (2011). *Aerosol measurement principles, techniques, and applications* (3rd ed). Hoboken, N.J.: Wiley.
- Kulkarni, Pramod, Baron, P. A., & Willeke, K. (2011). Appendix A: Glossary of Terms. *Aerosol Measurement: Principles, Techniques, and Applications*, 821–829. <https://doi.org/10.1002/9781118001684.app1>
- L Zhang, FXGu, JM Chan, AZ Wang, R. L. and O. F. (2007). Nanoparticles in Medicine: Therapeutic Applications and Developments. *Education Policy Analysis Archives*, 83(5), 761–769. <https://doi.org/10.1038/sj.clp>
- Langer, G., & Radnik, J. L. (1961). Development and preliminary testing of a device for

- electrostatic classification of submicron airborne particles. *Journal of Applied Physics*, 32(5), 955–957. <https://doi.org/10.1063/1.1736140>
- Lee, B. J., Kim, B., & Lee, K. (2014). Air pollution exposure and cardiovascular disease. *Toxicological Research*, 30(2), 71–75. <https://doi.org/10.5487/TR.2014.30.2.071>
- Lenggoro, I. W., Okuda, T., Gunji, Y., & Wuled Lenggoro, I. (2015). Measurement of the Electrostatic Charging State of Individual Particles in Ambient Aerosol Using Kelvin Probe Force Microscopy. *Eaorozu Kenkyu*, 30(3), 190–197. <https://doi.org/10.11203-/jar.30.190>
- Li, W., Li, L., & Chen, D.-R. (2006). Technical Note: A New Deconvolution Scheme for the Retrieval of True DMA Transfer Function from Tandem DMA Data. *Aerosol Science and Technology*, 40(12), 1052–1057. <https://doi.org/10.1080/0278682060094-4331>
- Liao, C. M., Chio, C. P., Chen, W. Y., Ju, Y. R., Li, W. H., Cheng, Y. H., ... Ling, M. P. (2011). Lung cancer risk in relation to traffic-related nano/ultrafine particle-bound PAHs exposure: A preliminary probabilistic assessment. *Journal of Hazardous Materials*, 190(1–3), 150–158. <https://doi.org/10.1016/j.jhazmat.2011.03.017>
- Lin, G. G., & Scott, J. G. (2012). Toxicological considerations when creating nanoparticle based drugs and drug delivery systems?, 100(2), 130–134. <https://doi.org/10.1016/-j.pestbp.2011.02.012>. Investigations
- Liu, B. Y. H., & Pui, D. Y. H. (1974). A submicron aerosol standard and the primary, absolute calibration of the condensation nuclei counter. *Journal of Colloid And Interface Science*, 47(1), 155–171. [https://doi.org/10.1016/0021-9797\(74\)90090-3](https://doi.org/10.1016/0021-9797(74)90090-3)
- Liu, Q. (2015). *Ultrafine particle generation and measurement*. Virginia Commonwealth University.
- Liu, Q., & Chen, D.-R. (2016a). Performance evaluation of a miniature plate Electrostatic Aerosol Analyzer (mini-plate EAA). *Journal of Aerosol Science*, 95, 30–42. <https://doi.org/10.1016/j.jaerosci.2016.01.001>
- Liu, Q., & Chen, D. (2016b). Experimental evaluation of miniature plate DMAs ( mini-plate DMAs ) for future ultrafine particle ( UFP ) sensor network, 6826(April). <https://>

doi.org/10.1080/02786826.2016.1149547

- Lucht, P. (2015). *Bipolar Coordinates and the Two-Cylinder Capacitor*. Salt Lake City, Utah. Retrieved from [https://www.researchgate.net/publication/273123774\\_Bipolar\\_-\\_Coordinates\\_and\\_the\\_Two-Cylinder\\_Capacitor](https://www.researchgate.net/publication/273123774_Bipolar_-_Coordinates_and_the_Two-Cylinder_Capacitor)
- Mai, H., & Flagan, R. C. (2018). Scanning DMA Data Analysis I. Classification Transfer Function. *Aerosol Science and Technology*, 52(12), 1382–1399. <https://doi.org/10.1080/02786826.2018.1528005>
- Masset, L., Bröls, O., & Kerschen, G. (2011). Partition of the circle in cells of equal area and shape, 6. Retrieved from <http://hdl.handle.net/2268/91953>
- McClelland, J. A. (1898). On the Conductivity of the Hot Gases from Flames. *Phil. Magazine*, 46, 29–42.
- Montet, X., Montet-Abou, K., Reynolds, F., Weissleder, R., & Josephson, L. (2006). Nanoparticle Imaging of Integrins on Tumor Cells. *Neoplasia*, 8(3), 214–222. <https://doi.org/10.1593/neo.05769>
- Müschelborn, P. M. (2007). Development of a differential mobility particle sizer applied to industrial gas phase synthesis processes for nanoscaled powders, 15–41. Retrieved from [http://duepublico.uni-duisburg-essen.de/servlets/DocumentServlet/Document-16630/Dissertation\\_Mueschenborn.pdf](http://duepublico.uni-duisburg-essen.de/servlets/DocumentServlet/Document-16630/Dissertation_Mueschenborn.pdf)
- Oberdörster, G., Oberdörster, E., & Oberdörster, J. (2005). Nanotoxicology: an emerging discipline evolving from studies of ultrafine particles. *Environmental Health Perspectives*, 113(7), 823–839. <https://doi.org/10.1289/ehp.7339>
- Oberdörster, G., Sharp, Z., Atudorei, V., Elder, A., Gelein, R., Kreyling, W., & Cox, C. (2004). Translocation of inhaled ultrafine particles to the brain. *Inhalation Toxicology*, 16(6–7), 437–445. <https://doi.org/10.1080/08958370490439597>
- Oliveira, M. L. S., Navarro, O. G., Crissien, T. J., Tutikian, B. F., da Boit, K., Teixeira, E. C., ... Silva, L. F. O. (2017). Coal emissions adverse human health effects associated with ultrafine/nano-particles role and resultant engineering controls. *Environmental Research*, 158(May), 450–455. <https://doi.org/10.1016/j.envres.2017.07.002>
- Pomareda, V., Lopez-Vidal, S., Calvo, D., Pardo, a, & Marco, S. (2013). A novel differential



- mobility analyzer as a VOC detector and multivariate techniques for identification and quantification. *The Analyst*, 138(12), 3512–3521. <https://doi.org/10.1039/c3an00078h>
- Rader, D. J., & McMurry, P. H. (1986). Application of the tandem differential mobility analyzer to studies of droplet growth or evaporation. *Journal of Aerosol Science*, 17(5), 771–787. [https://doi.org/10.1016/0021-8502\(86\)90031-5](https://doi.org/10.1016/0021-8502(86)90031-5)
- Ramechecandane, S., Beghein, C., Allard, F., & Bombardier, P. (2011). Modelling ultrafine / nano particle dispersion in two differential mobility analyzers ( M-DMA and L-DMA). *Building and Environment*, 46(11), 2255–2266. <https://doi.org/10.1016/j.buildenv.2011.05.005>
- Ranft, U., Schikowski, T., Sugiri, D., Krutmann, J., & Krämer, U. (2009). Long-term exposure to traffic-related particulate matter impairs cognitive function in the elderly. *Environmental Research*, 109(8), 1004–1011. <https://doi.org/10.1016/j.envres.2009.08.003>
- Ranjan, M., & Dhaniyala, S. (2008). A new miniature electrical aerosol spectrometer (MEAS): Experimental characterization. *Journal of Aerosol Science*, 39(8), 710–722. <https://doi.org/10.1016/j.jaerosci.2008.04.005>
- Reischl, G. P. (1991). Measurement of ambient aerosols by the differential mobility analyzer method: Concepts and realization criteria for the size range between 2 and 500 nm. *Aerosol Science and Technology*, 14(1), 5–24. <https://doi.org/10.1080/02786829108-959467>
- Roduner, E. (2006). Size matters: Why nanomaterials are different. *Chemical Society Reviews*, 35(7), 583–592. <https://doi.org/10.1039/b502142c>
- Rosell-Llompart, J., Loscertales, I. G., Bingham, D., & Fernández De La Mora, J. (1996). Sizing nanoparticles and ions with a short differential mobility analyzer. *Journal of Aerosol Science*, 27(5), 695–719. [https://doi.org/10.1016/0021-8502\(96\)00016-X](https://doi.org/10.1016/0021-8502(96)00016-X)
- Rosser, S., & de la Mora, J. F. (2005). Vienna-Type DMA of High Resolution and High Flow Rate. *Aerosol Science and Technology*, 39(12), 1191–1200. <https://doi.org/10.1080/02786820500444820>
- Rus, J., Moro, D., Sillero, J. A., Royuela, J., Casado, A., Estevez-Molinero, F., & Fernández

- de la Mora, J. (2010). IMS-MS studies based on coupling a differential mobility analyzer (DMA) to commercial API-MS systems. *International Journal of Mass Spectrometry*, 298(1–3), 30–40. <https://doi.org/10.1016/j.ijms.2010.05.008>
- Santos, J. P., Hontañón, E., Ramiro, E., & Alonso, M. (2009). Performance evaluation of a high-resolution parallel-plate differential mobility analyzer. *Atmospheric Chemistry and Physics Discussions*, 8(5), 17631–17660. <https://doi.org/10.5194/acp-9-2419-2009>
- Seol, K. S., Yabumoto, J., & Takeuchi, K. (2002). A differential mobility analyzer with adjustable column length for wide particle-size-range measurements. *Journal of Aerosol Science*, 33(11), 1481–1492. [https://doi.org/10.1016/S0021-8502\(02\)00094-0](https://doi.org/10.1016/S0021-8502(02)00094-0)
- Sergeev, Gleb B. Klabunde, K. J. (2013). *Nanochemistry*. Elsevier. Retrieved from <https://app.knovel.com/hotlink/toc/id:kpNE000003/nanochemistry-2nd-edition/nanochemistry-2nd-edition>
- Seto, T., Nakamoto, T., Okuyama, K., Adachi, M., Kuga, Y., & Takeuchi, K. (1997). Size distribution measurement of nanometer-sized aerosol particles using DMA under low-pressure conditions. *Journal of Aerosol Science*, 28(2), 193–206. [https://doi.org/10.1016/S0021-8502\(96\)00071-7](https://doi.org/10.1016/S0021-8502(96)00071-7)
- Steer, B., Gorbunov, B., Muir, R., Ghimire, A., Rowles, J., Steer, B., ... Rowles, J. (2014). Portable Planar DMA : Development and Tests Portable Planar DMA : Development and Tests, 48(3), 251–260. <https://doi.org/10.1080/02786826.2013.868863>
- Stolzenburg, Mark R, & McMurry, P. H. (2008). Equations Governing Single and Tandem DMA Configurations and a New Lognormal Approximation to the Transfer Function. *Aerosol Science and Technology*, 42(6), 421–432. <https://doi.org/10.1080/0278682-0802157823>
- Stolzenburg, Mark Richard. (1988). *An ultrafine aerosol size distribution measuring system*. ProQuest Dissertations and Theses. University of Minnesota. Retrieved from <http://www.researchgate.net/publication/230691922%0AAn>
- Stratmann, F., Hummes, D., Kauffeldt, T., & Fissan, H. (1995). Convolution and its application to DMA transfer function measurements. *Journal of Aerosol Science*, 26(September), S143–S144. [https://doi.org/10.1016/0021-8502\(95\)96979-h](https://doi.org/10.1016/0021-8502(95)96979-h)

- Tanaka, H., & Takeuchi, K. (2002). C60 monomer as an inherently monodisperse standard nanoparticle in the 1 nm range. *Japanese Journal of Applied Physics, Part 1: Regular Papers and Short Notes and Review Papers*, 41(2 A), 922–924. <https://doi.org/10.1143/JJAP.41.922>
- Tanyeri, M., Ranka, M., Sittipolkul, N., & Schroeder, C. M. (2011). A microfluidic-based hydrodynamic trap: design and implementation. *Lab on a Chip*, 11(10), 1786. <https://doi.org/10.1039/c0lc00709a>
- TSI INCORPORATED. (2018). ELECTROSTATIC CLASSIFIERS AND DMAS. Retrieved July 8, 2018, from <http://www.tsi.com/electrostatic-classifiers-and-dmas/>
- Uin, J., Tamm, E., & Mirme, A. (2011). Very Long DMA for the Generation of the Calibration Aerosols in Particle Diameter Range up to 10  $\mu\text{m}$  by Electrical Separation, 1980, 531–538. <https://doi.org/10.4209/aaqr.2011.05.0068>
- Vlasenko, S. S., Su, H., Pöschl, U., Andreae, M. O., & Mikhailov, E. F. (2016). Tandem configuration of differential mobility and centrifugal particle mass analyzers for investigating aerosol hygroscopic properties. *Atmospheric Measurement Techniques Discussions*, (September), 1–23. <https://doi.org/10.5194/amt-2016-249>
- von Klot, S., Wölke, G., Tuch, T., Heinrich, J., Dockery, D. W., Schwartz, J., ... Peters, A. (2002). Increased asthma medication use in association with ambient fine and ultrafine particles. *European Respiratory Journal*, 20(3), 691–702. <https://doi.org/10.1183/09031936.02.01402001>
- Wen, T., Krichtafovitch, I., & Mамishev, A. V. (2016). Numerical study of electrostatic precipitators with novel particle-trapping mechanism. *Journal of Aerosol Science*, 95, 95–103. <https://doi.org/10.1016/j.jaerosci.2016.02.001>
- Whitby, K. T., & Clark, W. E. (1966). Electric aerosol particle counting and size distribution measuring system for the 0.015 to 1  $\mu\text{m}$  size range. *Tellus A*, 18(2–3), 573–586. <https://doi.org/10.3402/tellusa.v18i2-3.9340>
- Winklmayr, W., Reischl, G. P., Lindner, A. O., & Berner, A. (1991). A new electromobility spectrometer for the measurement of aerosol size distributions in the size range from 1 to 1000 nm. *Journal of Aerosol Science*, 22(3), 289–296. <https://doi.org/10.1016/>

S0021-8502(05)80007-2

- Yonemichi, T., Fukagata, K., Fujioka, K., & Okuda, T. (2019). Numerical simulation of parallel-plate particle separator for estimation of charge distribution of PM<sub>2.5</sub>. *Aerosol Science and Technology*, *0*(0), 1–20. <https://doi.org/10.1080/02786826.2019.1569198>
- Zeleny, J. (1898). On the Ratio of the Velocities of the Two Ions Produced in Gases by Rontgen Radiation; and on Some Related Phenomena. *Phil. Mag.*, *46*, 120–154.
- Zeleny, John. (1900). The velocity of the ions produced in gases by Röntgen rays. *Philosophical Transactions*, *195*, 193–234.
- Zhang, M., & Wexler, A. S. (2006). Cross flow ion mobility spectrometry: Theory and initial prototype testing. *International Journal of Mass Spectrometry*, *258*(1–3), 13–20. <https://doi.org/10.1016/j.ijms.2006.05.012>
- Zhang, S.-H., & Flagan, R. C. (1996). Resolution of the radial differential mobility analyzer for ultrafine particles. *Journal of Aerosol Science*, *27*(8), 1179–1200.
- Zhang, S., Akutsu, Y., Russell, L. M., Flagan, R. C., Seinfeld, J. H., Akutsu, Y., ... Seinfeld, J. H. (1995). Radial Differential Mobility Analyzer, *23*(3), 357–372. <https://doi.org/10.1080/02786829508965320>
- Zhu, Y., Hinds, W. C., Kim, S., & Sioutas, C. (2002). Concentration and size distribution of ultrafine particles near a major highway. *Journal of the Air & Waste Management Association (1995)*, *52*(9), 1032–1042. <https://doi.org/10.1080/10473289.2002.10470842>

## **Appendices**

## **APPENDIX A: Bipolar Coordinate System**

In the case of shifting the center of the inner cylinder, the spacing between the inner and outer cylinders is constant. This leads to the unsymmetrical flow, electrical field and particle traveling distance around the cylinder. In other word, on the widest space, the axial flow is at its maximum value and it is at its minimum value at the narrowest spacing. The highest value of the electrical potential intensely at the narrowest spacing and the lowest value occurs at the wider spacing. This deviates (or drifts) particles from its designated path, which changes the transfer function value. The derivation of the eccentric transfer function is based on Knutson & Whitby, (1975) at which we calculate particle traveling distance and develop a procedure to calculate a non-diffusive eccentric transfer function. Since the eccentric DMC consists of two eccentric cylinders, it is more convenient to analyze the flow and the electric field in the spacing between the eccentric cylinders using the bipolar coordinate system.

We define DMC eccentricity ( $\epsilon$ ) as a ratio of the shift between the center of the inner and outer cylinders ( $S$ ) to the spacing ( $R_2 - R_1$ ) between them.

$$\epsilon = \frac{S}{(R_2 - R_1)} \quad (\text{A.1})$$

Figure A.1a shows the bipolar coordinate system which is a 2D coordinate system formed by an orthogonal intersection of two groups of curves-circles ( $\eta$  &  $\xi$ ) (Lucht, 2015). The first coordinate ( $\eta$ ) are circles with the center at  $x, y=S.\text{coth}(\eta),0$ , and radius  $S.\text{csch}(\eta)$

is denoted by  $\eta$  coordinate. Where  $S$  is foci coordinate distance and it is related to the inner and outer radii, and the shifting  $s$  is given as:

$$S = \frac{\sqrt{(s^2 - (R_2 + R_1)^2)(s^2 - (R_2 - R_1)^2)}}{2s} \quad (\text{A.2})$$

The second coordinate ( $\xi$ ) are the circles that intersect at two foci and intersect the  $\eta$ -circles tangentially with angles from  $0 \rightarrow 2\pi$ . The bipolar coordinate curves have a constant value of  $\eta$  and  $\xi$ , and also have two focal points at  $x, y = (\pm S, 0)$ . To calculate the particle traveling distance (path) for the eccentric DMC, we assume it is laminar flow and fully developed velocity profile. The bipolar coordinates are mapped into the computational domain and shown in [figure A.1b](#) and [A.1c](#) respectively. The three dimensional computational domains are extended in

- $\eta$ -coordinate is from  $\beta$  to  $\alpha$ , which are the values of the inner and outer cylinder respectively
- $\xi$ - coordinate is from  $0$  to  $\pi$  (not  $2\pi$ ) because the computational domain is symmetric
- $z$ - coordinate is from  $L$  to  $0$  (from the inlet slit down to the exit slit heights)

The axial traveling distance in the  $z$ -directions are shown in [figure A.1.c](#) and can be expressed in the following equation

$$\frac{dz}{d\eta} = \frac{-(\beta - \alpha)}{Z_p V} J_W \quad (\text{A.3})$$

Where  $\beta$  and  $\alpha$ : are the value of the  $\eta$ -coordinate at the outer and inner cylinders respectively, and they mapped to Cartesian coordinates using the formulas  $\eta = \frac{1}{2} \frac{(x+S)^2 + y^2}{(x-S)^2 + y^2}$ ;  $\beta =$

$\frac{1}{2} \frac{(x+S)^2+y^2}{(x-S)^2+y^2}$ ,  $\alpha = \frac{1}{2} \frac{(x+S)^2+y^2}{(x-S)^2+y^2}$ ;  $Z_p$ : particle mobility;  $V$ : The voltage;  $J$ : Jacobean bipolar

coordinate transformation and is derived as  $J = \begin{vmatrix} \frac{\partial x}{\partial \xi} & \frac{\partial y}{\partial \xi} \\ \frac{\partial x}{\partial \eta} & \frac{\partial y}{\partial \eta} \end{vmatrix} = \frac{(1+\cos \xi \cdot \cosh \eta)^2 + (\sin \xi \cdot \sinh \eta)^2}{(\cos \xi \cdot \cosh \eta)^4} S^2$ ;

$W$  : The fully developed velocity profile is given in the literature (Cummings, 1998), Same velocity profile is utilize for the numerical solution in the cases of the fully develop inlet flow, which is mapped to the Cartesian coordinate to be used utilized on the COMSOL Multiphysics® using conversion procedure given by Lucht (2015).

Equation (A.3) can further be simplified to find the particle traveling distance  $L$  as shown below

$$L = \frac{-(\beta-\alpha)}{Z_p V} \int_{\alpha}^{\beta} J W d\eta \quad (\text{A.4})$$

In the above equation for at each  $\eta$  value, particles motion begins at the outer cylinder at  $\eta=\alpha$  and ends at the inner cylinder at  $\eta=\beta$ . The results for particle traveling distance rely on the value of  $\zeta$ , which is the location of the particle release point around the outer cylinder on the aerosols inlet slit. Since the eccentric DMC computational domain is symmetric, the range of  $\zeta$  reduces to the interval  $[0, \pi]$ .

Finding the value of  $L$  is associated with specific mobility which then yields the transfer function for each mesh element. All transfer functions are weighted based on the velocity and size of the element to find the theoretical eccentric DMC transfer function.

## References

- 1) Howell, W. (1998). Information to users, 1–83. <https://doi.org/10.16953/deusbed.74839>

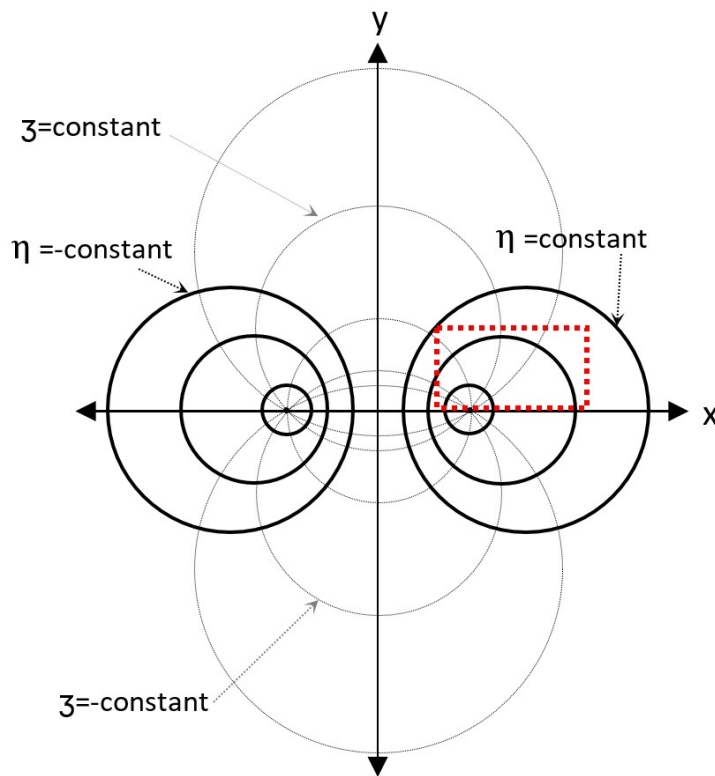


- 2) Knutson, E. O., & Whitby, K. T. (1975). Aerosol classification by electric mobility: apparatus, theory, and applications. *Journal of Aerosol Science*, 6(6), 443–451.

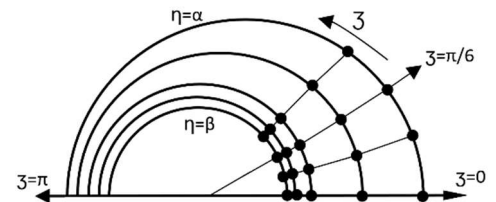
[https://doi.org/10.1016/0021-8502\(75\)90060-9](https://doi.org/10.1016/0021-8502(75)90060-9)

- 3) Lucht, P. (2015). Bipolar Coordinates and the Two-Cylinder Capacitor, 53(c), 1–71.

(a) Bipolar coordinate system



(b) Cross-section of the computational domain



(c) The computational domain

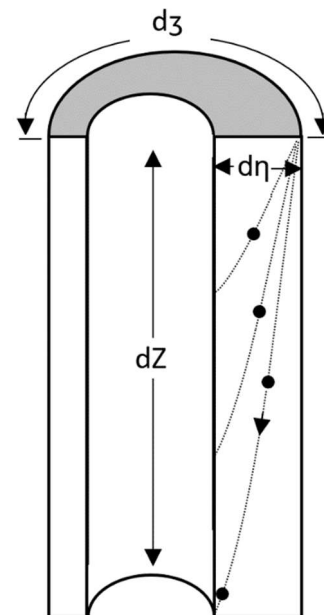


**Figure A.1** (a) The bipolar coordinate system used to analyze the computational domain (b) the cross-section of the mapped bipolar coordinate grids system (c) the theoretical computational domain.

## **APPENDIX B: The Developing Length for the Eccentric DMC**

The inner cylinder shifting (eccentricity) affects the flow field, which impacts the velocity profile and the developing length inside the DCM channel. Therefore, the ratio of the developing length (L) to the classifying channel hydraulic diameter (Dh)<sup>10</sup> has been calculated for different eccentricities and Reynold numbers. [Figure B.1](#) shows the relation between the ratio L/Dh and the Reynold number (Re) for the concentric and the eccentric cases of 1, 3, 5 %, and for the range of Reynold numbers of 2 to 100 respectively. The results show an increase in the L/Dh ratio as Reynold number increases. This raise in of developing length will be a rapid increased as the eccentricity increased and that because increasing in the unsymmetrical spacing which increases the variance in the flow and that requires a longer distance for the flow field to reach to the stable fully-develop flow case.

In the calculation, we consider the axial velocity reaching  $\approx 0.99$  of the fully developed flow maximum velocity. Another criteria was considered for the eccentric fully develop flow, which is the tangential flow reaching to a negligible value as parameters for the fully developed flow status, and similar to the work of Poole (2010).

---

<sup>10</sup> The hydraulic diameter for the hollow (Annulus) cross-section is defined as  $D_h = 4A/P$  ; and for the Annulus DMC can be simplified to  $D_h = D_2 - D_1$ ; -where A is the cross-section area; P is the wetted perimeter of the cross-section; D<sub>1</sub> and D<sub>2</sub> is the inner and outer cylinders diameter respectively.

From all the curves on [figure A-1](#), we found a general relation between the entrance length and the Reynold number and eccentricity using statistical software (OriginPro 2017<sup>®</sup>) which gives the relation

$$\frac{L}{D_h} = 6.886 \exp(\varepsilon/3.083 + Re/208.589)$$

where L: channel length,  $D_h$ : hydraulic diameter,  $\varepsilon$ : eccentricity, and Re : Reynold number.

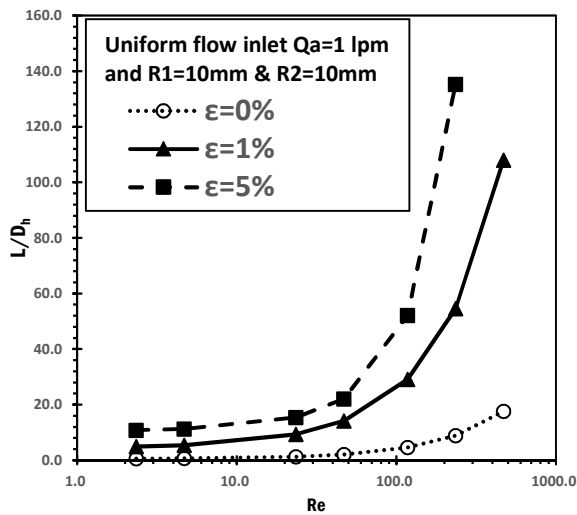
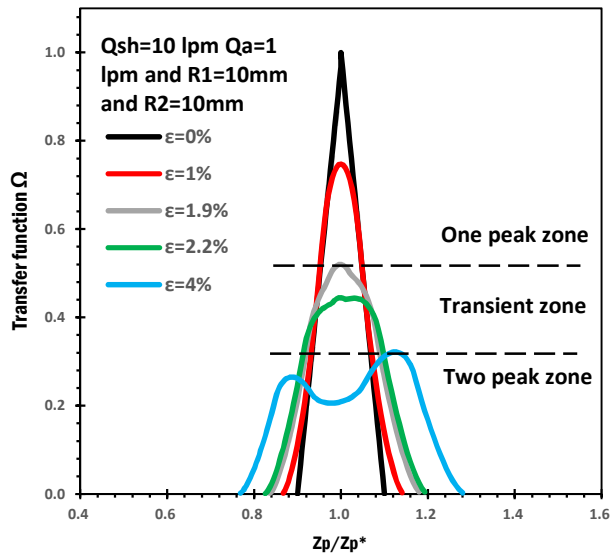


Figure B.1 the relation between Reynold number (Re) and the ratio of the fully develop entry length (L) to the hydraulic diameter ( $D_h$ ) for both concentric and eccentric DMC with eccentricities of 0%, 1%, and 5%.

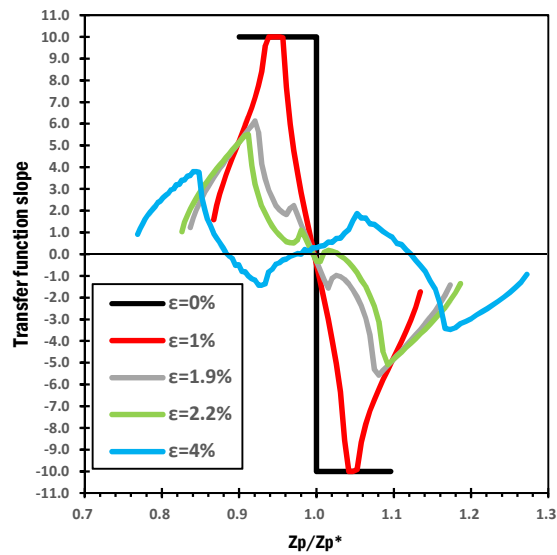
## **APPENDIX C: The Transfer Function Slope**

The cylindrical eccentric particle transfer function was gradually transferred from the one peak zone to the double peak zone, as shown in [figure C.1 a](#), through which the sharp peak is gently flattened as the eccentricity increases. Using the slope an indicator to identify these zone was very precise to cut off the zone.

We divide these zones based on data/curves slopes, especially near the transfer function peak. [Figure C.1.b](#). The first region is the unipolar distribution zone, at which the slope will vary rapidly around the peak. If the slope had a little fluctuation, especially on the data near the peak of the eccentric transfer function peak, then the data is in a transition to the double peaks. The third zone will be the double peak zone at which the data will follow the bimodal data distribution. The slope indication for this zone has low positive and negative values for the slopes around the peak, and for higher eccentricities, these values will be zeroes.



(a)



(b)

Figure C.1 (a) The three zones of the eccentric DMC transfer function for with eccentricities range from 0 to 4% for particle size ( $D_p$ ) of 160 nm and classify region length of 5 cm (b) the slope of the transferee function curves.

Note that these results are compatible in cases of using channel lengths and particle sizes of 45 cm with 815 nm and for 15 cm of 340 nm respectively because on this research we utilize a 30 kV as a maximum limit for electric field intensity.

## APPENDIX D: Maximum Inner Rod Tilting Angle $\theta_m$ for The Cylindrical DMC

In general, the maximum tilting angle  $\theta_m$  of inner rod in the cylindrical DMC classification channel can be calculated given the DMC dimensions of the classifying channel length  $L$  and the inner and outer cylinders radii  $R_1$  and  $R_2$ . The derivation of the equation for the maximum tilting angle can be found in the following:

Shown in [Figure D.1a](#) is the extreme tilting of the inner rod in the DMC classification channel. Accordingly,  $X_1 = X_2 + R_1$ . More, the values of  $X_1$  and  $X_2$  can be calculated via the trigonometric relation as  $X_1 = R_2 \cos \theta_m$  and  $X_2 = L \tan \theta_m$  (as shown in the [Figures D.1b](#) and [D.1c](#)). Thus, the final relation for determining the  $\theta_m$  can be expressed as:  $R_2 \cos \theta_m - L \tan \theta_m = R_1$

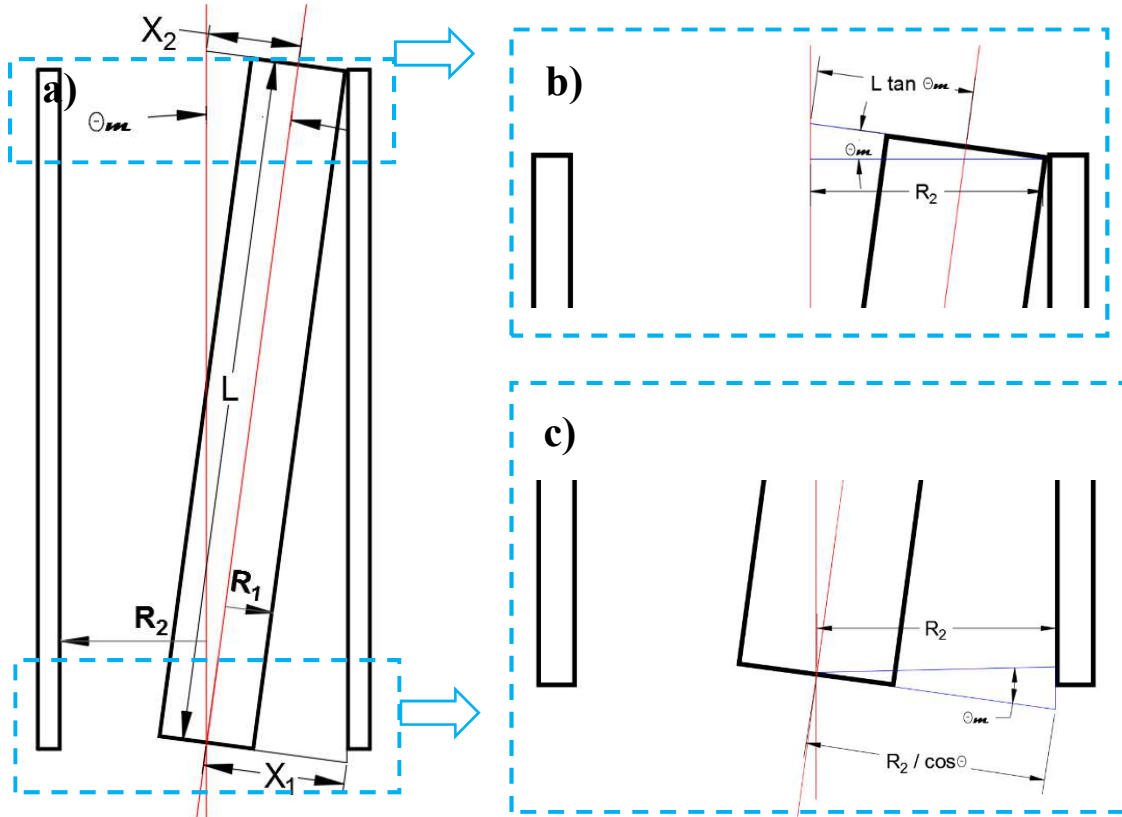


Figure D.1 Geometrical illustration of the relationship of  $L$  and  $R_1$  and  $R_2$  to the maximum tilting angle  $\theta_m$  of inner rod in a cylindrical DMC.

## VITA

Thamir Alsharifi | [thamirha@vcu.edu](mailto:thamirha@vcu.edu)

### EDUCATION

Ph.D. in Mechanical and Nuclear Engineering 2015-2019  
Virginia Commonwealth University, Richmond, VA, USA

M.Sc. in Mechanical Engineering 2005-2008  
University of Technology, Baghdad, Iraq

### PUBLICATIONS

- **Alsharifi, T., & Chen, D.-R.** (2018). On the Design of Miniature Parallel-Plate Differential Mobility Classifiers. *Journal of Aerosol Science*.  
<https://doi.org/10.1016/j.jaerosci.2018.04.003>.
- **Alsharifi, T., & Chen, D.-R.** (2019). Effect of axial eccentricity on the performance of a cylindrical differential mobility classifier. *Aerosol Science and Technology*, 0(0), 1–14. <https://doi.org/10.1080/02786826.2019.1599097>.
- **Alsharifi, T., & Chen, D.-R.** (2019). The influence of plate tilt on the transfer function of small plate differential mobility analyzers. *Journal of Aerosol Science*, 136(June), 48–59. <https://doi.org/10.1016/j.jaerosci.2019.06.006>.
- **Alsharifi, T., & Chen, D.** (2019). Effect of Inner Rod Tilting on the Performance of a Cylindrical Differential Electrical Mobility Analyzer (DEMC), (1972), 1–9. <https://doi.org/10.4209/aaqr.2019.01.0037>.

### Conferences

- **Alsharifi, T., & Chen, D.-R.** (2017). “Numerical Study of Miniature Plate Differential Mobility Analyzers (Mini-plate DMAs).” AAAR 36th Annual Conference, Raleigh, NC, USA.
- **Alsharifi, T., & Chen, D.-R.** (2018). “Effect of Eccentricity on the Performance of a Cylindrical Differential Mobility Classifier.” 10th International Aerosol Conference, St. Louis, MO, USA.

### LANGUAGES

Arabic – native language

English – speak fluently and read/write with high proficiency